STRATIGRAPHY, SEDIMENTOLOGY, AND TIDAL PROCESSES OF THE LATE MIOCENE TO EARLY PLIOCENE SOUTHERN BOUSE FORMATION, SOUTHEAST PALO VERDE MOUNTAINS, CALIFORNIA

by

KEVIN KORTUM GARDNER

A THESIS

Presented to the Department of Earth Sciences
and the Graduate School of the University of Oregon
in partial fulfillment of the requirements
for the degree of
Master of Science

September 2019

THESIS APPROVAL PAGE

Student: Kevin Kortum Gardner

Title: Stratigraphy, Sedimentology, and Tidal Processes of the Late Miocene to Early Pliocene Southern Bouse Formation, Southeast Palo Verde Mountains, California

This thesis has been accepted and approved in partial fulfillment of the requirements for the Master of Science degree in the Department of Earth Sciences by:

Dr. Rebecca J.Dorsey	Advisor
Dr. Marli Miller	Chair
Dr. Gregory Retallack	Member

and

Janet Woodruff-Borden	Vice Provost and Dean of the Graduate School

Original approval signatures are on file with the University of Oregon Graduate School.

Degree awarded September 2019

THESIS ABSTRACT

Kevin Kortum Gardner

Master of Science

Department of Earth Sciences

September 2019

Title: Stratigraphy, Sedimentology, and Tidal Processes of the Late Miocene to Early Pliocene Southern Bouse Formation, Southeast Palo Verde Mountains, California

Contrasting hypotheses for the depositional paleoenvironments of the late Miocene to early Pliocene southern Bouse Formation currently hinder progress toward a consensus on tectonic and paleogeographic reconstructions for the lower Colorado River region. The basal carbonate member of the southern Bouse Formation has been interpreted to record deposition in either (i) a large inland lake isolated from the ocean, or (ii) a transgressive intertidal to subtidal marine seaway. In this study, we analyze sedimentary lithofacies, facies associations, paleocurrents, and architecture of large-scale compound bedforms to develop a comprehensive depositional model. Our paleocurrent data and analyses of bedform architecture and facies association support a tidal origin for the southern Bouse Formation. Our paleogeographic reconstruction constrains the location of marine connection required by paleontological and sedimentary data. Our interpretation provides strong evidence in favor of a tidal origin and requires post-Miocene regional uplift.

This paper includes unpublished, coauthored material.

CURRICULUM VITAE

NAME OF AUTHOR: Kevin Kortum Gardner

GRADUATE AND UNDERGRADUATE SCHOOLS ATTENDED:

University of Oregon, Eugene
Whitman College, Walla Walla

DEGREES AWARDED:

Master of Science, Geological Sciences, 2019 University of Oregon
Bachelor of Arts, Geology, 2016, Whitman College

AREAS OF SPECIAL INTEREST:

Analytical Process Sedimentology
Stratigraphy
Basin Analysis
Structural Geology
Geologic Mapping

PROFESSIONAL EXPERIENCE:

Graduate Teaching Fellow, University of Oregon, 2017-2019

Undergraduate Researcher, Keck Geology Consortium, 2015

GRANTS, AWARDS, AND HONORS:

Outstanding Teaching Assistant Award, University of Oregon, 2019

Graduate Student Research Grant, Geological Society of America, 2018

Dr. Albert R. Leeds Prize for Excellence in Geology, Whitman College, 2016

ACKNOWLEDGMENTS

I wish to express the utmost appreciation for my advisor Becky Dorsey for providing funding for this research and for consistent support of my work through thoughtful discussion and review. Under your guidance I have learned to be a better geologist, to integrate observations both large and small, create unique solutions to unique problems, and to strive towards excellence in science. Your enthusiasm for geology is second to none, and it has been an exciting journey with you. I would also like to thank my committee members Marli Miller and Gregory Retallack for their thoughtful feedback and their review of my work.

I would like to express thanks to my field assistants Anthony Downey, Patrick Nonte, and Stephen Wainwright. Your company and support over four wild months in the desert made much of this work possible. From finding a dead body or climbing Palo Verde Peak to eating Albertacos and rock-hunting with desert folk; you all have made my field work the adventure of a lifetime. I would also like to thank Imperial County Sheriff's Department and Coroner for their timely 2.5 hour response time to finding human remains. An additional thanks goes out to Dave and Ski. Thank you for the generosity, kindness, and friendship you extended towards me while researching near your home.

I would like to thank the University of Oregon Department of Earth Sciences, National Science Foundation, and Geological Society of America for financial support.

I want to acknowledge the following very special people; Renee and Stephen Gardner for always encouraging me to follow my heart, be curious and do my best; Sophia Cromartie for being my partner, best friend, joy bring, and for listening to me ramble on

about rocks and graduate school for probably countless hours. You are amazing; James Hogan for being a fantastic friend, a source of interesting conversation, and my brewery buddy; Brennah McVey for your friendship and hospitality throughout school; Josh W and Tyler for your humor, and awesome cookouts; Larry Lai for being a peer mentor. Your advice was invaluable. I know you will do great things!; Michelle and Anne for being excellent office mates.

Finally, I want to acknowledge how amazing the earth is. It is an absolute privilege to be able to learn about how its various systems work. The earth and all its life are beautiful beyond compare. I will treasure it for the rest of my life and teach others to do so.

TABLE OF CONTENTS

Chapter Page

LIST OF FIGURES

Figure Page

Figure Page

LIST OF TABLES

Table Page

CHAPTER I

INTRODUCTION

The late Miocene to early Pliocene Bouse formation is exposed discontinuously along the margins of the lower Colorado River corridor. The three members: (1) basal carbonate, (2) siliciclastic, and (3) upper bioclastic record the conditions prior to and throughout the first integration of the Colorado River with the Gulf of California. The focus of this study is the basal carbonate member of the southern Bouse Formation along the range front of the southeastern Palo Verde Mountains, CA, and constrains the depositional environment of the region prior to the arrival of the Colorado River.

There is no consensus among researchers regarding the depositional paleoenvironment of the basal carbonate member of the southern Bouse Formation. The basal carbonate member has been interpreted to record deposition in either (1) a large inland lake isolated from the ocean, or (2) a transgressive intertidal to subtidal marine seaway. Lack of consensus regarding the origins of the basal carbonate member currently hinders constraints on the tectonics and paleogeography of the region, and understanding the processes by which the Colorado River integrated with the Miocene Gulf of California. A marine origin for the basal carbonate requires at least 330 m of regional uplift since the late Miocene. Conversely, a lacustrine origin requires no uplift, and does not provide any useful constraints.

In this thesis I present detailed sedimentologic, stratigraphic, and quantitative data from the basal carbonate member of the southern Bouse Formation, interpret them to provide constraints on depositional paleoenvironments, hydraulic conditions,

paleogeographic reconstructions. Additionally, I discuss the implication of these analyses. In Chapter II, I present detailed analyses of lithofacies, bedform architecture, paleocurrents, and paleogeographic reconstructions. I use this data to reconstruct the depositional environments of the basal carbonate member and propose a detailed depositional model that includes hydrodynamics of tidal processes based on empirical studies and published studies of similar tidal deposits.

This thesis emphasizes analytical process sedimentology integrated with stratigraphy through interpretation of bedforms and detailed descriptions of lithofacies. Data for this thesis was collected during two winter terms (January-March) in 2018 and 2019. Measured sections, geologic mapping, and paleocurrent data were collected along the rangefront of the southeastern Palo Verde Mountains, CA. Outcrops of the basal carbonate member in the Palo Verde Mountains are the focus of this study because outcrops record the transition from pre-Bouse deposition conditions and highlight the effect of pre-depositional, erosional paleotopography on the facies distribution of the basal carbonate member. Chapter II is presented in manuscript form for the journal *Sedimentary Geology* and is co-authored with Dr. Rebecca Dorsey.

CHAPTER II

STRATIGRAPHY, SEDIMENTOLOGY, AND TIDAL PROCESSES OF THE LATE MIOCENE TO EARLY PLIOCENE SOUTHERN BOUSE FORMATION, SOUTHEAST PALO VERDE MOUNTAINS, CALIFORNIA

The data in this chapter was developed by both my advisor Dr. Rebecca J. Dorsey and myself. Dr. Dorsey contributed substantially to this work by participating in the development of a depositional model, reviewing manuscripts, and planning data collection I was the primary contributor to the data collection and analysis, constructed a majority of the figures, and did all the writing.

1. Introduction

The late Miocene to early Pliocene Bouse Formation, exposed discontinuously along the margins of the lower Colorado River valley (Figure 1), records conditions that existed prior to and during integration of the Colorado River to the Gulf of California. The Bouse Formation is divided into three distinct members – basal carbonate, siliciclastic, and upper bioclastic members – that reflect major changes in depositional processes, sediment sources, and paleoenvironments during initiation and early evolution of the river (e.g., Dorsey et al., 2018). Interpretation of these processes affects our understanding of the regional tectonic evolution and origins of the Colorado River, but contrasting hypotheses hinder progress toward a general consensus on paleogeographic and tectonic reconstructions for this enigmatic formation.

Most workers agree that the northern Bouse Formation, north of Parker, Ariz. (Fig. 1), was deposited in a series of interconnected lakes that filled with water and sediment of the first-arriving Colorado River (Spencer and Patchett, 1997; Spencer and Pearthree, 2001; House et al., 2008; Spencer et al., 2013; Pearthree and House, 2014;

Bright et al., 2016). However, ongoing debate centers on the depositional paleoenvironments of the southern Bouse Formation in the Blythe Basin (Fig. 1). Two hypotheses have been proposed for the basal carbonate member of the southern Bouse Formation: (1) carbonate deposits accumulated in a saline lake with no connection to the ocean, similar to northern Bouse lakes (Spencer and Patchett, 1997; Roskowski et al., 2010; Spencer et al., 2013; Pearthree and House, 2014; Bright et al., 2016, 2018a, 2018b); or (2) southern Bouse carbonates formed in a tidally-influenced marine seaway at the north end of the Miocene Gulf of California oblique rift basin (Metzger, 1968; Buising, 1990; McDougall, 2008; McDougall and Martínez, 2014; Miller et al., 2014; O'Connell et al., 2017; Dorsey et al., 2018). Previous studies identified tide-generated sedimentary structures and sequences in the southern Bouse basal carbonate member (Buising, 1990; Turak, 2000; O'Connell et al., 2017; Dorsey et al., 2018), but additional data and observations are needed to further test the tidal seaway hypothesis.

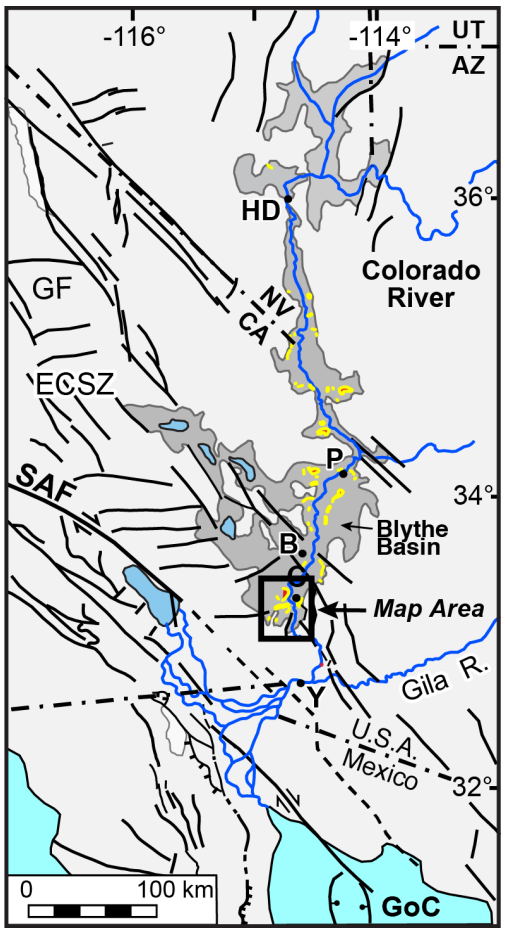

Figure 1: Map of SE California along the lower Colorado River Corridor. Outcrops of Bouse Fm. Are in yellow. Black box indicates area of Figures 2 and 17. P = Parker, AZ; C = Cibola, AZ, B = Blythe, CA.

This paper presents the results of a detailed sedimentologic study of the basal carbonate member of the southern Bouse Formation in the Palo Verde Mountains (Fig.

2). We use process-based analysis of sedimentary lithofacies, facies associations, paleocurrent data, and architecture of large-scale bedforms to develop an integrated depositional model for these deposits. The results support a tidal interpretation for mixed carbonate-siliciclastic facies of the basal carbonate member and allow us to clarify the hydrodynamics of this macro- or mega-tidal system. Our paleogeographic reconstruction of the southern Bouse tidal seaway provides new support for post-Miocene uplift in the lower Colorado River region and highlights the value of integrative sedimentology and stratigraphic analysis for understanding the consequences of long-wavelength vertical crustal motions adjacent to an active transform plate boundary.

2. Geologic Background

2.1 Summary of Models for the Bouse Formation

The southern Bouse Formation in the Blythe Basin (Fig. 2) has been studied over the past ca. 50 years with the aim of understanding the geologic and hydrologic evolution of the lower Colorado River region, starting with early studies of Metzger (1968) and Smith (1970). The lake hypothesis postulates that the southern Bouse Formation accumulated in a large inland lake that filled with water derived from downstream-directed lake spillover events recorded in the northern Bouse Formation (Spencer and Patchett, 1997; Spencer et al., 2013; House et al., 2008; Pearthree and House, 2014; Bright et al., 2016, 2018a, 2018b). Based on the observation that the $^{87}Sr/^{86}Sr$ ratio of southern Bouse carbonates is closer to that of Colorado River water than Miocene seawater, Spencer and Patchett (1997) concluded that Bouse carbonates accumulated in a lake filled with Colorado River water. Subsequent studies of carbonate chemistry,

isotopes, water budgets, and stratigraphic evidence have lent additional support to the inland saline lake model for the southern Bouse Formation (Poulson and John, 2003; Roskowski et al., 2010; Spencer et al., 2013; Pearthree and House, 2014; Bright et al., 2016, 2018a, 2018b).

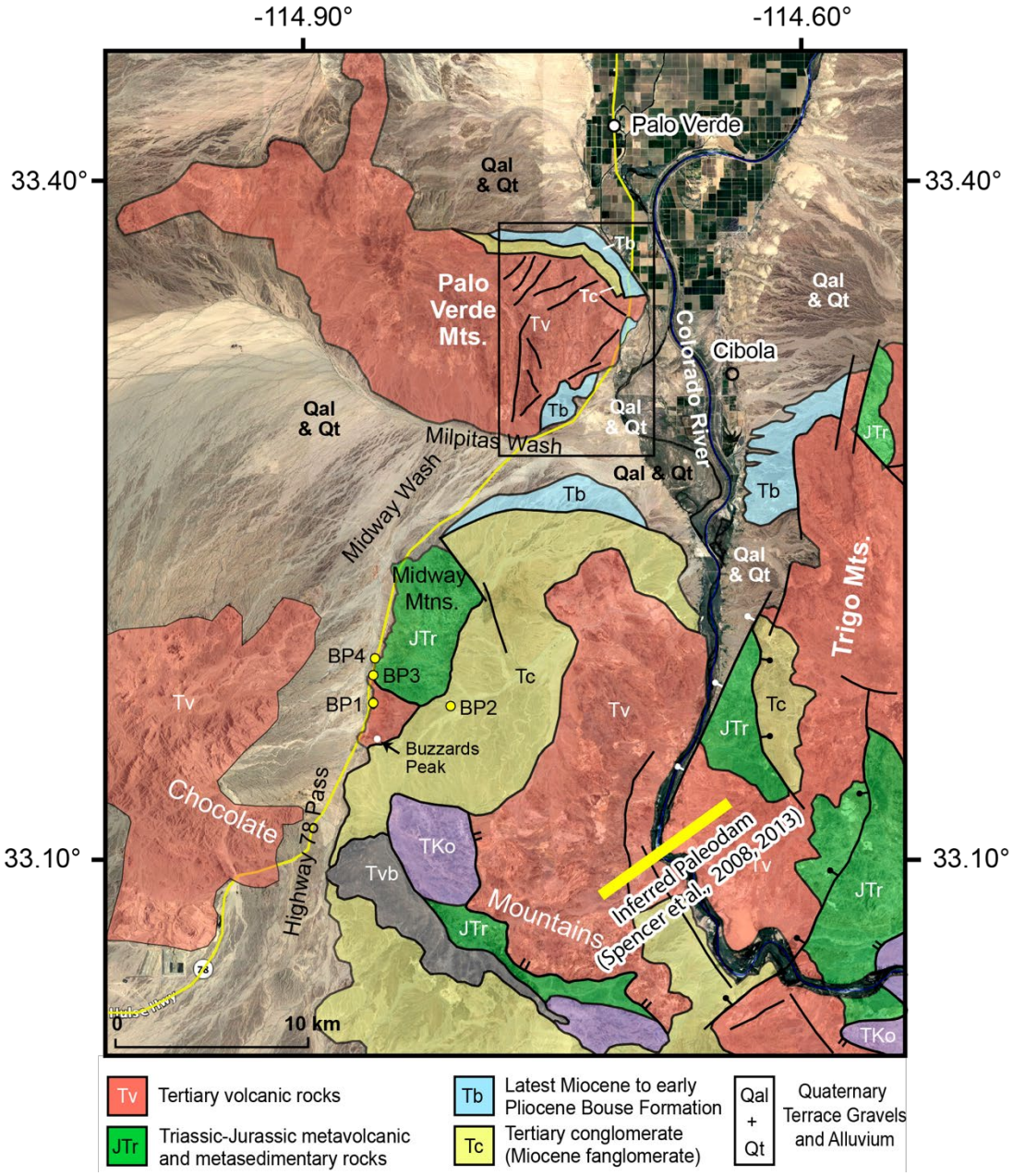

Figure 2: Geologic map of the southern Blythe Basin (Compiled from Sherrod and Tosdal, 1991; Richard, 1993; Ricketts et al., 2011; Gootee et al., 2016; this study).

The marine hypothesis for the southern Bouse Formation postulates that the basal carbonate member accumulated in a marine seaway at the north end of the Miocene Gulf of California oblique-rift basin. In this interpretation the basal carbonate member is interpreted to pre-date arrival of the earliest through-flowing Colorado River and its sediment load (e.g., McDougall, 2008; McDougall & Miranda-Martínez 2014; Dorsey et al., 2018). Previous studies have identified a variety of marine and brackish-water fossils in the southern Bouse Formation, as far north as Parker, AZ, including bivalves, gastropods, barnacles, calcareous algae, ostracodes, and foraminifers (Metzger, 1968; Smith, 1970; Buising, 1990; McDougall, 2008; McDougall and Miranda-Martínez, 2014). Based on physical sedimentology and Fourier transform analysis of rhythmically bedded bioclastic deposits, O'Connell et al. (2017) concluded that the basal carbonate member was deposited by tidal currents in a tide-dominated marginal marine environment. Tide- and wave-generated bedforms have also been documented in Milpitas Wash, AZ, and the Palo Verde Mountains (Buising, 1990; Turak, 2000; Homan, 2014; Dorsey et al., 2018), but recent papers have questioned the tidal origin of these features (e.g., Bright at al., 2018a, 2018b), indicating the need for a more detailed analysis of proposed tidal features.

Some studies of stable isotopes (O and C) in Bouse carbonates reveal light isotopic signatures interpreted to support a lacustrine depositional model for the basal carbonate member (e.g., Roskowski et al., 2010; Bright et al., 2016, 2018a, 2018b). Some datasets reveal a southward increase in $\delta^{13}C$ toward seawater values (0 per mil) over a distance of ~200 km along the lower Colorado River valley (Poulson and John, 2003), and O and C isotopes show linear covariation toward seawater (Roskowski et al., 2010;

Crossey et al., 2015) in a trend that is commonly produced by mixing of river and ocean waters in marine estuaries (e.g., Ingram et al., 1996). Crossey et al. (2015) showed that Sr-isotope ratios in southern Bouse carbonates could be produced by mixing of Colorado River water, radiogenic spring water, and seawater with a plausible range of mixing fractions of ~5 to 50% seawater. Thus, the isotopic data presented to distinguish between lake and marine interpretations appear inconclusive.

2.2 Stratigraphic Framework

In this paper we divide the southern Bouse Formation in the Palo Verde Mountains into the basal carbonate member, siliciclastic member, and upper bioclastic member (Fig. 3; Dorsey et al., 2018). The Bouse basal carbonate member overlies Miocene alluvial fan conglomerate and older volcanic rocks in the Palo Verde Mountains (Fig. 3). We divide the basal carbonate member into three units that occur in consistent stratigraphic order: (1) basal travertine that commonly is encrusted directly on Miocene volcanic rock, and rarely is seen in small amounts on Miocene conglomerate; (2) bioclastic unit (focus of this study) comprising a wide range of grain sizes and sedimentary lithofacies documented below; and (3) very fine-grained upper marl.

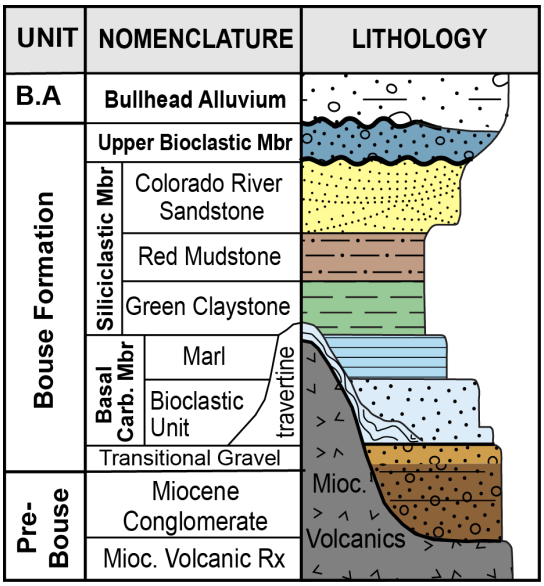

Figure 3: Generalized Stratigraphy of the southern Bouse Formation in the southeastern Palo Verde Mountains.

The siliciclastic member overlies the basal carbonate along a conformable but abrupt contact that records the first arrival of Colorado River sediment (Homan, 2014; Dorsey et al., 2018). It ranges up to 200 m thick in subsurface sections (Metzger et al., 1973) and thins to zero thickness where it is cut out along a regional unconformity at the base of the upper bioclastic member. The siliciclastic member is sub-divided into three units: (1) pale to dark green, massive to thinly laminated claystone; (2) red mudstone interbedded with small-scale cross-bedded siltstone and sandstone; and (3) fine to medium-grained channelized, trough cross-bedded Colorado River channel sandstone. Systematic coarsening up-section from green clays to channelized trough cross-bedded fluvial sandstones is interpreted to record progradation of the Colorado river delta (Buising, 1990; Pearthree and House, 2014) and integration of the Colorado river to the northern Gulf of California (Dorsey et al., 2018).

The upper bioclastic member unconformably overlies the two older members of the southern Bouse Formation (Fig. 3), and varies in composition from nearly pure carbonate to mixed carbonate-siliciclastic facies to dominantly siliciclastic sand and gravel (Homan, 2014; Dorsey et al., 2018; O'Connell, 2016). Wave-formed ripple bedforms and presence of marine fossil mollusks and calcareous coralline red algae indicate that the upper bioclastic member records deposition in high-energy shallow marine waters in the lower Colorado River valley, after earliest initiation of the Colorado river (Dorsey et al., 2018, 2019). The upper bioclastic member plays a central role in testing hypotheses for processes involved in the initiation and early evolution of the Colorado River (Beard et al., 2016; Dorsey et al., 2018, 2019).

This study is focused on exposures of the Bouse basal carbonate member exposed in the southeastern Palo Verde Mountains (Fig. 4). The mountains are composed of Miocene and older volcanic rocks including mafic to dacitic flows and rhyolitic tuffs that dip steeply to the east (Sherrod and Tosdal, 1991). Large normal and oblique faults are common in the Palo Verde Mountains (Fig. 4) and mostly pre-date deposition of the Bouse Formation. Widespread travertine deposits of the basal carbonate member are encrusted directly on volcanic bedrock, thus preserving the latest Miocene to early Pliocene erosional paleotopography of the Palo Verde Mountains. Proximity of the basal carbonate member to the steep range front, and preservation of pre-Bouse erosional paleotopography, make the southeast Palo Verde Mountains an excellent natural laboratory for studying the topographic controls on depositional processes.

3. Overview of Lacustrine and Tidal Sedimentation

Shallow, low energy lacustrine settings are dominated by deposition of mud and sand. In these environments, reversing wind directions produce bi-directional currents and temporarily expose parts of the shoreline (Ainsworth et al., 2012). Bi-directional wind currents can produce small scale crossbedding in two dominant directions, and fluctuations in energy levels throughout the lake can produce mud drapes, mud cracks and wavy-lenticular bedding. In higher energy lakes, lateral migration of gravelly longshore bars and sandy stream mouth bars can also produce bi-directional paleocurrents (Fraser and Hester, 1977). Multi-meter scale lake-shore structures, such as gravelly beach ridges formed during the late Pleistocene Lake Lahontan highstand in Nevada, may display opposing cross-bedding directions on lakeward and landward faces

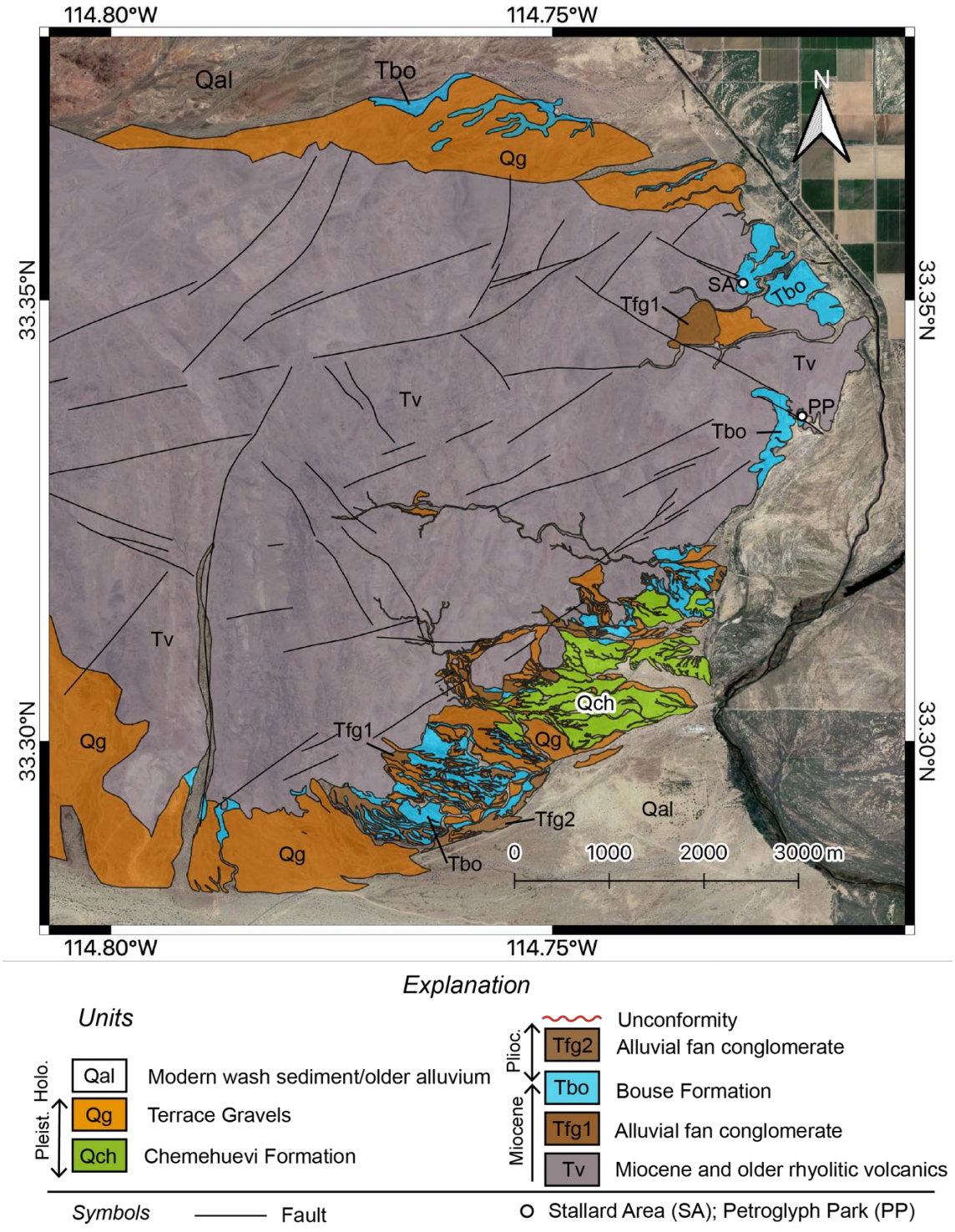

Figure 4: Geologic map of the southeastern Palo Verde Mountains showing the major units in the region. All members of the Bouse Formation have been included in a single unit (Tbo). Terrace Gravels (Qg) include all ages of Qi from Gootee et al. (2016). Qal is not colored on the map.

(e.g., Blair, 1999). Lakeward dipping strata are deposited by wave processes such as swash on the lakeward face (Schuster and Nutz, 2017), whereas landward dipping tabular cross-beds form as washover deposits during storms on the landward faces of beach ridges (Shaw et al., 2015). Bioclastic carbonate grainstones also form in lacustrine environments characterized by dominance of continental faunal assemblages (Gierlowski-Kordesch, 2010). Bioclastic carbonates can form wavy-lenticular bedding and crossbedding in shallow lake environments (e.g., Ainsworth et al., 2012).

In marginal-marine settings, cyclical fluctuations in water depth during daily tides induce horizontal flood (onshore-directed) and ebb (offshore-directed) currents that result in daily filling and draining of coastlines and ocean-connected basins (e.g., Davis, 2012). In tidal environments these currents are the dominant mechanism of sediment transport and can build multi-meter scale compound bedforms. The net transport of sediment in the flood or ebb direction determines whether a tidal system is classified as flood- or ebb-*dominant*, whereas the duration and velocity of each current determines the *asymmetry* of a tidal system (Dronkers, 1986; Brown and Davies, 2010). Bathymetry and geometry of tidal basins exert the primary control on tidal range, current duration, and current velocity in tidal environments (Brown and Davies, 2010). Deposits most commonly associated with tidal depositional systems include wavy-flaser-lenticular bedding (Reineck and Wunderlich, 1968) and herringbone crossbedding formed by bimodal, bipolar currents with interceding periods of slackwater (e.g., Davis, 2012; Daidu et al., 2013). While mud-rich deposits often are not diagnostic of deposition by tidal currents (Stride, 1982; Davis, 2012), the internal structures and geometries of cross-bedded sands and gravels have been shown to be uniquely diagnostic of tidal depositional processes and

environments (Stride, 1982; Brown and Davies, 2010; C. Olariu et al., 2012; Davis, 2012; Longhitano et al., 2012; Longhitano, 2013; Longhitano and Steel, 2017), especially when coupled with mud-rich facies that commonly are found in tidal facies associations.

Large sand sheets and isolated sand banks are well described from modern and ancient tidal environments (Dalrymple, 1984; Berné, 2000; Santoro et al., 2002; Olariu et al., 2012; Reynaud and Dalrymple, 2012; Longhitano, 2013; Longhitano and Steel, 2017), and are characteristic features of high energy tidal currents in shoreface and offshore environments. Large sand sheets are produced by the growth and migration of compound bedforms that are built from smaller bedforms (Dalrymple, 1984; C. Olariu et al., 2012; M. I. Olariu et al., 2012). Large compound bedforms in tidal environments typically are constructed by deposition from smaller-scale individual bars or dunes (Fig. 5). Tidal bars and dunes are distinctly different types of bedform that represent unique stratal geometries, mechanisms of formation, and depositional conditions.

Compound dunes (Fig. 5a) are large bedforms (1-15 m) with crests oriented transverse to flow direction, in which bedform migration occurs primarily by forward accretion (Dalrymple, 1984; Berné, 2000; C. Olariu et al., 2012). Superimposed, smaller-scale simple dunes have foresets oriented similar to down-current-dipping lee faces that make up the master surfaces of compound dunes. Compound dunes can form within tidal channels or as isolated sand sheets and bars. Importantly the height of compound dunes is typically no more than ~20% of water depth (C. Olariu et al., 2012), providing a minimum constraint on paleo-water depth. In contrast, tidal bars are elongate bedforms with crests oriented parallel to the dominant current direction (Fig. 5; Dalrymple, 1984; Dalrymple et al., 1990; Fenies and Tastet, 1998; C. Olariu et al., 2012; M. I. Olariu et al.,

2012). Tidal bars migrate by lateral accretion, perpendicular to current direction, and often are found at the margins of tidal channels, and tidal bar heights are commonly up to 100% of water depth (Dalrymple et al., 1990; Dalrymple and Choi, 2007; M. I. Olariu et al., 2012; Reynaud and Dalrymple, 2012; C. Olariu et al., 2012). The different behavior and scales of bars versus dunes provide useful criteria for constraining paleoenvironmental reconstructions and interpretation of paleocurrent data from the stratigraphic record.

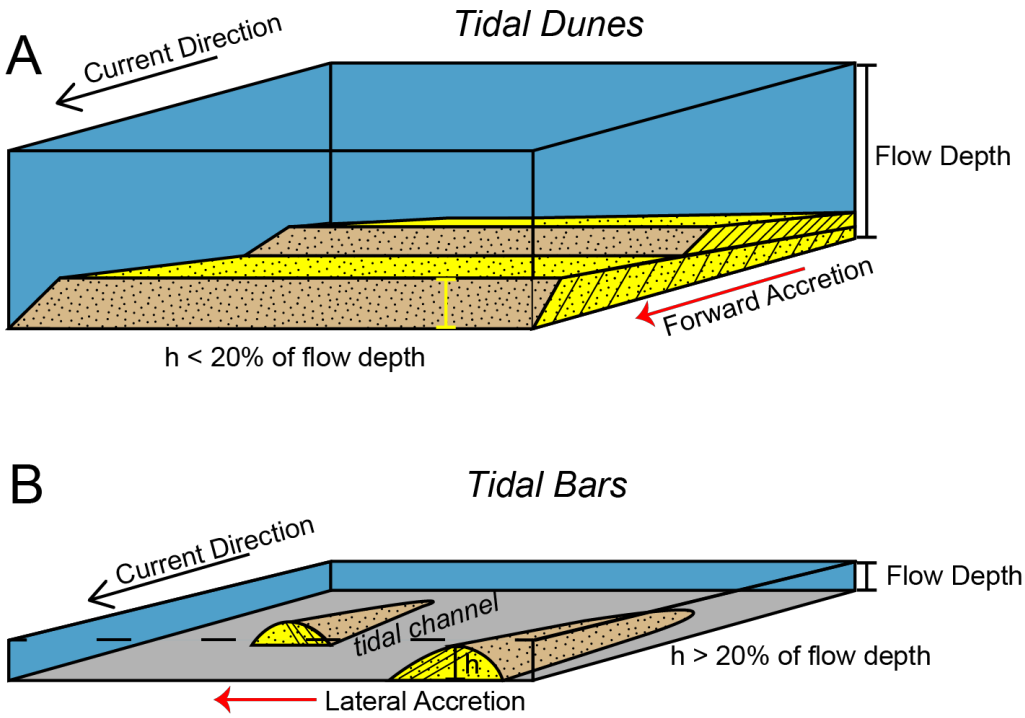

Figure 5: Schematic diagram of A) tidal dunes and B) tidal bars showing the relationship between bedform geometry, flow depth, current direction, and accretion direction. Flow depths in A and B are equal. h = bedform thickness.

In this paper we use the terminology of Ashley (1990) and C. Olariu et al. (2012) to document the major architectural features of tidal dune and bar cross bedding in the southern Bouse Formation. This system is the only published classification that is suitable for describing and interpreting the wide array of cross-bedding scales and

geometries observed in this study. The smallest architectural components of compound dunes are 2D and 3D simple dunes with foresets (1st-order surfaces) whose down-dip direction is parallel to the current direction (Fig. 6). Master surfaces (2nd-order surfaces) mark the boundaries between stacked simple dunes and represent the lee faces of migrating compound dunes (Dalrymple, 1984; Berné, 2000; C. Olariu et al., 2012).

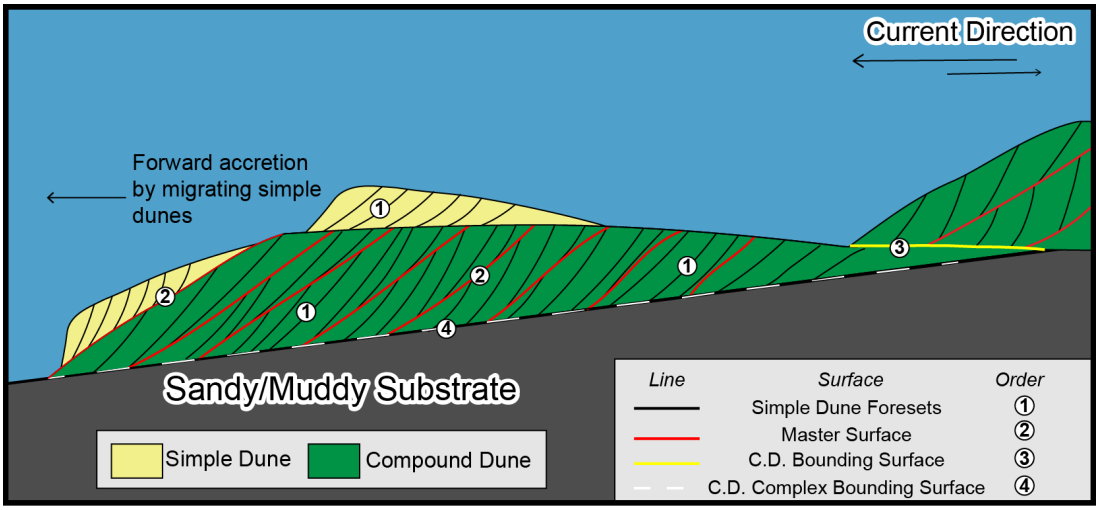

Figure 6: Fundamental architectural components of a tidal compound dune and their relation to bedform migration and current direction. Vertical exaggeration is ~5x to illustrate geometric relations. C.D. = Compound Dune

Compound dunes are built by successive stacking of simple dunes, and the direction of compound dune migration is recorded in dip direction of the master surfaces. Migration of compound dunes through forward accretion is facilitated by the migration of simple dunes over the crest and down the lee faces of compound dunes (Allen, 1980). Compound dune complexes (Fig. 6) are built by the stacking of compound dunes bounded by 3rd order surfaces, and can extend for kilometers as a result of compound dune migration over regional 4th order surfaces (C. Olariu et al., 2012). Simple dunes and compound dunes may be 2D or 3D, and may have sigmoidal or planar-tabular

geometries, which are indicative of differing flow conditions. Recognition of these architectural elements and their relationships in outcrop is necessary to differentiate dunes from bars and allows us to identify tidal process in near-shore and off-shore environments.

4. Methods

Data collected for this study include representative measured sections, field photos that display important features of sedimentary lithofacies, bedform geometries and stratal architecture, measurements of bedset and compound dune thicknesses, and paleocurrent measurements (primarily dip direction on well-defined foreset surfaces). Stratigraphic sections (see Appendices A&B) were measured bed-by-bed and include bed thickness and geometry, grain size, sorting, composition, sedimentary structures, and fossils. Bed set thicknesses of sigmoidal and planar-tabular simple dunes were measured within and outside of compound dunes at their thickest point. Compound dune thicknesses were measured at the thickest point with a meter stick where possible and (where cliff exposures were not accessible) using a Nikon laser rangefinder. Measurements of paleocurrent indicators, master surfaces, and bedding include strike, dip, and dip angle, and are corrected for gentle structural dips using Stereonet 9 software (see appendices C-E).

We constructed and interpreted facies associations by comparison to similar published case studies. Interpretations of depositional environments from this and previous studies (Metzger, 1968; Homan, 2014; O'Connell, 2016; Dorsey et al., 2018) were used as constraints for our paleogeographic reconstruction (Fig. 16). Reconstruction

of the paleo-shoreline was completed using minimum water depth estimates from compound dune thicknesses from the Stallard Area, Petroglyph Park, BP4, and BP5 (Fig. 2). Using a locality-by-locality approach, we calculated the intersection of present topography and a plane representing the height of water over each locality in QGIS. Measured gentle tectonic dips were used to restore cross bedding and other features to their original, pre-tilting orientation.

5. Sedimentary Lithofacies Analysis

We divide the bioclastic unit of the Bouse basal carbonate member into 15 distinct lithofacies based on grain size, composition, sedimentary structures, and sorting (Table 1). These lithofacies are grouped into two categories based on dominant composition: siliciclastic-dominant versus carbonate-dominant. Interbedding of different facies and sediment types permits designation of two main facies associations: (1) Tidal Fan Delta Facies Association, and (2) Tidal Dune Field Facies Association (Table 2).

5.1 Siliciclastic-Dominant Facies

Four types of siliciclastic-dominant facies in the study area include: horizontally stratified pebbly sandstone; horizontally stratified conglomerate; unstratified conglomerate; and cross-bedded conglomerate. Carbonate percentage in conglomerate matrix ranges from 0 to 80% in these facies. Siliciclastic-dominant facies alternate vertically and laterally with carbonate-dominant facies along the margins of the basin.

Horizontally stratified pebbly sandstone (Facies S1, Table 1) consists of medium- to coarse-grained, moderately sorted sandstone containing 20-30% subrounded, sub-equant pebbles (Fig. 7a). No preferred orientation was observed in the pebbles. Sand and

pebbles are derived from local volcanic bedrock. Facies S1 contains 0% carbonate grains. Stratified conglomerate (Facies S2, Table 1) is matrix-supported, moderately to poorly sorted, granule to pebble conglomerate with minor cobble lenses (Fig. 7b). This facies displays horizontal to low-angle cross stratification. Granule and pebble-sized lasts are subangular to subrounded, and cobbles are angular to subangular. Facies S2 matrix ranges from 0-20% carbonate.

Unstratified conglomerate (Facies S3, Table 1) consists of clast-supported, poorly sorted, unstratified, subangular pebble to boulder conglomerate (Fig. 7C). This unit can be either ungraded or inversely graded. Clasts are locally-derived volcanic rocks. Boulder-sized clasts may be up to 2 meters across. This lithofacies is laterally discontinuous and thins to zero thickness over horizontal distances of <200 m (often <50 m). Facies S3 displays the greatest variation in matrix composition, with matrix composition ranging from 0-80% carbonate. Where facies S3 directly overlies carbonate-dominant facies, the matrix composition contains higher percentages of carbonate (Fig. 7e). Cross-bedded conglomerate (Facies S4, Table 1) consists of matrix-supported, moderately to well sorted, granule to pebble conglomerate with subrounded volcanic clasts (Fig. 7D). Facies S4 has planar-tabular cross-bedding with bedsets ranging from 0.2-0.8 m thick. Cross-bedding may be uni-directional or bi-directional and is often channelized. Matrix composition ranges from 10-80% bioclastic carbonate. Facies S4 is systematically observed stratigraphically above the first occurrence of bioclastic carbonate.

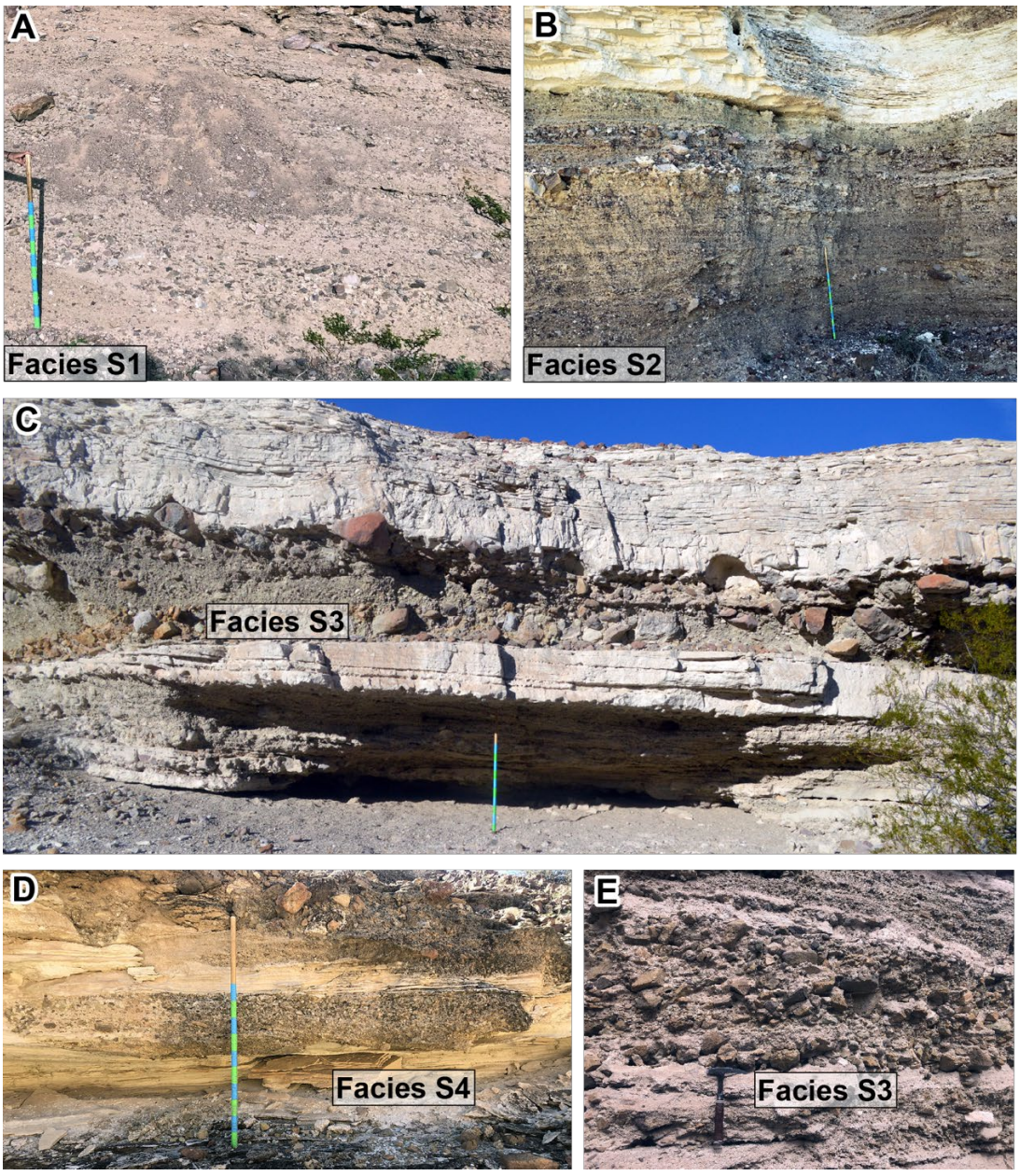

Figure 7: Field photos of siliciclastic-dominant facies with interbedded carbonate-dominant facies. A) Horizontally stratified, pebbly sandstone. B) Horizontally stratified to low angle cross-bedded sandy pebble conglomerate overlain by horizontally stratified calcisiltite and sandy grainstone. C) Unstratified, inversely graded, pebble to boulder conglomerate, with carbonate-dominant facies above and below. D) Well sorted, subrounded, cross-bedded, granule to pebble conglomerate. E) Unstratified, ungraded, pebble to cobble conglomerate interbedded with pebbly, sandy grainstone.

Table 1: Lithofacies

Lithofacies	Facies #	Description	Interpretation
Siliciclastic Dominant	S1	Horizontally bedded Medium- to coarse-grained pebbly sandstone.	Upper plane bed deposition in distal alluvial fan.
	S2	Moderately- to poorly-sorted, horizontally to low-angle cross-stratified, granule-pebble conglomerate with minor cobble lenses. Carbonate composition of matrix varies from 0-20%	Deposition by sheet floods on medial alluvial fan.
	S3	Poorly sorted, unstratified, ungraded to inversely graded, pebble to boulder conglomerate. Matrix composition varies from 100% siliciclastic to 70-80% bioclastic carbonate.	Deposition by debris flow in proximal to medial alluvial fan.
	S4	Moderately- to well-sorted, sub-rounded, granule to pebble conglomerate with tabular cross-bedding. Cross-bed sets range from 0.2 - 0.8m thick and have channel geometries.	Deposition by migration of gravelly point bars in braided channels of a fan delta.
	SC1	Poorly sorted, unstratified, clast-supported, pebble to cobble conglomerate with fine-grained carbonate grainstone matrix. Clasts display travertine encrustation.	Deposition by sediment gravity flow.
Carbonate Dominant	C1	Massive to rhythmically bedded calcisiltite with interbedded siliciclastic and lime mud.	Deposition by suspension settling in upper intertidal flats
	C2a	Wavy-flaser-lenticular bedded and horizontally laminated, interbedded, very fine- to fine-grained sandy grainstone and calcisiltite.	Deposition by low energy wave oscillation and suspension settling on intertidal flats.
	C2b	Wave ripple laminated, very fine to fine-grained sandy grainstone with thin lime mud interbeds. Lime mud interbeds display desiccation cracks	Deposition by low energy wave oscillation and suspension settling on intertidal flats.
	C2c	Massive/bioturbated very fine- to med-grained sandy grainstone with or without calcisiltite component. Rhodoliths, micro mollusks and gastropods common. Bioturbated variety displays contains Thalassinoides burrows locally.	Deposition by sub-critical flow in bottom sets of small-scale intertidal compound dunes

Table 1 (continued)

Lithofacies	Facies #	Description	Interpretation
	C3a	Massive to weakly stratified, medium-grained to granule-sized sandy grainstone with abundant rhodoliths, mollusks, and barnacles.	Rapid deposition in bottomsets of subtidal compound dunes.
	C3b	Horizontally stratified, fine- to coarse-grained sandy grainstone. Locally contains angular to sub-rounded pebbles.	Deposition by critical to flow in bottomsets of large-scale subtidal compound dunes.
	C3c	Weakly stratified, poorly sorted, fine- to coarse-grained pebbly, sandy grainstone.	Rapid deposition by high energy currents.
	C3d	Weakly stratified, coarse-grained to granule-sized, sandy grainstone with thin, granule-pebble conglomerate lenses.	High energy re-working of granule-pebbles in intertidal flats.
	C4	Well sorted, fine-grained to granule-sized sandy grainstone with small- to intermediate-scale tabular cross-bedding. Cross-bed sets range from 0.05-0.5m thick. Crossbed sets display bi-directional transport.	Deposition by migrating 2D tidal dunes in lower intertidal flats.
	C5	Well sorted, medium-grained to granule sized sandy grainstone with large-scale sigmoidal cross-bedding. Cross-bed sets range from 0.4-2.5 m thick. Granule sized shell fragments on foresets are common.	Deposition by migrating 2D to 3D tidal bedforms in a shallow to middle subtidal environment.

5.2 Carbonate-Dominant Facies

We divide carbonate-dominant facies into 5 lithofacies with internal variations (Table 1, Figure 8). When describing carbonate-dominant facies, we used the terms "sandy" and "pebbly" in reference to the siliciclastic component which ranges from 5-40%. Carbonate-dominant facies are commonly interbedded and are differentiated on the basis of grain size, scale, and style of sedimentary structures. Carbonates were produced in-situ by organisms or through inorganic precipitation.

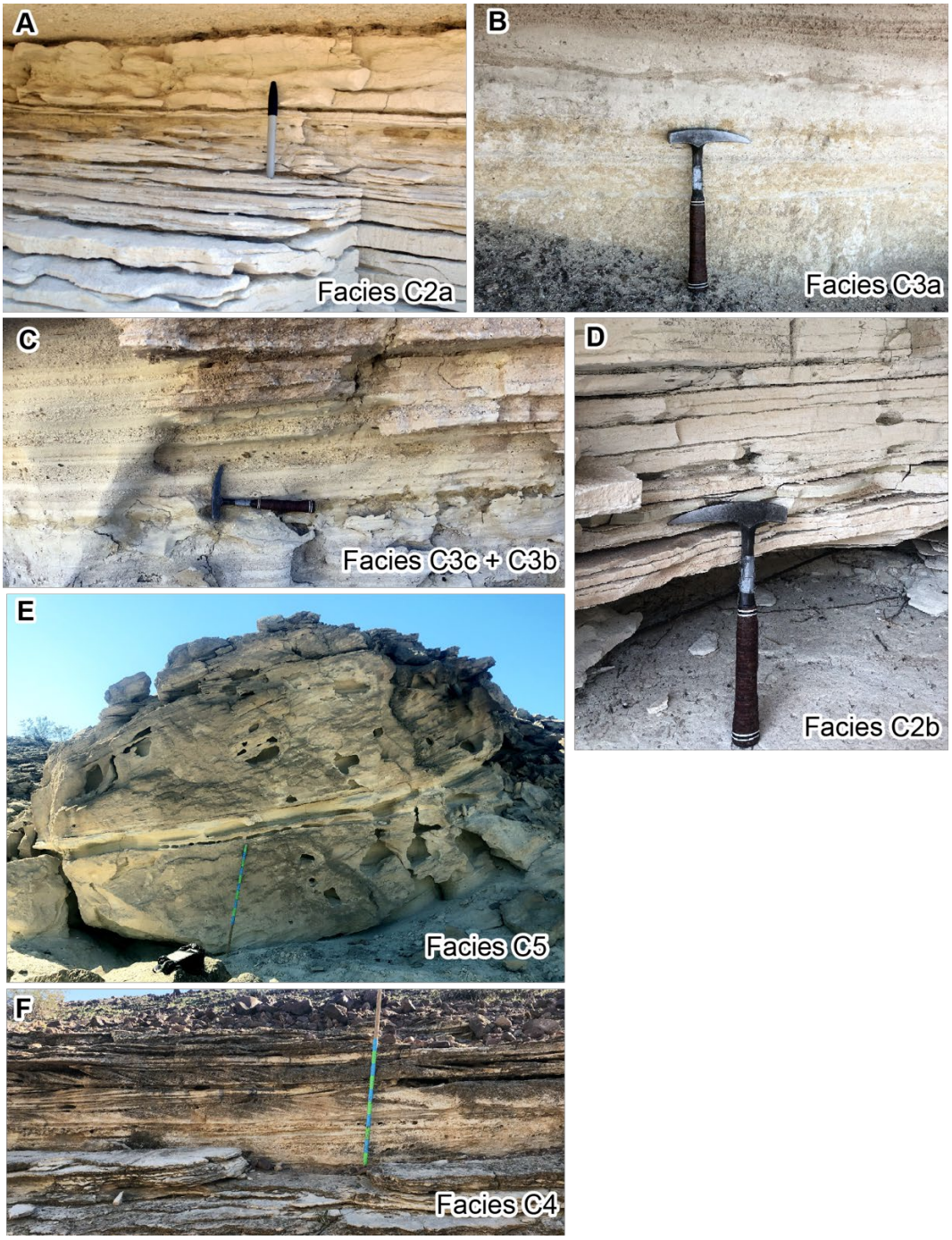

Figure 8: Field photos of carbonate dominant facies. A) Wavy-Flaser-Lenticular bedded grainstone and calcisiltite. B) Massive to weakly stratified grainstone. C) Horizontally stratified, fine- to medium-grained pebbly, sandy grainstone. D) Horizontally stratified, very fine- to fine-grained sandy grainstone with lime mud interbeds. E) Large-scale (0.5-2 m thick), medium-grained to granule-sized, sigmoidal, cross-bedded grainstone. F) Small scale (10-20 cm thick) medium-grained to granule-sized, planar cross-bedded sandy grainstone. Color divsions on staff are 10 cm; Hammer = 32.5 cm; Sharpie = 13.6 cm

.

Encrusted-clast conglomerate (Facies SC1, Table 1) consists of poorly sorted, unstratified, subrounded pebble to cobble conglomerate with fine-grained sandy grainstone matrix. Locally-derived clasts are fully encrusted by travertine and surrounded by a sandy carbonate matrix. Facies SC1 is not observed in contact with volcanic bedrock and is instead found as a discontinuous, 6-10 cm thick unit overlying Miocene conglomerate and Bouse conglomerate. Interbedded calcisiltite (Facies C1, Table 1) is well-sorted, massive to rhythmically bedded silt-sized carbonate unit interbedded with siliciclastic and carbonate mud. Facies C1 displays reed casts and burrows along bedding plane exposures. Massive beds are up to 10 cm thick, and rhythmite beds are <1 cm thick. Stratigraphically, Facies C1 is the oldest facies of the bioclastic unit. This unit is equivalent to the fine-grained heterolithic facies used in fourier transform analysis by O'Connell et al. (2016).

Facies C2a, C2b and C2c (Table 1) contain ripple-scale cross-laminations, horizontal laminations, and massive bedding. Facies C2a and C2b are very fine- to fine-grained sandy grainstone with interbeds of calcisiltite and lime mud. Facies C2c consists of fine- to medium-grained sandy grainstone that locally contains calcisiltite. C2a displays abundant wavy-flaser-lenticular bedding (Figure 8a) along with minor horizontal laminations. C2b displays horizontal and wave ripple laminations and bedding plane exposures of lime mud in Facies C2b show grainstone-filled desiccation cracks (Fig. 8d). Facies C2c contains micromolluscs, rhodoliths and gastropods, commonly associated with *Thalassinoides* burrows. Individual grainstone beds in Facies C2a and C2b range from 2 to 6 cm thick, and finer interbeds are typically <1 cm thick. Bed thicknesses in Facies C2c range from 3 to 10 cm.

Facies C3a-d (Table 1) consist of fine-grained to granule-sized, moderately to poorly sorted sandy grainstone with locally-derived volcanic pebbles. Facies C3a, C3c, and C3d are weakly stratified and have an average bed thickness of 5 cm. Facies C3b (Figure 8c) is well stratified and has an average bed thickness of 3 cm. Facies C3a (Fig. 8b) has no pebble sized clasts and contains abundant molluscs, gastropods, and barnacles. Locally, Facies C3a contains *Thallasinoides* burrows. Facies C3b contains angular, locally-derived pebbles within well stratified beds. C3c lacks internal stratification observed in C3b, and contains locally-derived pebbles. Facies C3d contains abundant poorly sorted, siliciclastic granule and pebble lenses.

Facies C4 and C5 (Table 1) comprise fine-grained to granule-sized, well sorted, cross-bedded sandy grainstone. Cross-beds in Facies C4 (Fig. 8d) have planar-tabular geometries and bed set thicknesses ranging from 0.05-0.5 m thick. Paleocurrents in Facies C4 are bidirectional and rectilinear. Facies C5 (Fig. 8e) has sigmoidal cross-beds with thicknesses from 0.4-2.5 meters. Paleocurrents in Facies C5 are unidirectional. Shell fragments are concentrated on reactivation surfaces and foresets within simple dunes. Facies C4 and C5 are observed individually, and are also commonly observed within larger, multi-meter thick compound bedforms.

5.3 Facies Associations

In this study we recognize distinctive vertical and lateral stacking and interbedding of lithofacies that comprise three main facies associations (Table 2): (1) Distal Alluvial Fan; (2) Tidally-Influenced Fan Margin, and (3) Tidal Dune Field facies.

5.3.1 Alluvial Fan Facies Association (FA1)

Miocene conglomerate of FA1 directly overlies Miocene and older bedrock and underlies the Bouse Formation. This unit includes Facies S1-S3 (pebbly sandstone and conglomerate), but without any carbonate in clast or matrix compositions. Facies S2 (stratified conglomerate) and S3 (unstratified conglomerate) are common constituents of FA1 (Fig. 9). Facies S1 is less common and occurs as discontinuous beds of stratified pebbly sandstone within conglomerate facies. This facies association can be 10s of meters thick, although a maximum thickness cannot be determined because the contact with underlying bedrock dips into the subsurface.

Table 2: Facies Associations

Facies Association	**Lithofacies**	**Interpretation**
Alluvial Fan (FA1)	S1, S2, S3	Deposition by sheet floods and debris flows in a proximal to distal alluvial fan setting.
Tidally-influenced Fan Margin (FA2)	S1, S2, S3, S4, SC1, C1, C2a, C2b, C2c, C4	Transgression of tidal flats onto alluvial fans. Sheet floods and debris flows build out shoreline in active alluvial channels. Inactive alluvial channels are dominated by tidal processes.
Tidal Dune Field Facies Association (FA3)	C2b, C3a, C3b, C3c, C3d, C4, C5	Deposition by large scale (5m thick) 2D and 3D tidal compound dunes migrating along axis of an ebb-dominated tidal seaway.

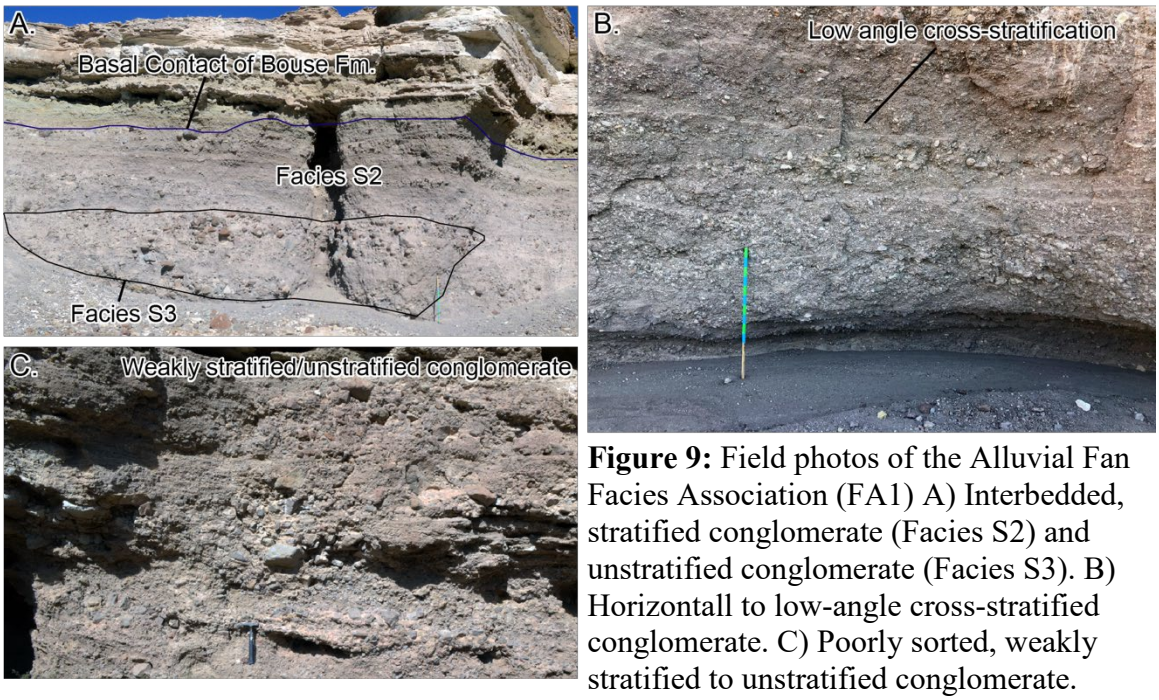

Figure 9: Field photos of the Alluvial Fan Facies Association (FA1) A) Interbedded, stratified conglomerate (Facies S2) and unstratified conglomerate (Facies S3). B) Horizontall to low-angle cross-stratified conglomerate. C) Poorly sorted, weakly stratified to unstratified conglomerate. Hammer is 32.5 cm; Staff is 1m and has 10 cm divisions.

We interpret the Alluvial Fan Facies Association to record deposition in subaerial alluvial fans. Where facies S2 and facies S1 are most abundant, sheetfloods were the primary mode of deposition. In localities where facies S3 (unstratified conglomerates) is abundant, deposition by debris flows was the dominant mechanism for building alluvial fans. These two processes are not mutually exclusive, and evidence for both processes in a single alluvial fan is common. Large boulders (> 2m across) are observed within extensive sheet flood deposits. This suggests initial transport via debris flow and subsequent winnowing and reworking of fines through sheet floods, leaving behind large boulder lags. The presence of both sheetflood and debris flow deposits could reflect lateral changes in depositional environments from proximal to distal alluvial fan, or intermittent debris flows extending out into distal alluvial fan environments.

5.3.2 Tidally-Influenced Fan Margin Facies Association (FA2)

This facies association is characterized by complex interbedding of siliciclastic-dominant and carbonate-dominant lithofacies near the margins of the basin (Table 2, Figs. 10, 11). FA2 is transitional between late Miocene alluvial fan conglomerate (FA1) and subtidal carbonate-dominant facies (FA3), and is absent in areas where subtidal deposits of FA3 rest directly on travertine-encrusted Miocene volcanic rock. Measured sections display variations in the ratio of siliciclastic-dominant to carbonate-dominant facies (S:C ratio) and relative abundance of Facies S2 and S3 (stratified and unstratified conglomerate). These differences define two variants: FA2a with a higher ratio of siliciclastic deposits and mainly stratified conglomerate in the siliciclastic component; and FA2b with a higher ratio of carbonate deposits and dominantly unstratified conglomerate in the siliciclastic component.

In sections with a high S:C ratio, the base of FA2a is marked by the lowest carbonate-rich deposits above Miocene conglomerate (Fig. 11a). Typically, the lowest carbonate is a <30 cm thick bed of fine-grained calcisiltite or grainstone (C1 or C2). Facies S2, stratified conglomerate, is the dominant lithofacies occurring in thick (0.25-2 m) continuous beds, with thinner (0.15-0.3 m) interbeds and discontinuous lenses of S3 (unstratified conglomerate). We observe an up-section decrease in the S:C ratio and a subtle increase in grain size of carbonate-dominant facies (Fig. 11). Stratigraphically higher unstratified conglomerate forms laterally discontinuous beds averaging 0.2 m thick. Sections with a low S:C ratio (FA2b, Fig. 11b, 11c) are characterized by abundant carbonate-dominant facies and unstratified conglomerate (S3) beds in the siliciclastic

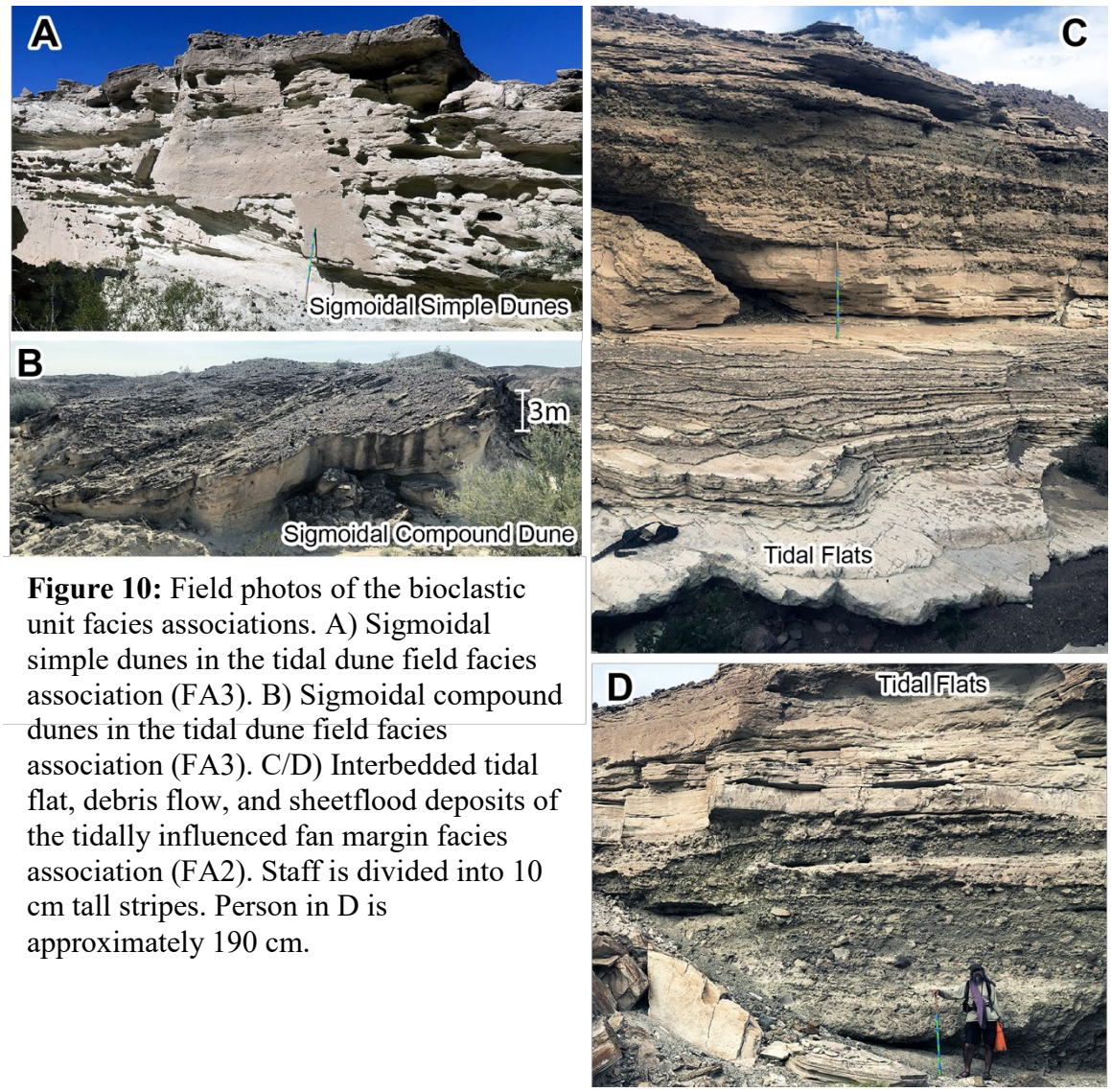

Figure 10: Field photos of the bioclastic unit facies associations. A) Sigmoidal simple dunes in the tidal dune field facies association (FA3). B) Sigmoidal compound dunes in the tidal dune field facies association (FA3). C/D) Interbedded tidal flat, debris flow, and sheetflood deposits of the tidally influenced fan margin facies association (FA2). Staff is divided into 10 cm tall stripes. Person in D is approximately 190 cm.

Tidally Influenced Fan Margin Facies Association

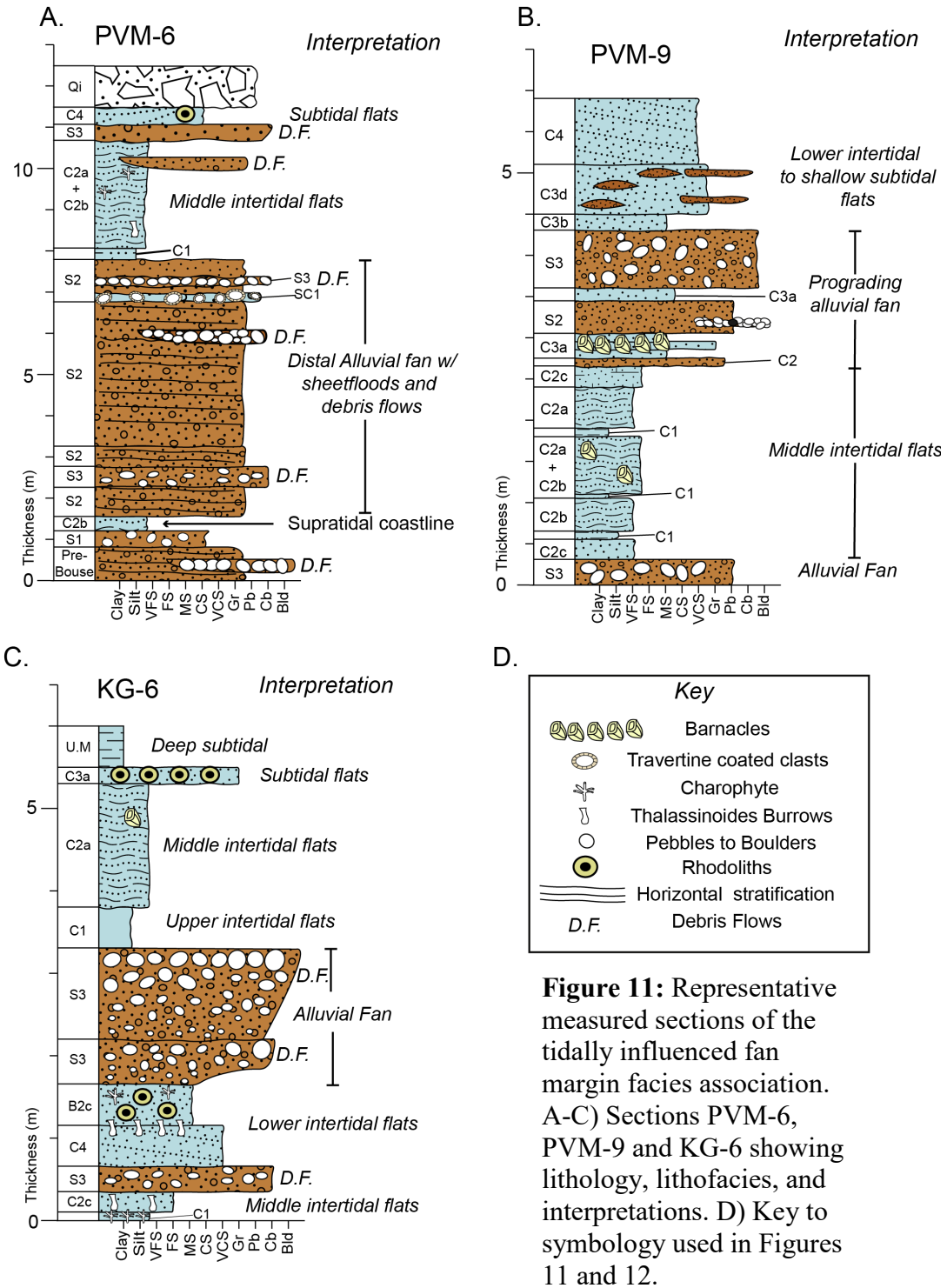

Figure 11: Representative measured sections of the tidally influenced fan margin facies association. A-C) Sections PVM-6, PVM-9 and KG-6 showing lithology, lithofacies, and interpretations. D) Key to symbology used in Figures 11 and 12.

component. In these sections, Facies S2 and S3 occur in laterally discontinuous beds 0.2-1 m thick, or as thin lenses (0.1-0.15 m) in Facies C3d.

We interpret facies association FA2 to record the transition from pre-inundation Miocene alluvial fans (FA1) to high-energy subtidal conditions that produced the cross-bedded bioclastic deposits of FA3. Pre-Bouse Miocene conglomerate (FA1) was deposited in distal alluvial fans by sheet floods (Facies S1, S2) and debris flows (Facies S3). Conglomerate interbeds of FA2a have similar composition and texture as the deposits of underlying alluvial-fan association FA1. Carbonate-dominant facies C1-C3 record deposition by wave action and tidal currents with intermittent suspension settling during slackwater conditions (Table 1). Common interbedding and lateral interfingering of alluvial fan and tidal deposits records migration of active alluvial channels that built out the shoreline, while abandoned portions of alluvial fans became inundated by intertidal flats at the margins of a tidal seaway (see below). Sections with high S:C ratios and abundant Facies S2 (stratified conglomerate) formed on active, sheetflood-dominated distal alluvial fans that underwent rare inundation and tidal deposition during rare marginal-marine floods produced by storm-driven anomalously high hides. Tidal-flat conditions became dominant up-section following abandonment of the alluvial fan, decreased siliciclastic sediment supply, or an increase in average water depth due to rising relative sea level. Sections with low S:C ratios and more unstratified conglomerate formed on fan-fringing tidal flats where sediment supply from debris flows was intermittent. Coarsening-up rends in carbonate-dominant facies record a transition from low-energy upper intertidal flats, to increased energy conditions associated with lower intertidal to shallow subtidal environments. Our observations are consistent with studies

of modern tectonically-confined transgressive tidal environments (e.g. Longhitano et al., 2013).

5.4 Tidal Dune Field Facies Association (FA3)

This facies association contains coarsening-up successions of cross-bedded sandy grainstones and calcisiltites with little to no siliciclastic-dominant facies (Figs. 9, 11; Table 2). Facies C5 (cross-bedded sandy grainstone) is the dominant sediment type and includes abundant inclined surfaces where paleocurrent measurements were collected. FA3 makes up the majority of bioclastic carbonate deposits in the southeastern Palo Verde Mountains. This facies association is distinguished by abundance of medium-grained to granule sized, multi-meter scale cross-bedded sandy grainstone. Cross-beds are abundant and provide useful paleocurrent and hydrodynamic information (Section 6, below). All localities of FA3 reveal strong coarsening-up in carbonate-dominant deposits, with facies S2-S4 making up ≤ 10% of this facies association.

We interpret Facies Association 3 to record migration and deposition of coarse-grained bioclastic sediment in subtidal compound dune fields that formed large carbonate sand sheets in a transgressive tidal seaway. Large-scale compound bedforms with bimodal paleocurrent directions (see below) documented in this study are characteristic of tidal environments (e.g. Dalrymple, 1984; Berné, 2000; C. Olariu et al., 2012; M. I. Olariu et al., 2012) and are not seen in lakes. Coarsening-up trends record increased water depth and current velocities during deposition. Fine-grained carbonate sand, silt, and mud in the lower parts of each section accumulated in low-energy intertidal flats and are overlain by large-scale compound dunes (Fig. 12) that require increased current velocity and water depth during deposition.

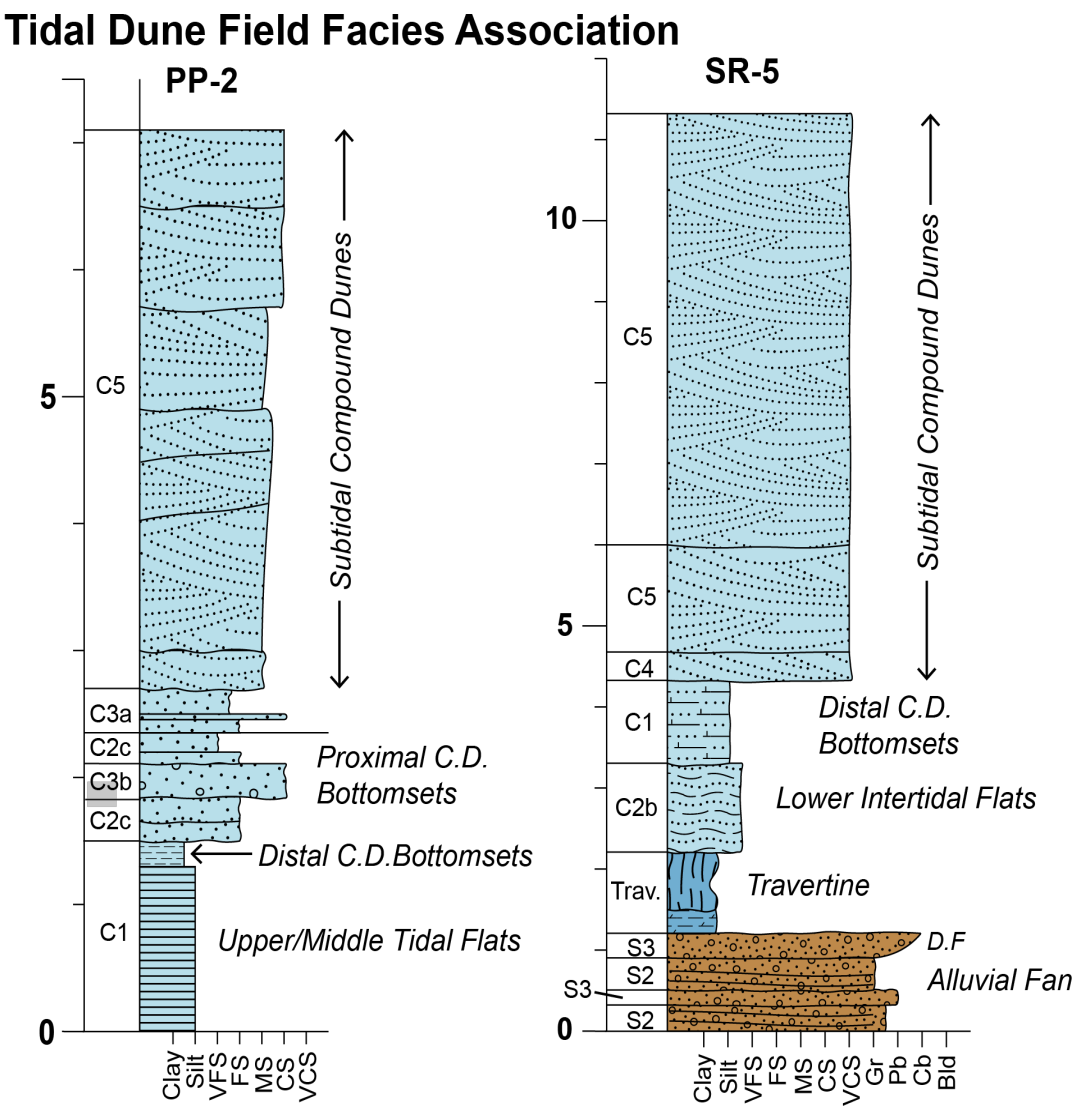

Figure 12: Representative measured sections of the tidal dune field facies association. Section PP-2 in Petroglyph Park shows a transition from shallow intertidal flats to subtidal compound dunes. Section SR-5 from the Stallard Area shows a transition from Miocene alluvial fan deposits covered by Bouse travertine into shallow intertidal flats and then into subtidal compound dunes. Both sections coarsen upwards, and represent an up section rise in relative seal level RSL.

Up-section coarsening in large-scale cross beds also reflects hydraulic sorting during traction transport. Coarse-grained to granule-sized particles are deposited on the lee-faces of compound bedforms, and very-fine to medium sand is transported out in front of the compound bedform and deposited as bottomsets. An upward increase in grain size is typical of compound dunes and results from forward migration of coarse-grained foresets over finer-grained proximal to distal bottomsets (C. Olariu et al., 2012; M. I. Olariu et al., 2012). In contrast, fining-upward is commonly seen in deposits of tidal bars. Only upward-coarsening vertical trends were observed in compound bedforms in this study. The absence of mud-rich and siliciclastic-dominant facies in FA3 indicates deposition away from basin-margin alluvial fans. The characteristics of this facies association are consistent with large sand sheets in modern and ancient transgressive tidal systems (Stride, 1982; C. Olariu et al., 2012; M. I. Olariu et al., 2012; Reynaud and Dalrymple, 2012; Longhitano, 2013; Longhitano and Steel, 2017).

6. Sedimentary Bedform Analysis

Analysis of sedimentary bedforms provides insights into hydraulic conditions, current dynamics, and water depth of tidal depositional systems (Stride, 1982; Dalrymple, 1984; Dalrymple et al., 1990; C. Olariu et al., 2012; Longhitano et al., 2012; Longhitano, 2013; Longhitano and Steel, 2017). Two areas in the southeastern Palo Verde Mountains, the Stallard Area and Petroglyph Park (Fig. 2), contain excellent exposures of large-scale cross bedding in carbonate-dominant facies (FA3) that permit detailed analysis of stratal geometries and their origins. In this section we use data from these exposures to document the architecture of compound and simple dune bedforms, measure and classify

master surfaces and simple foresets, and analyze paleocurrent data to reconstruct hydraulic conditions and paleogeography.

6.1 Compound Dune Architecture

Exposures of cross-bedding at Petroglyph Park and the Stallard Area (Fig. 4) reveal architectural elements ranging from simple dunes to compound dunes to compound-dune complex scale. In one example at Petroglyph Park, two compound dunes are defined by 3rd-order bounding surfaces and each compound dune is composed of numerous smaller-scale simple dunes measuring 0.05-1.8 m thick (Fig. 13a). Internal foresets (1st-order surfaces) within simple dunes dip 18-29°, whereas master surfaces that define the boundaries of simple dunes (2nd-order surfaces) are generally shallower and dip 8-20° (Fig. 13a). Master surfaces are non-uniform and irregular. Larger (0.5-2.5 m) simple dunes at Petroglyph Park have sigmoidal geometries with south-dipping lee faces, while smaller dunes (0.05-0.5 m) are both sigmoidal and tabular. Tabular varieties are laterally discontinuous, often truncated by foresets of larger sigmoidal simple dunes. Compound dunes at Petroglyph Park range from 4.0 to 5.5 m tall. Their geometry is distinctly sigmoidal, with thin tails in the north and thick lee faces in the south. The dune field here rests on a regional 4th order surface above shallow tidal rhythmites (Fig. 13 a).

Simple dunes in the Stallard Area (Fig. 4) are similar to those observed at Petroglyph Park. Foresets (1st-order surfaces) dip 18-31° east, and master (2nd-order) surfaces have a range of dips from 3° to 23°. Simple dunes at all scales are dominantly sigmoidal with uncommon tabular cross-beds. One representative exposure (Fig. 14a) reveals a network of nested and laterally stacked compound dunes within a larger-scale compound dune complex spanning 100s of meters in horizontal distance.

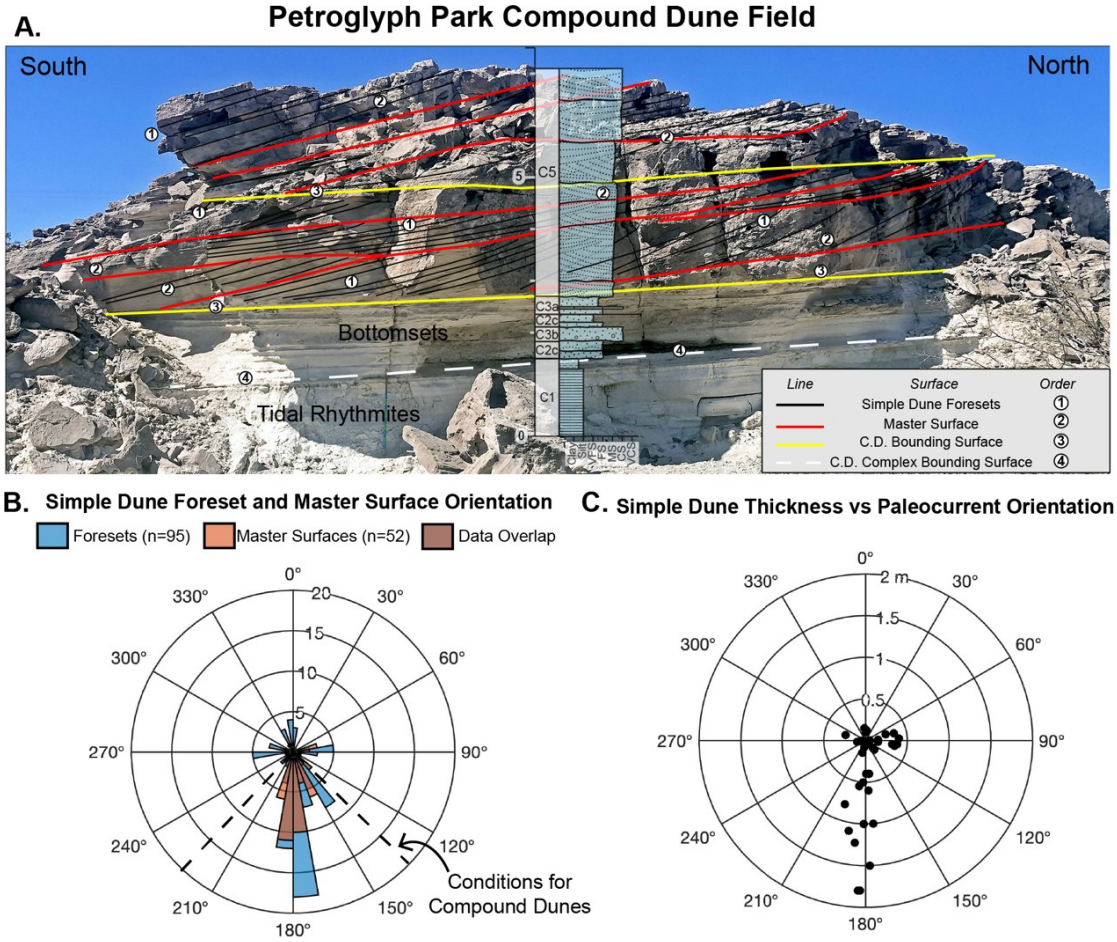

Figure 13: Petroglyph Park compound dune field. A) Annotated photo showing architectural elements of two compound dunes. B) Rose diagram showing orientations of foresets and master surfaces. Area where conditions are met for compound dunes is bounded by dashed lines. C) Polar plot of simple dune thickness versus paleocurrent orientation. Note that larger bedforms are directed to the south.

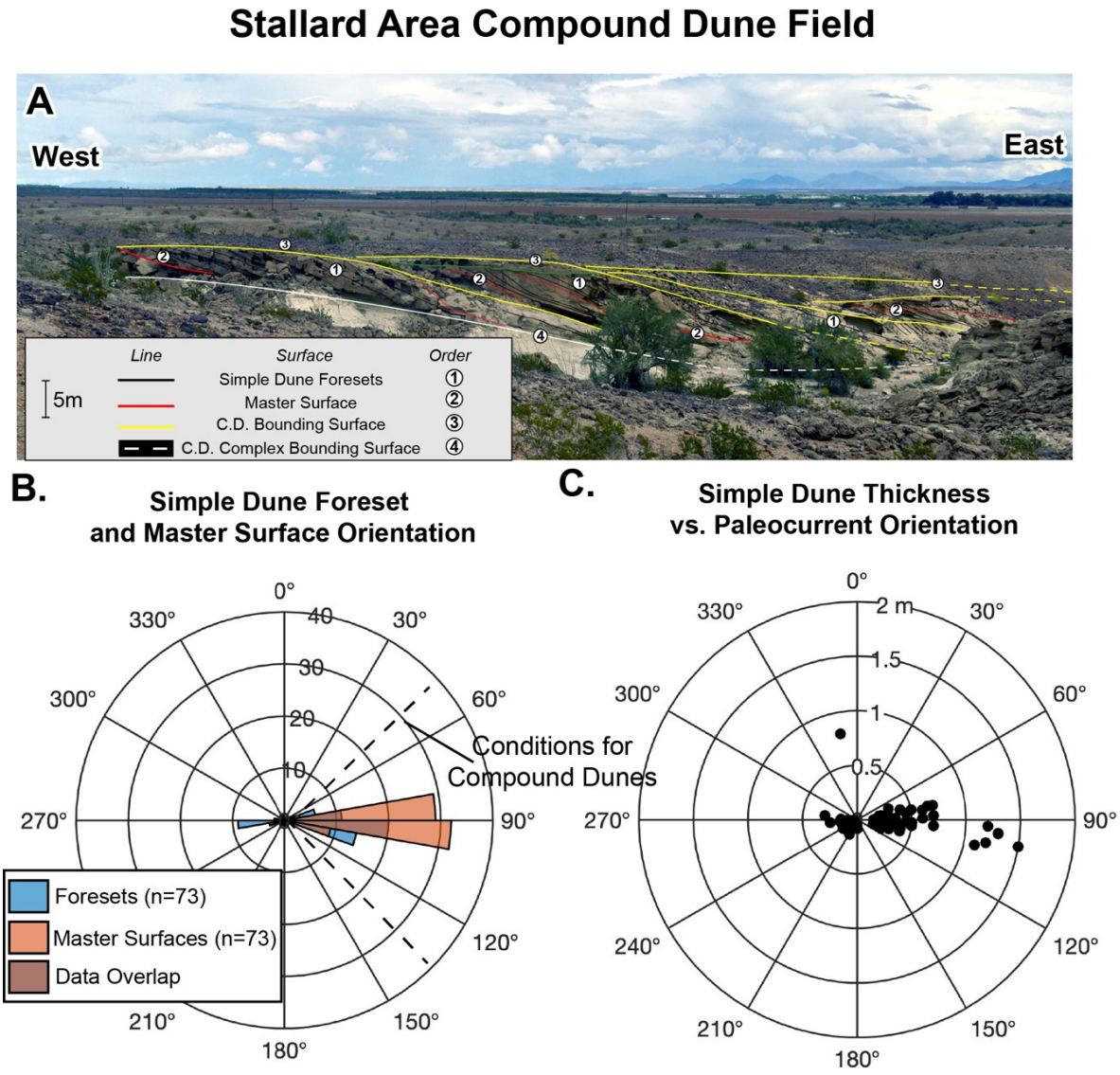

Figure 14: Stallard Area Compound Dune Field. A) Annotated photograph showing the architectural elements of compound dunes in a compound dune complex, B) Rose diagram comparing orientations of simple dune foresets and master surfaces. Area that fits criteria for compound dunes is bounded by dashed lines. C) Polar plot comparing simple dune thickness. Note that east directed simple dunes are the thickest.

`Compound dunes in the Stallard Area range from 3.0 to 5.5 m high and are separated from adjacent compound dunes by third order surfaces dipping 15-25° (Fig. 14a). Individual compound dunes have strongly sigmoidal geometries with east-dipping lee faces that transition laterally to the east into ripple laminated and bioturbated bottomsets over distances of 20-30 m. Planar tabular compound dunes are rare. The architecture of the compound dune complex (Fig. 14a) is consistent with east-directed migration and stacking of compound dunes in a dune field to form a laterally continuous sand sheet.

6.2 Paleocurrents and Bedform Thickness

Paleocurrent data collected for this study permit recognition of cross-bedding created by dunes versus bars. At Petroglyph Park, dip directions of simple dune foresets (1^{st}-order surfaces) are oriented within 45° of master surfaces (2^{nd}-order surfaces) (Fig. 13b), consistent with conditions required for compound dunes (Dalrymple, 1984). Simple dunes show bi-directional, rectilinear paleocurrent directions oriented N-S, and a minor number of E-W directions (Fig. 13b). Most master surfaces of compound dunes at Petroglyph Park dip south, and a smaller number dip east. No north- or west-dipping master surfaces were observed. Figure 12c shows that north-directed simple dunes are <0.25 m thick, whereas south-directed simple dunes are typically larger (most are >0.5 m) and range up to 1.85 m thick. East-directed simple dunes are <0.5m thick, and are consistently larger than north- and west-dipping simple dunes (Fig. 13c).

Data from the Stallard Area similarly show that simple dune foresets and master surfaces are oriented within 45° of each other (Fig. 14b), confirming their classification as compound dunes. Paleocurrents from simple dunes in this area are bi-directional and

rectilinear with E-W orientations and dominantly eastward-directed paleocurrents. Master surfaces in the Stallard Area dip only in the dominant paleocurrent direction (east); west-dipping master surfaces were not observed. A plot of simple dune thickness vs. paleocurrent direction (Fig. 14c) shows a systematic and significant difference between thicknesses of east-dipping versus west-dipping cross-bed sets. This comparison shows that east-directed simple dunes are 0.1-1.5 m thick, whereas west-directed simple dunes are <0.4 m and most are <0.25 m thick (Fig. 14c). One 0.8-m thick simple dune has NNW-directed paleoflow, but other bedforms of similar scale and orientation were not observed.

In summary, paleo-dune fields in the study area show a consistent pattern of paleocurrents and simple dune thicknesses that shed light on the hydrodynamics of the system where they formed. Data from the Stallard area and Petroglyph Park localities reveal highly organized bi-modal paleocurrent directions with dominant and subordinate modes, and evidence that compound dunes migrated only in the dominant current direction (Figs. 13, 14). Simple dunes that dip in the dominant current direction are consistently larger than simple dunes that dip in the subordinate direction, and all subordinate simple dues are <0.5 m thick.

6.3 Water Depth Estimates from Compound Dune Thicknesses

Compound dunes that form in tidal environments develop in quasi-equilibrium with fluctuating water, and therefore provide information about average water depth (Allen & Friend, 1976; Dalrymple et al., 1978; Dalrymple, 1984; C. Olariu et al., 2012). Empirical and theoretical studies have shown that compound dune heights are ≤20% of average water depth, whereas bars are commonly up to 100% of average water depth (C.

Olariu et al., 2012). These bounding values, and presence of abundant cross-bedding formed by migrating dunes in the study area, allow us to estimate minimum average water depth based on measured compound dune thicknesses (Table 3). Minimum water depths were calculated using two methods: (1) compound dune height = 20% of water depth, and (2) inverting the empirical relation $H=0.086*h^{1.19}$ (H=Dune height; h=water depth; Allen, 1984) and solving for water depth.

The average thickness of 18 compound dunes measured in this study is 3.9±0.8 m. Petroglyph Park compound bedforms are on average larger (4.5±0.9 m) than those in the Stallard Area (3.8±0.7m). Estimates of water depth based on all measured compound dunes using the first method above give an average water depth of 20 ± 1 meters, and calculations using the empirical relationship (second method) yield an average water depth of 25 ± 1 m. Average water depth estimated from the empirical relation is consistently 5 m deeper than values calculated using the 20% estimate in both the Stallard Area (20%: 19 ± 1 m; empirical: 24 ± 1 m) and Petroglyph Park (20%: 22 ± 2 m; empirical = 27 ± 2 m). Both estimates indicate that the Stallard Area dune field formed in shallower water than the Petroglyph Park dune field, though this difference could be negligible if compound dune heights in the Stallard Area represent less than 20% of average water depth. In the absence of any evidence to suggest a different relationship between water depth and dune height in the two dune fields, we use the estimated minimum average water depth at both localities using the same equation from Allen (1984), since calculations using this equation closely match empirical observations. Summarizing, we estimate paleowater depths of 24 ± 1 m for the Stallard area and 27 ± 2 m for the Petroglyph Park dune field.

Table 3: Compound Dune Thicknesses and Water Depth Estimates

Compound Dune	Compound Dune height (m)	Min Water depth (h = 20% of Wd)	Water depth (Allen 1984)
SR1	4.4	22	27
SR2	5.2	26	31
SR3	4.5	23	28
SR4	4.1	21	26
SR5	3.2	16	21
SR6	3.8	19	24
SR7	3.4	17	22
SR8	3.4	17	22
SR9	3.2		21
SR10	3.6	18	23
SR11	3.1	16	20
SR12	2.8	14	19
SR13	3.1	16	20
SR14	4.9	25	30
PP1	4.8	24	29
PP2	5.2	26	31
PP3	4.6	23	28
PP4	3.2	16	21
Petroglyph Park Average	4.5 ± 0.9	22 ± 2	27 ± 2
Stallard Area Average	3.8 ± 0.7	19 ± 1	24 ± 1
Total Average	3.9 ± 0.8	20 ± 1	24 ± 1

7. Depositional Model and Buzzards Peak Localities

Lithofacies analyses, paleocurrent data, and water depth estimates presented above shed light on depositional processes and paleoenvironments of the Bouse basal carbonate member in the Palo Verde Mts. Based on comparison to similar deposits documented in other studies (e.g. Longitano et al., 2013), we developed a depositional model and paleogeographic reconstruction for the basal carbonate member (Figs 15 – 17). The model is further constrained by other studies of the southern Bouse Formation (Homan, 2014; O'Connell et al., 2017; Dorsey et al., 2018) and the physiography of the lower Colorado River valley and southern Blythe Basin (Figs. 1, 2).

7.1. Depositional Model

Data and results presented above show that the basal carbonate member accumulated in a transgressive, macro- to mega-tidal, tide-dominated marine seaway (Fig. 15). Tidal seaways are marine connections between adjacent basins that are dominated by strong tidal currents flowing parallel to the long axis of the seaway (Longhitano and Steel, 2017). Tidal straits are similar to tidal seaways but they are narrower than seaways and become tide-dominated only after amplification of tidal currents due to reduction in cross-sectional area of the basin (Pugh, 1987; Longhitano, 2013; Longhitano and Steel, 2017). A diagnostic feature of tidal straits and seaways is the strait-margin zone, where siliciclastic sediment from adjacent highlands is transported toward the basin axis by mass-flow and traction processes (Longhitano, 2013). Tidal straits and seaways are also characterized by large sand sheets and dune fields that form in in deeper subtidal environments (C. Olariu et al., 2012; Longhitano, 2013; Longhitano

and Steel, 2017). Cross-bedded sand sheets and dune fields with bimodal rectilinear flow patterns are diagnostic of tidal conditions (e.g. Dalrymple et al., 1992), though they are not formed exclusively in tidal seaways.

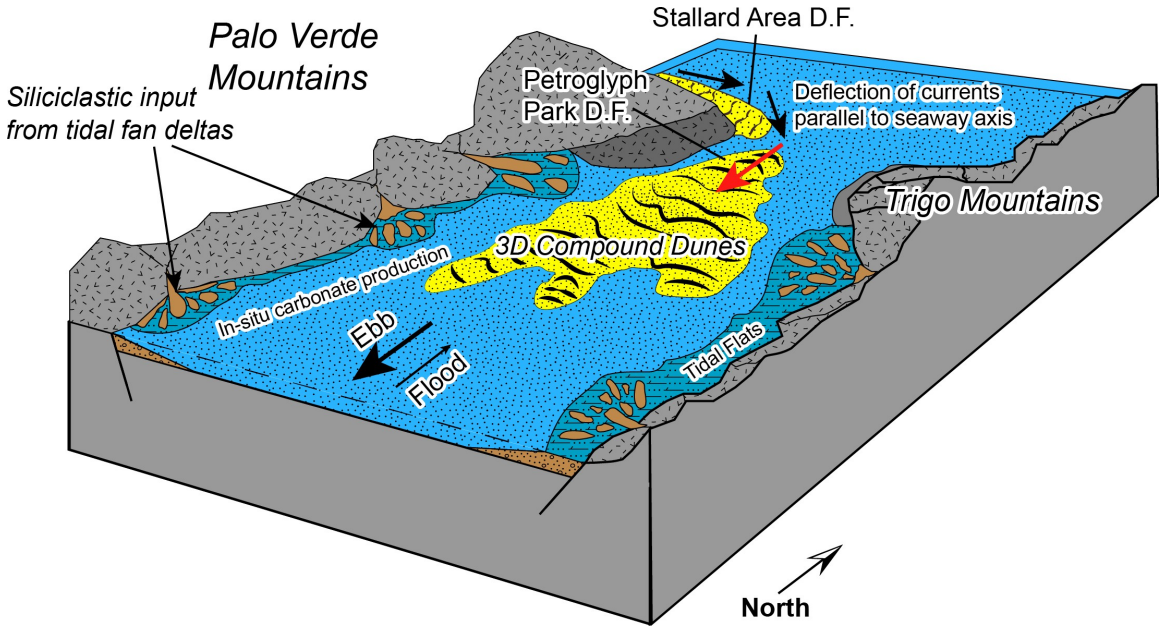

Figure 15: Schematic model for the deposition of the basal carbonate member in an ebb-dominated tidal seaway. Siliciclastic material is derived from local tidally influenced alluvial fan deltas. Paleocurrents between the Stallard Area Dune Field (D.F.) and Petroglyph Park Dune Field are deflected to the south along the seaway axis.

The occurrence and distribution of facies associations FA2 (tide-influenced fan margin) and FA3 (tidal dune field) provide evidence for a tidal seaway setting (Fig. 15). FA2 contains tidal shoreface deposits interbedded with locally-derived sediment that was transferred from local alluvial fans by sheet floods and debris flows. This association closely resembles strait-margin facies described by Longhitano (2013). FA3 records deposition by migrating compound dunes in large subtidal dune fields. Compound dunes in the Stallard area migrated to the east, while those in Petroglyph Park (closer to the basin center) migrated south and parallel to the basin axis (Fig. 15). The change from

east-directed to south-directed currents appears to record deflection of the transport direction by axial tidal currents, a process that commonly affects deltas prograding into tidal seaways (Longhitano and Steel, 2013). This process may also be facilitated by bedrock control on tidal currents. We infer that active channels of alluvial fans delivered siliciclastic material into the basin, while inactive areas of fans were inundated by marine water and reworked by tidal flat processes (Fig. 15).

7.2 Buzzards Peak Bouse Localities

The location of the marine connection between the southern Blythe Basin and the latest Miocene to early Pliocene Gulf of California has been poorly understood until now. Some studies propose a connection through Midway Wash over the Chocolate Mountains Anticlinorium (CMA) at the Highway 78 pass (Fig. 2; Dillon, 1976; Sherrod and Tosdal, 1991), consistent with broad post-Miocene tilting of the Bouse Formation and uplift along the axis of the CMA adjacent to the San Andreas fault (Olmstead et al., 1973; Beard et al., 2016). Other studies conclude that the southern Bouse Formation formed in a large lake isolated from the ocean, and that Bouse deposits accumulated at modern elevations with no uplift in the past ca. 5 Ma (e.g. Spencer and Patchett, 1997; Spencer et al., 2008, 2013). In this view, the Blythe Basin lake was blocked at its southern end by an inferred paleodam across the modern course of the Colorado River southeast of Buzzards Peak (Fig. 2). Recognition of Bouse tidal deposits at two previously undocumented localities near Buzzards Peak (BP3 and BP4; Figs. 2 and 16) provides new constraints on this question.

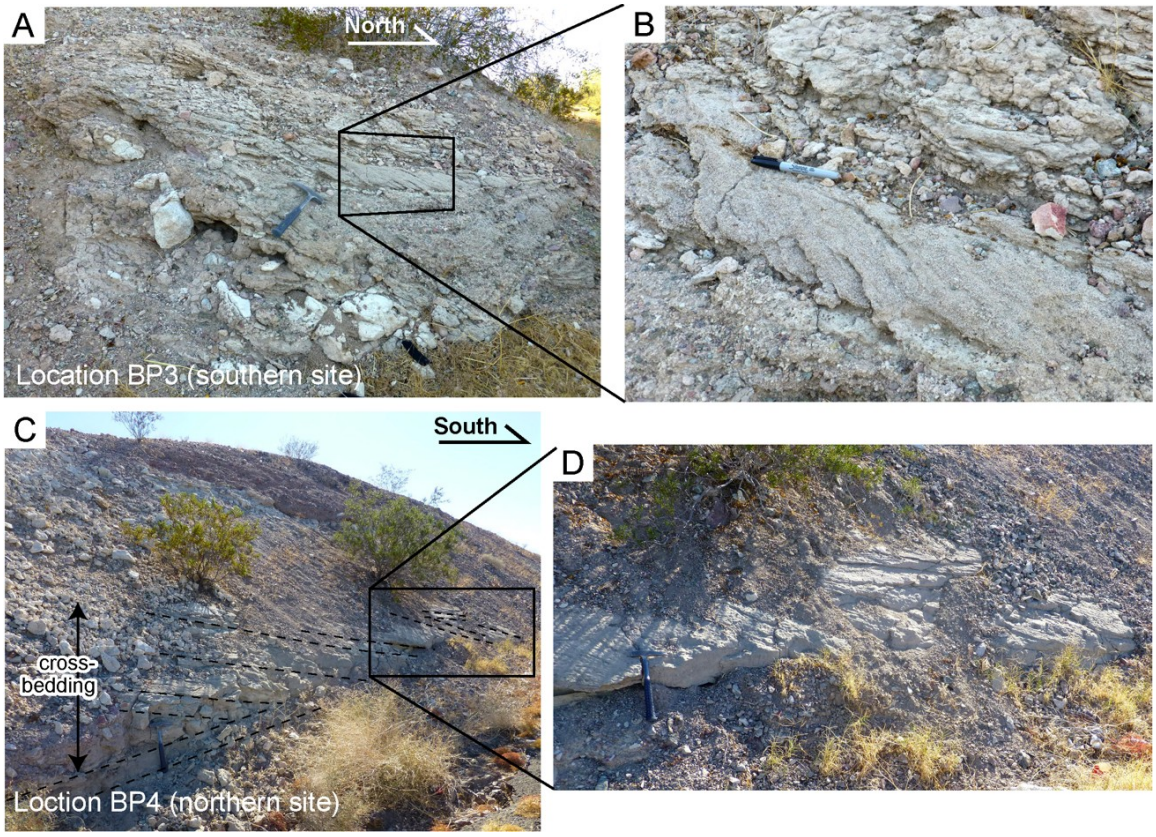

Figure 16: Photos of mixed carbonate-siliciclastic tidal facies in Bouse Formation basal carbonate member near Buzzards Peak (See location in Fig. 17). Interpretations are given in parentheses. A) Vertical succession consisting of: (1) matrix-rich conglomerate with carbonate-rich matrix and clasts of reworked travertine carbonate (alluvial-fan debris flows); (2) poorly sorted, stratified pebble conglomerate (fan-margin sheet floods); (3) well sorted calcerenitic sandstone with 20-cm high tabular cross-bedding, transport to north (shallow-flow, flood-tide dune bedform); and (4) bioturbated sandy calcarenite with relict larger scale cross-bedding (transition to subtidal). B). Close-up of cross-bedded calcarenitic sandstone and bioturbated calcarenite in A**.** C)~ 1 m high cross-bed set in well sorted sandy calcarenite, transport to south (ebb-tidal dune bedform). D) Close up of cross-bedding in C.

Locality BP3 reveals carbonate-rich unstratified conglomerate (Facies S3) and stratified pebble conglomerate (Facies S2) overlain by small-scale tabular cross-bedded calcarenitic sandstone (Facies S4/C4) (Fig. 16A). Cross-beds at this location dip north and record deposition in shallow water by north-flowing currents that we interpret as flood-tidal flow based on comparison to Petroglyph Park. Cross-bedded calcarenitic sandstone is overlain by bioturbated sandy calcarenite with relict cross bedding (Fig. 16B) that records a change to deeper water and colonization by benthic organisms. At locality BP4, south-directed cross-beds in sandy calcarenite are 1 m thick (Fig. 16C,D), similar to Facies C5, and record deposition by subaqueous dunes in deeper water (~5-8 m) by ebb-tide currents. North- and south-dipping cross-bed foresets are consistent with measurements from the Palo Verde Mountains and indicate similar hydraulic conditions. The secular change from alluvial-fan to tidal processes at BP3 and BP4 is also recorded in tidally influenced deposits in the Palo Verde Mts. (this study), Milpitas Wash (Homan, 2014), and southeast of Cibola (O'Connell et al., 2017; Dorsey et al., 2018) (Fig. 2). We conclude this transition records latest Miocene or early Pliocene regional marine transgression when the deposits were at sea level, prior to broad crustal warping that uplifted Bouse carbonates in the Chocolate Mountains to present elevations of ~330 m above sea level (e.g., Beard et al., 2016).

8. Discussion

There presently is no consensus regarding the depositional environment for the basal carbonate member of the southern Bouse Formation. Some stratigraphic and sedimentological studies interpret bioclastic carbonate as a record of deposition by tidal

processes in a marine embayment or estuary (Buising, 1990; Turak, 2000; O'Connell, 2016; O'Connell et al., 2017; Dorsey et al., 2018; this study). Other studies conclude that southern Bouse carbonate formed in a lake isolated from the ocean (e.g., Spencer and Patchett, 1997; Spencer et al., 2013; Pearthree and House, 2014; Bright et al., 2018a, 2018b), in which case the cross-bedded gravels and coarse-grained bioclastic carbonate would represent deposits of high-energy beach ridges or Gilbert deltas. Below we discuss sedimentary processes and structures of high-energy lakes and their similarities to lithofacies of the southern Bouse basal carbonate member, and evaluate important similarities and differences between them.

8.1 Lacustrine depositional processes

Horizontal laminations, wavy-flaser-lenticular bedding and desiccation cracks (Facies C1, C2a-c) are formed by regular changes in current velocity and water depth, which are known to affect lakes. Playa lakes in arid environments can accumulate deposits in sandy mud flats as a result of regular fluctuations in water depth through evaporation and filling (e.g. Ainsworth et al., 2012; Zanor et al., 2012). Perennial lakes such as Lake Michigan and Lake Eyre produce sedimentary structures that are commonly associated with weak tidal processes produced by wind-generated and fluvial currents (Fraser and Hester, 1977; Bye and Will, 1989; Ainsworth et al., 2012). Daily fluctuations in wind velocity and direction in Lake Eyre commonly produce "wind tides" that cause water levels to fluctuate by ca. 5 cm over the course of a day (Bye and Will, 1989). A 5-cm drop in lake level could repeatedly expose and re-submerge mud flats to produce desiccation cracks. Wind-driven currents created by bi-directional winds can form <0.5m thick herringbone crossbedding in lake deposits (Facies C4) (Ainsworth et al., 2012).

Similarly, wavy-flaser-lenticular bedding may be created when fluvial currents entering a lake are intermittently slowed by opposing wind-generated currents.

Beach-ridge gravel complexes formed at lake margins contain cross-bedding structures similar to those observed in tidal environments, but they are produced almost entirely by wave processes (e.g., Fraser and Hester, 1977; Lichter, 1995; Otvos, 2000; Schuster and Nutz, 2017). Davis et al. (1972) compared ridge and runnel systems in nearshore tidal and lacustrine environments, and found that the morphology of migrating ridges is nearly identical in the two types of environment. Where stream channels enter a lake, fining-upward sequences of tabular to trough cross-beds dip in a lakeward direction and are produced by lateral-accretion point bars in meandering streams (Fraser and Hester, 1977). Beach-ridge complex dunes are often composed of smaller superimposed bedforms, similar to compound bedforms observed in Facies Association 3 (this study). Lakeward migration of eolian beach-ridge dunes is facilitated by high vegetation and a net positive sediment supply to the beach, and/or lowering of lake water level, resulting in shoreline regression (Pye, 1990; Lichter, 1995)

High-angle cross-bedding in upper shoreface sands and gravels of Lake Michigan records deposition by reversing longshore currents during storm events that produce bi-polar current directions perpendicular to the shoreline (Fraser and Hester, 1977). Bi-directional paleocurrents have also been recorded in beach ridge gravels associated with the Lake Lahontan Pleistocene highstand (e.g. Blair, 1999). These deposits contain lakeward-dipping, low-angle gravel beds interbedded with landward dipping tabular cross-bedded gravels that represent beach to upper shoreface deposits and washover deposits in back-barrier ponds behind beach ridges. Washover fans with tabular cross

bedding are “micro-deltas” that record landward transport of sediment by storm waves breaching a beach ridge (Shaw et al., 2015; Schuster and Nutz, 2017). Beach ridges are the most common deposits of high energy lakes, and near-shore spits and bars are also commonly observed (Schuster and Nutz, 2017). They are produced by longshore currents that produce lateral accretion bars and often contain ridges and coastal dunes formed by shore-normal wind transport (Lichter, 1995; Schuster and Nutz, 2017).

8.2 Tidal versus Lacustrine Origin

Although high-energy lakes can produce sedimentary structures similar to those of tidal systems, the deposits of the southern Bouse Formation formed under unique conditions that could not have been generated in a lake. Bimodal currents in lake-margin settings are produced by lateral accretion of point bars at the mouths of streams, reversing wind-driven currents, lateral accretion from reversing long-shore currents, and storm waves breaching beach ridges (e.g., Fraser and Hester, 1977; Blair et al., 1999; Ainsworth et al., 2012; Schuster and Nutz, 2017). Bimodal, rectilinear paleocurrent indicators in the Bouse basal carbonate member are most commonly observed in deeper-water large-scale compound dunes, not shoreline deposits. Bouse compound dunes migrated by forward accretion and display overall coarsening-upward intervals, indicating that they did not form by lateral accretion which most likely would produce fining-upward sequences typical of channel deposition. Thus we conclude that reversing longshore lake currents and meandering channels cannot explain the unique structures and sequences observed in the Bouse basal carbonate member in the Palo Verde Mts.

Lakeward-dipping beds and landward-dipping cross-beds on gravelly beach ridges in lakes do record a type of reversing-transport process (e.g., Schuster and Nutz,

2017). Low-angle, lakeward dipping beds in well-rounded gravels often are deposited by wave processes such as swash. High-angle, landward dipping tabular cross-beds are generated when storm swells and waves transport gravel over beach ridges into back-barrier lagoons (Shaw et al., 2015). Compound dunes in the Bouse basal carbonate member (this study) are composed of angular to subrounded carbonate grains and lack thick tabular crossbedding. Opposing paleocurrent indicators in the Bouse deposits are found within compound dunes indicating their formation in the same location and time. In contrast, landward-dipping cross-beds in lake-margin gravels are formed separately in space and time from lakeward-dipping low angle cross-beds.

Compound dunes in the basal carbonate member average around 4 m thick, whereas tabular cross-bedding produced by reversing winds in lakes are typically about 0.5 meters high (Ainsworth et al., 2012). The largest simple dunes in the basal carbonate member are 1.8 m thick, almost 4 times larger than lacustrine cross-bedding documented by Ainsworth et al. (2012). The large scale of bedforms documented in this study indicate a minimum water depth of 25 meters (e.g. Allen, 1980). At this depth wind-driven current velocities in the Great Lakes are <2.5 cm/s (Beletsky et al., 1999), much weaker than the velocity required to transport grain sizes of Facies C4 and C5 (Allen, 1982; Flemming, 2000). In lacustrine settings, large bedforms are often eolian dunes formed on beach ridges and contain some reversing paleocurrent indicators from changes in wind direction. However, an eolian origin can be ruled out for compound dunes of the southern Bouse deposits because foresets alternate between granule and coarse sand and often contain pebbles in the bottom sets. Grainstones have been documented in lakes

(Gierlowski-Kordesch, 2010), but bioclasts in lake deposits are composed of continental fauna, not the dominantly marine fauna observed in the Bouse basal carbonate member.

The northern Bouse Formation, which all workers agree formed in a lake (e.g. House et al., 2008; Pearthree and House, 2014; Crossey et al., 2015), notably lacks coarse bioclastic facies and marine fossils. In contrast, the southern Bouse Formation contains both high-energy tidal bedforms (Buising, 1990; Turak, 2000; O'Connell et al., 2017; this study) and marine fauna (Winterer, 1975; Taylor, 1983; McDougall, 2008; McDougall and Miranda-Martínez, 2014). The presence of tidal structures in association with marine fossils is a fundamental criterion that is widely used to confirm a tidal origin in ancient deposits (Ainsworth et al., 2012), and we therefore reject a lacustrine origin for coarse bioclastic facies of the southern Bouse basal carbonate.

8.3 Paleogeographic Reconstruction

Figure 17 shows interpreted paleogeography for the southern Bouse tidal seaway based on shoreline modeling from water depth estimates, and observations of diagnostic sedimentary lithofacies, structures, and sequences (Homan, 2014; O'Connell, 2016; O'Connell et al., 2017; Dorsey et al., 2018; this study). This reconstruction includes a marine connection through Midway Wash over the Chocolate Mountains at the Highway 78 pass, as inferred by previous workers (Dillon, 1976; Sherrod and Tosdal, 1991). The reconstructed seaway has an overall north-south orientation with a distinct east-west jog south of the Palo Verde Mts, and displays a geometry conducive to a large tidal range and/or tidal amplification (Fig. 17). We infer that basin subsidence and uplift in flanking ranges was controlled by a diffuse system of transtensional strike-slip and normal faults in the southern part of the Eastern California Shear Zone (e.g., Sherrod and Tosdal, 1991;

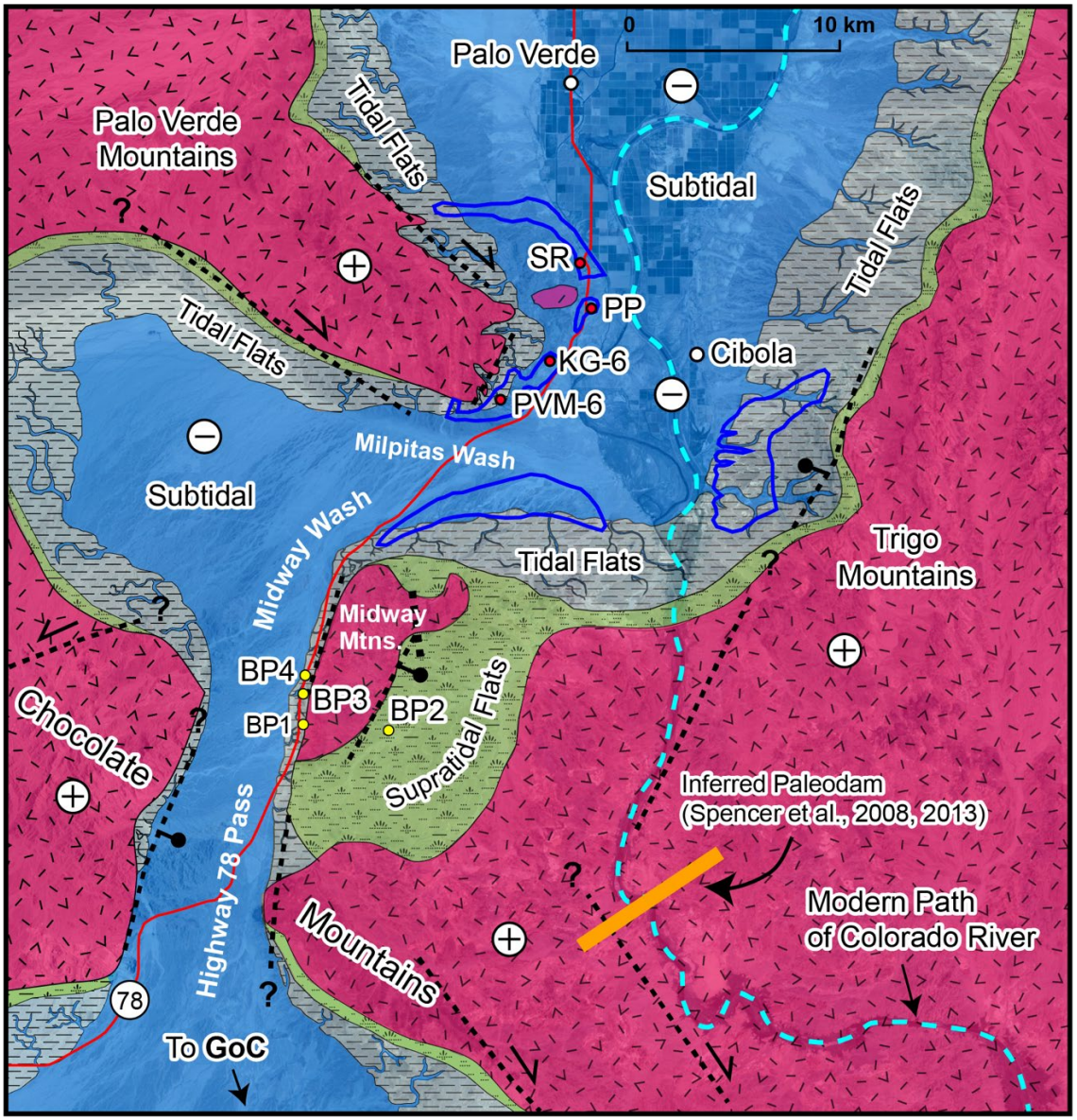

Figure 17: Paleogeographic reconstruction of the southern Bouse tidal seaway based on data and shoreline estimates presented above (see text for details). Correlation of tidal facies at localities BP3 & BP4 to those in the SE Palo Verde Mountains, Milpitas Wash and Cibola area provides evidence for a marine connection to the paleo-Gulf of California (**GoC**) over the Highway 78 Pass. Dashed heavy lines are inferred syn-depositional faults, some of which likely were subsurface structures (Sherrod and Tosdal 1991; Richard, 1993; Ricketts et al., 2011; Beard et al., 2016; Dorsey et al., 2017). Plusand mins signs indicate direction (uplift or subsidence) of inferred vertical crustal motions related to syn-basinal fault deformation. Blue outlines indicate present day exposures of the Bouse Formation

Richard, 1993; Ricketts et al., 2011; Beard et al., 2016; Dorsey et al., 2017). The paleo-seaway is fairly narrow (<8 km) from localities BP3 and BP4 south to the Highway 78 Pass, and it widens northward from the Stallard Area, producing a funnel-shaped geometry that may have enhanced tidal range and ebb-dominance. The overall geometry is similar to that of the Messina Strait, Italy, and its size is similar to Cook Strait between North and South Island, New Zealand.

Tidal seaways and straits are defined as narrow marine connections between two wider bodies of water where tidal processes are dominant (Longhitano and Steel, 2017). The overall geometry of seaways is largely dictated by bedrock topography, but the morphology of coastlines can vary depending on local depositional conditions (i.e. local river input) and local gradient which may be structurally controlled. Our reconstruction shows that coastlines east of the Cibola area had much wider intertidal flats with greater development of tidal channels (O'Connell et al., 2017) than in the southeastern Palo Verde Mountains (Fig. 17). Low energy facies and tidal-channel bar deposits are relatively uncommon in the Palo Verde Mountains, suggesting narrower tidal flats and a steeper basin margin compared to the eastern margin of the seaway. While large alluvial fans provided a broad, low-gradient surface that promoted development of extensive tidal flats on the east side of the tidal seaway, Bouse basal carbonate facies in the Palo Verde Mountains formed directly adjacent to the steep range front and onlap directly onto steep erosional paleotopography. The combination of steep paleotopography and relative paucity of low-gradient alluvial fan surfaces prevented formation of wide tidal flats in the Palo Verde Mountains.

8.4 Ebb/Flood Dominance and Asymmetry

The magnitude of daily tides is often unequal, and either the flood or ebb current may be stronger (Dronkers, 1986; Kvale et al., 1995; Brown and Davies, 2010). Rarely is the strength of both flood and ebb currents equal. Dominance of a single current (ebb or flood) is dictated by the direction of net sediment transport within a system (Brown and Davies, 2010). These systems can either be ebb- or flood-asymmetrical, where the direction of asymmetry is the current with the highest peak velocity and shortest duration. Asymmetry does not imply dominance of a system, and can change through time as the morphology changes (Brown and Davies, 2010). Although studies of ebb/flood dominance and asymmetry have primarily focused on estuaries, the concepts are applicable to other tidal systems since they do not require fluvial input to be applicable.

Voluminous compound dunes in the southern Bouse basal carbonate member migrated in the ebb direction, toward the strait axis (in the Stallard Area) and southward (at Petroglyph Park) toward the late Miocene Gulf of California. These results show that the basal carbonate member accumulated in an ebb-dominant system, consistent with the conclusion of O'Connell et al. (2017). Comparison of bedform thickness between ebb-directed (E, S) and flood-directed (W, N) simple dunes (Figs. 13c, 14c) show that ebb-directed simple dunes are systematically larger than flood-directed dunes, further supporting our conclusion that the basal carbonate member accumulated in an ebb-dominated seaway. However, it is much more difficult to determine tidal asymmetry in the rock record. Although water depth can be estimated from the thicknesses of compound dunes and sedimentary structures (Allen, 1980; this study), estimates of tidal amplitude and surface areas during low and high tides can only be loosely constrained.

Studies of estuaries have shown that in the initial stages of formation estuaries have a greater width-averaged depth at high tide than low tide giving rise to a short, fast flood phase and a long, slow ebb phase (flood-asymmetry) (Dronkers, 1986; Pethick, 1994; Townend, 2003; Brown and Davies, 2010). A flood-asymmetric system facilitates accumulation of fine sediments and the build-up of broad intertidal flats along the margins. Buildup of shallow intertidal flats creates deep, narrow subtidal channels, and a threshold is crossed where the width-averaged water depth during high tide is reduced, the ebb duration decreases, and peak ebb velocity increases, changing the system to ebb-asymmetric (Kang and Jun, 2003; Townend, 2003; Fortunato and Oliveira, 2005; Moore et al., 2009; Brown and Davies, 2010). Faster currents during the ebb phase promote erosion of intertidal flats and net export of the sediment from the system. An estuary may remain in dynamic equilibrium over time through feedback driven by the buildup and erosion of intertidal flats and subtidal channels.

Our paleogeographic reconstruction (Fig. 17) provides some insight into the asymmetry of the southern Bouse Formation. The eastern margin of the seaway was dominated by broad intertidal flats, whereas the western margin had significantly narrower intertidal flats adjacent to a steep basin margin. While this difference may reflect structurally controlled asymmetry of topography across the seaway, it could also be related to a change from flood-asymmetry to ebb-asymmetry. Pethick (1994) suggested that an estuary may change asymmetry about every 100 years to maintain dynamic equilibrium, and this basin may have also fluctuated between flood and ebb asymmetries. Basin subsidence and relative sea-level rise (Dorsey et al., 2018) allowed for aggradation of tidal flats along the margins and formation of deep subtidal

environments along the axis of the tidal seaway. Large bedforms require deep water (Allen, 1980) and, to lesser extent, fast current velocities to transport large volumes of sediment. Ebb-directed simple dunes documented in this study are larger than flood-directed simple dunes (Figs. 13c, 14c), which requires deeper water and/or faster velocities for the ebb-directed bedforms. Because the simple dunes are found within compound dunes that formed at ca. 25 m depth, it is unlikely that water depth was the limiting factor in simple dune thickness. Thus, the difference in scale of ebb- and flood-directed bedforms probably was controlled by a difference in peak velocity. We speculate that the ebb phase was short but with higher peak velocities that drove larger bedforms and a larger-volume sediment transport compared to a longer but slower flood phase. Although the tidal asymmetry cannot be quantified for the southern Bouse Formation, the available data and observations suggest deposition in an ebb-dominated, ebb-asymmetric tidal system.

9. Conclusions

This study examined sedimentary lithofacies, paleocurrent directions, and architecture of large-scale bedforms in the basal carbonate member of the southern Bouse Formation in the Palo Verde Mountains, southeastern California. Our results lead to the following conclusions:

(1) Bi-modal, rectilinear paleocurrent data reveal dominant transport to the east and south with a subordinate current in the opposing directions.

(2) Cross-bedding records migration by forward accretion, not lateral accretion, indicating that the bi-modality of paleocurrents reflects changes in current direction rather than lateral migration of bars or meandering channels.

(3) Large-scale compound dunes formed at ca. 25 m depth, well below the depth at which wind-driven currents in lakes become incapable of transporting coarse bioclastic sediment.

(4) Intertidal flat and alluvial fan deposits are interbedded at the basin margin, a feature diagnostic of tidal strait and seaway margins.

(5) Large-scale compound dunes are only found near the basin axis, which we interpret to be a subtidal zone where strong axial currents formed large dune fields.

The data and results of this study reveal a suite of depositional processes that are inconsistent with deposition in a lacustrine environment, but are consistent with abundant marine fauna in the southern Bouse Formation. We therefore conclude that the basal carbonate member accumulated in an ebb-dominated tidal seaway during regional marine transgression.

Our paleogeographic reconstruction includes a marine connection over the Chocolate Mountains through the Highway 78 pass, providing new evidence for broad post-Miocene uplift in the lower Colorado River region. If the Chocolate Mountains had been at or near their present elevation during deposition of the southern Bouse Formation, a marine connection would not have been possible and strong tides could not have existed in this basin. Thus, much of the uplift to present-day elevations must have occurred since late Miocene or early Pliocene time. These results highlight the value of integrative

sedimentology and stratigraphic analysis in reconstructing depositional paleoenvironments, and provide important constraints on the timing and magnitude of long-wavelength vertical crustal motions adjacent to an active transform plate boundary.

APPENDIX A

MEASURED SECTION LOCATIONS (DATUM: WGS84)

Section	Latitude	Longitude	Elevation (m asl)
KG1	33.32039	-114.73746	83
KG2	33.31437	-114.74540	93
KG3	33.31295	-114.74428	83
KG4	33.31183	-114.74389	82.95
KG5	33.31183	-114.74289	81.75
KG6	33.31179	-114.74217	78.5
KG7	33.29614	-114.76691	119.4
KG8	33.29594	-114.26629	119
KG9	33.29575	-114.76555	115.6
KG10	33.29534	-114.76462	119
KG11	33.29489	-114.76685	123
KG12	33.29262	-114.76450	118
KG13	33.29098	-114.75822	107.25
KG14	33.29202	-114.76241	110
KG15	33.30200	-114.76243	121
KG16	33.30159	-114.76090	115
KG17	33.30159	-114.76051	112
KG18	33.30138	-114.75999	110.5
KG19	33.30075	-114.75938	107.6
KG20	33.29731	-114.75668	104.4
KG21	33.29673	-114.75426	97
KG22	33.29639	-114.75136	91
KG23	33.30758	-114.75134	94.5
KG24	33.30721	-114.74867	93
KG25	33.30688	-114.74545	89
KG26	33.30709	-114.74813	94
PVM-1	33.29730	-114.76793	131

PVM-2	33.29698	-114.76732	131
PVM-3	33.29609	-114.76482	130
PVM-4	33.30378	-114.75709	112
PVM-5	33.29330	-114.76836	123
PVM-6	33.29614	-114.76704	125
PVM-7	33.29603	-114.76652	124
PVM-8	33.29617	-114.76613	123
PVM-9	33.29606	-114.76577	122
PVM-10	33.29542	-114.76517	122
PVM-11	33.29160	-114.76213	111
PVM-12	33.29546	-114.75305	95
PVM-13	33.31554	-114.74169	86
PP-1	33.33668	-114.72139	74
PP-2	33.33668	-114.72122	76
SR-1	33.35899	-114.72660	77
SR-2	33.36895	-114.72639	75
SR-3	33.35910	-114.72628	75
SR-4	33.35553	-114.72463	74
SR-5	33.35162	-114.72609	68

APPENDIX B

TABULATED MEASURED SECTIONS

Section KG-1

Height in section (m)	Description
0-3.4	Poorly sorted sandy pebble conglomerate with angular casts and trough crossbedding. Trough axes oriented 70°. Troughs 0.3-0.5m thick.Unit: Miocene Conglomerate
3.4-3.8	Moderately sorted sandy pebble conglomerate with surrounded clasts a trough crossbedding. Unit: Reworked Conglomerate (Bouse)
3.8-4.4	Well sorted, fine grained sandy grainstone. Thins to the east due to erosion.Unit: basal carbonate member
4.4-5.6	Horizontally bedded pebble conglomerate with sandy matrix. Sparse barnacle rich medium grained grainstone interbeds. Erosional boundary with underlying unit. Thins eastward into condensed unit. Unit:Basal Carbonate Member
5.6-6.7	Interbedded horizontally stratified fine-grained sandy grainstone and sandy pebble conglomerate. Grainstone beds: 0.2-0.25 m thick; Conglomerate beds: 0.2-0.25m thick; Unit: basal carbonate member
6.7-7.4	Calcisiltite with horizontal laminations and minor soft sed deformation. Unit: basal carbonate member
7.4-7.6	Travertine interbed with small bioherms (<1m across). Passes eastward into fine to medium-grained grainstone; Unit: basal carbonate member
7.6-8	Calcisiltite with horizontal laminations and minor soft sed deformation. Unit: Bioclastic Unit of Basal Carbonate Member
8.0-8.2	Travertine interbed with small bioherms (<1m across). Passes eastward into fine to medium-grained grainstone; Unit: basal carbonate member
8.2-10.0	Interbedded calcisiltite and siliciclastic-rich calcisiltite with horizontal laminations. Unit: Bioclastic Unit of the basal carbonate member.
10.0-12.2	Interbedded coarse- to very coarse-grained grainstone and fine-grained grainstone. Unit: basal carbonate member.
12.2-13.1	Pebbly fine-grained grainstone with siliciclastic pebbles; Structureless. Basal 0.2m contains travertine rip up clasts. Unit: basal carbonate member.

13.1-15.6	Horizontally bedded, very coarse-grained gravestone with abundant barnacle and shell fragments. Individual beds range from 0.03-0.1m thick. Unit: Bioclastic unit of basal carbonate member.
15.6-19.9	Poorly sorted, angular pebble-cobble conglomerate. Quaternary Gravel

Section KG-2

Height in section (m)	Description
0-7.4	Poorly sorted, moderately cemented pebble to cobble conglomerate with siliciclastic matrix; No discernible structures; Unit: Miocene Conglomerate.
7.4-7.5	Moderately sorted cobble conglomerate with sub=rounded clasts; cobble lag; Unit: basal carbonate member
7.5-7.6	Moderately sorted pebbly granule conglomerate with <30% carbonate in matrix. Unit: basal carbonate member.
7.6-8.7	Horizontally bedded, well sorted, very fine- to fine-grained grainstone with 3-5cm interbreeds of calcisiltite; Wavy bedding and rippled tops present in grainstone beds; Unit: basal carbonate member.
8.7-9.2	Poorly sorted, angular, pebble to cobble conglomerate; Quaternary Gravel

Section KG-3

Height in section (m)	Description
0.0-5.1	Poorly sorted, sandy pebble to cobble conglomerate with angular to sub-angular clasts; trough cross-bedded; cross-beds 0.3m thick with axes oriented 172°; Unit: Miocene Conglomerate
5.1-6.0	Poorly sorted, granule to pebble conglomerate with weak horizontal stratification; sandy matrix supported; Unit: Miocene Conglomerate
6.0-6.1	Well sorted, very fine-grained sandy grainstone with poorly exposed tabular cross-bedding
6.1-6.8	Moderately sorted, pebbly, granule conglomerate with 30cm thick bi-directional tabular cross-bed sets; well rounded clasts; Unit: Reworked conglomerate.

6.8-7.1	Massive lime mud; Unit: basal carbonate member
7.1-8.3	Interbedded very fine to fine-grained grainstone with wavy to planar bedding. Individual beds range from 3-5cm thick. Unit: basal carbonate member

Section KG-4

Height in section (m)	Description
0.0-5.7	Poorly sorted, pebble to cobble conglomerates with infrequent small boulders; angular-subangular clasts; trough cross-bedding throughout, but is absent in upper 40cm; Unit: Miocene Conglomerate
5.7-7.0	Poorly sorted, pebble to cobble conglomerate with <20% carbonate in the matrix; Horizontal to low-angle stratification; Unit: Reworked conglomerate
7.0-9.6	Interbedded calcisiltite and very fine-grained calcarenite; horizontal to wavy-falser bedding; <10% siliciclastics; individual beds range from 1-5cm; Unit: Basal carbonate member
9.6-11.0	Horizontally bedded, fine grained calcarenite with <10% siliciclastics. Unit: Basal carbonate member.
11.0-11.1	Pebble conglomerate; Quaternary Gravel

Section KG-5

Height in section (m)	Description
0.0-1.7	Moderately to poorly sorted, sub rounded, pebble to cobble conglomerate; inverse grading with large boulders in upper 40cm; Unit: Miocene conglomerate
1.7-2.5	Moderately sorted; normally graded with small boulders at base; pebble to cobble conglomerate with weak bi-directional cross-bedding; Minor carbonate in matrix; Unit: Reworked conglomerate
2.5-2.9	Massive lime mud bed; Unit: Basal carbonate member
2.9-4.4	Interbedded calcisiltite and very fine-grained grainstone; horizontal to wavy bedding; wave ripple surfaces on grainstone beds; individual beds range from 1-5cm; Unit: Basal carbonate member

4.4-6.4	Horizontally bedded, granular grainstone; abundant barnacles, mollusks and rhodolite fragments; grades laterally eastward into poorly cemented lime mud; Unit: Basal carbonate member
6.4-7.6	Fine to medium-grained fossiliferous sandy grainstone; weak bidirectional crossbedding and rippled surfaces; ~40% siliciclastics; grades lateral eastward into poorly cemented lime mud; Unit: basal carbonate member
7.6-8.3	Poorly sorted pebble conglomerate; Quaternary Gravel

Section KG-6

Height in section (m)	Description
0.0-0.1	Very fine-grained silty grainstone; abundant reed casts; Sample GB-4
0.1-0.4	Fine-grained sandy grainstone with basal cobble lag; 50% siliciclastics; Unit: Basal carbonate member.
0.4-0.7	Poorly sorted, sandy cobble conglomerate; surrounded clasts; clast supported; Unit: Basal carbonate member
0.7-1.2	Well sorted, sub-rounded, very coarse-grained sandy grainstone; horizontal to low-angle stratification; Unit: Basal carbonate member.
1.2-1.7	Well to moderately sorted, medium- to coarse-grained sandy grainstone; abundant wave ripple laminations; ostracodes and shell fragments common; thalassinoides burrows present at base of unit; marine gastropod casts and molds abundant; Unit: Basal carbonate member.
1.7-2.2	Poorly sorted, sub-rounded, cobble conglomerate; inversely graded from very coarse sand at base to cobbles; unit pinches out 15m to the east; Unit: Basal carbonate member
2.2-3.3	Poorly sorted, pebble to cobble conglomerate; rounded to subangular clasts; inversely graded from pebbles at base to boulders at upper boundary; Unit pinches out 15m to the east: <10% carbonate in matrix; Unit: Basal carbonate member.
3.3-3.8	Massive lime mud with weakly defined bedding; drapes over underlying large boulders; Unit: Basal carbonate member
3.8-5.3	Interbedded calcisiltite and very fine-grained grainstone; >80% carbonate; wavy to planar bedding; Individual beds range from 2-8cm; lower 0.5m of unit appears to drape over mounds created in underlying unit; Unit: Basal carbonate member

5.3-5.5	Moderately sorted, granular grainstone; clasts entirely made of barnacle and mollusk fragments; Unit: Basal carbonate member
5.5-6.0	Horizontally laminated carbonate paper shale; highly fissile; Unit: Upper marl of basal carbonate member.
6.0-6.1	Quaternary Gravel

Section KG-7

Height in section (m)	Description
0.0-2.2	Poorly sorted, pebble to cobble conglomerate with horizontal stratification; angular to subangular clasts; alternates between clast and matrix supported beds (2-10 cm thick); clast supported intervals have clast imbrication with imbrication dipping towards 301°; Unit: Miocene Conglomerate
2.2-2.3	Very fine- to fine-grained sandy grainstone; <20% siliciclastics; structureless; Unit: Basal carbonate member
2.3-3.6	Poorly sorted, pebble to cobble conglomerate; horizontal bedding; ungraded; subangular clasts; clast imbrication dips toward 304°; Unit: Basal carbonate member
3.6-3.9	Structureless, very-fine- to fine-grained grainstone; abundant rhodoliths and Battalaria fossils; >85% carbonate; Unit: Basal carbonate member.
3.9-4.6	Interbedded calcisiltite and very fine- to fine-grained grainstone with horizontal stratification; calcisiltite beds are 1-3 cm thick; grainstone beds are 5 cm thick; Unit: Basal carbonate member
4.6-6.6	Interbedded lime mud and fine-grained grainstone; wavy bedding to horizontal stratification; lime mud beds are <1 cm thick; grainstone beds are 3-5 cm thick; Unit: Basal carbonate member
6.6-7.3	Poorly sorted, pebble to cobble conglomerate with calcareous matrix; weak cross-bedding; angular to subangular clasts; Unit: Basal carbonate member
7.3-8.8	Poorly sorted, unstratified, pebble to cobble conglomerate; Quaternary Gravel

Section KG-8

Height in section (m)	Description
0.0-0.4	Poorly sorted, pebble conglomerate; angular clasts; structureless; ungraded;
0.4-0.5	Well sorted, very fine-grained grainstone with minor siliciclastic component (<15%); Unit: Basal carbonate member
0.5-0.6	Well sorted, granule-sized grainstone; abundant mollusks and barnacles; Unit: Basal carbonate member
0.6-1.6	Poorly sorted, granule to pebble conglomerate; inversely graded with large cobbles in upper 20 cm; clasts are rounded; Unit; Basal carbonate member.
1.6-1.9	Well sorted, fine-grained sandy grainstone with no internal bedding; gastropod fossils and thalassinoides burrows common; Unit: Basal carbonate member
1.9-2.7	Interbedded calcisiltite and very fine- to fine-grained grainstone; wavy to planar stratification; individual beds range from 1-5 cm thick; Unit: Basal carbonate member
2.7-4.7	Inter bedded lime mude, calcisilitite, and very fine- to fine-grained sandy grainstone; wavy, flaser, and planar bedding throughout; individual beds range from 2-4 cm; Unit: Basal carbonate member
4.7-9.8m	Poorly sorted, weakly cemented, sandy, pebble conglomerate: Quaternary gravel.

Section KG-9

Height in section (m)	Description
0.0-1.0	Horizontally bedded calcisiltite with minor interbeds of very fine-grained grainstone; wavy bedding uncommon; Unit: Basal carbonate member
1.0-1.2	Calcisiltite with single coarse-grained fossiliferous grainstone bed; grainstone interbed is 6 cm thick; Unit: Basal carbonate member
1.2-1.6	Interbedded planar laminated calcisiltite and wavy bedded very fine grained grainstone; Unit: Basal carbonate member

1.6-2.0	Structureless calcisiltite that coarsens upward into a coarse-grained grainstone; wavy and planar laminations common in grainstone; mollusks and barnacles common; Unit: Basal carbonate member
2.0-2.3	Coarse grained, fossiliferous pebbly grainstone with no distinct internal structures; pebbles concentrated in upper 10 cm; Unit: Basal carbonate member
2.3-3.0	Tabular cross-bedded fossiliferous coarse-grained grainstone; forests average between 10-20 cm thick and dip 22-30° towards 125*; background dip is 7° to 130°; siliciclastic pebbles concentrated in lower 10 cm; Unit: Basal carbonate member
3.0-7.6	Horizontally to wavy bedded, very coarse-grained to granular fossiliferous grainstone with 20-30 cm thick interbeds of poorly sorted , angular pebble to cobble conglomerate; conglomerate matrix ranges from 20-60% carbonate; Upper 30 cm of unit contain bi-directional tabular cross beds (20-30 cm thick) oriented towards 130° and 310°; Unit: Basal carbonate member
7.6-13.4	Quaternary gravel and covered section; gravel appears to have eroded away Upper bioclastic member. Base of gravel (20 cm) is well cemented and may possibly be remnant of UBM.

Section KG-10

Height in section (m)	**Description**
0.0-0.3	Fine-grained grainstone with planar to wavy bedding; top of bioclastic unit
0.3-0.7	Green claystone; highly fissile; planar laminations; pale green color
0.7-1.1	Structureless, well sorted, fine-grained grainstone; few shell fragments;
1.1-1.6	Green claystone; highl fissile with planar bedding; dark green in lowest 5 cm; orange weathering in cracks; possible DCL;
1.6-1.7	Structureless, well sorted, fine-grained grainstone; no fossils present
1.7-5.0	Red mudstone with rare siltstone interbeds; planar laminations; highly fissile; Unit: Siliciclastic member
5.0-5.5	Moderately sorted, coarse grained sandy grainstone with abundant barnacle and mollusk fragments; structureless;
5.5-7.3	Red mudstone with minor silt; planar laminations; fissile; Unit siliciclastic member;

7.3-8.3	Coarse-grained sandy grainstone with planar to wavy bedding and abundan barnacles, mollusks, and coralline red algae; poorly preserved tabular cross-bedding visible; Unit: Upper bioclastic member
8.3-10.2	Quaternary gravel/cover

Section KG-11

Height in section (m)	Description
0.0-1.0	Moderately sorted, fine- to medium-grained grainstone with abundant mollusk fragments and rhodoliths; planar and wavy bedding common; uppermost surface exposes poorly preserved cross-beds; similar to dancefloor of the Cibola area; top of the bioclastic unit
1.0-2.8	Covered section; massive lime mud out of section projects into covered interval.
2.8-3.9	Massive lime mud with no distinct bedding or internal structures; Upper Marl
3.9-5.1	Carbonate paper shale with millimeter thick laminations; paper shale is interbedded every 40 cm by 10 cm thick interbeds of massive lime mud; background dip is 5° to 134°; Upper Marl
5.1-5.3	Coarse-grained to granular sandy grainstone with planar bedding and abundant shell fragments; Upper bioclastic member
5.3-5.8	Planar bedded, granule to pebble conglomerate with mixed siliciclastic and carbonate matrix; siliciclastic pebbles and granules are subrounded to rounded; shell fragments and coralline red algae fragments are abundant; Upper bioclastic member
5.8-6.0	Planar bedded, moderately sorted, very coarse-grained to granular sandy grainstone with abundant mollusk and barnacle fossils; individual beds are about 1 cm; Upper bioclastic member
6.0-6.6	Horizontally bedded, poorly sorted, coarse- to very coarse-grained pebbly grainstone; carbonate grains are almost entirely shell fragments; individual beds are 5 cm thick; coarse-grained beds have fewer shell fragments; 50% carbonate in matrix; Upper bioclastic member
6.6-8.0	Poorly sorted, rounded, granule to pebble conglomerate with calcareous matrix; matrix is >60% carbonate; shell fragments and coralline red algae common; Upper bioclastic member

8.0-9.8	Poorly sorted, weakly horizontal to low angle bedded, pebble to cobble conglomerate with mixed matrix (>50% carbonate); sub angular to angular clasts; matrix is very coarse-grained sandy grainstone; Upper bioclastic member
9.8-12.8	Poorly sorted, planar bedded, pebble to cobble conglomerate with minor boulders; individual beds range from 2-20cm; carbonate component of matrix in beds varies but does not fall below 20%; matrix supported; angular to subangular clasts; Upper bioclastic member
12.8-13.7	Quaternary Gravel

Section KG-12

Height in section (m)	Description
0.0-4.9	Interbedded fissile red mudstone and siltstone with minor sand interbeds; sandy beds are Colorado River derived sands; sand beds do not exceed 3 cm in thickness
4.9-5.0	Well sorted, very fine- to fine-grained Colorado River sandstone; unit thickens to the NW to over 1.5 meters thick; meter scale trough cross-bedding observed; trough axis oriented 140°;
5.0-12.4	Well sorted, well rounded, very fine- to fine-grained Colorado River sandstone; trough crossbedding and ripple cross laminations are abundant; poorly cemented.
12.4-12.6	Coarse-grained, planar bedded pebbly sandy grainstone with abundant coralline red algae fragments; Upper bioclastic member
12.6-13.3	Planar bedded, coarse-grained pebbly sandy grainstone with shell fragments; 60% carbonate; Upper bioclastic member;
13.3-15.0	Poorly sorted, subangular pebble to cobble conglomerate; inversely graded from pebbly, coarse-grained grainstone (30% siliciclastics) with hummocky cross stratification at the base to a clast supported pebble to cobble conglomerate (>80% siliciclastic in matrix) in the upper 0.7 m; carbonate content decreases upwards to zero; Upper bioclastic member
15.0-17.0	Poorly sorted, angular pebble conglomerate; transitional with underlying unit; no carbonate in matrix; clast supported; Tfg2;
17.0-17.2	Quaternary Gravel

Section KG-13

Height in section (m)	Description
0.0-6.3	Planar laminated, red mudstone; highly fissile until uppermost 1 m when occasional 10-20 cm thick massive mudstone interbeds appear.
6.3-6.5	Massive siltstone with ~10% carbonate
6.5-9.0	Poorly sorted, subangular, sandy pebble to cobble conglomerate; matrix supported; planar bedding throughout; coarsens upward into sandy cobble conglomerate; matrix is <20% carbonate shell fragments; Upper bioclastic member
9.0-9.5	Poorly sorted, subangular, sandy pebble conglomerate; ,matrix supported; no internal structures; Upper bioclastic member
9.5-11.2	Poorly sorted, coarse-grained pebbly sandstone with weak horizontal stratification; coarsens upward into a poorly sorted, sandy pebble to cobble conglomerate with horizontal stratification; <20% carbonate; Upper bioclastic member
11.2-13.2	Structureless, well sorted, fine- to medium-grained sandstone with minor silt; >10% carbonates; Upper bioclastic member
13.2-15.2	Weakly horizontally laminated poorly sorted, pebble to cobble conglomerate; angular to sub-angular clasts; erosional contact with underlying unit; no carbonate in matrix; moderately to weakly cemented; Tfg2

Section KG-14

Height in section (m)	Description
0.0-4.0	Planar laminated, fissile red mudstone with minor 5 cm thick calcisiltite interbeds; upper 10cm is silt-rich; Siliciclastic member

4.0-4.3	Very fine- to fine-grained Colorado River sandstone with climbing ripples; well sorted; rounded; Siliciclastic member
4.3-4.5	Silty red mudstone; highly fissile
4.5-4.7	Very fine- to fine-grained Colorado river sandstone with asymmetrical ripple laminations throughout; quite silty;
4.7-4.9	Silty red mudstone; highly fissile
4.9-7.7	Moderately sorted, silty, very fine- to fine-grained Colorado River sandstone with weakly preserved centimeter scale ripples; individual laminations are 1-2 mm thick; poorly cemented
7.7-10.7	Interbedded silty, very fine- fine to fine grained Colorado River sandstone and massive red mudstone; Individual beds range from 10-40 cm
10.7-11.9	Well sorted, fine-grained Colorado River sandstone with abundant climbing ripples and asymmetric ripple laminations;
11.9-12.8	Moderately to poorly sorted, pebble to cobble conglomerate; low angle crossbedding throughout; horizontally bedded otherwise; clast imbrications dip towards 307°<10% carbonate in matrix; coralline red algae; Upper bioclastic member
12.8-15.7	Poorly sorted, subrounded to subangular, pebble to cobble conglomerate; no carbonate fragments; weak, sub horizontal stratification; weakly cemented; Tfg2?

Section KG-15

Height in section (m)	**Description**
0.0-0.9	Very fine- to fine-grained crystalline travertine bioherms; spaces between mounds are filled by calcisilitite; Basal carbonate member
0.9-2.5	Interbedded calcisiltite and very fine-grained grainstone; individual beds range from 1-3 cm thick; 1-2 mm thick lime mud interbeds also present; flaser to wavy bedding common; planar bedding present throughout; Basal carbonate member; Background dip: 4° towards 128°

2.5-2.9	Fine-grained grainstone with abundant bivalve fragments and gastropod shells; very dense and well cemented in patches (silicification?); Sample GB6; Basal carbonate member
2.9-3.5	Barnacle and bivalve rich, very coarse-grained to granular grainstone with minor coarse-grained grainstone interbeds; 5 cm tall foresets dipping 12* towards 134°; planar to wavy beds on uppermost 10 cm; Basal carbonate member
3.5-6.2	Quaternary Gravel

Section KG-16

Height in section (m)	**Description**
0.0-2.3	Planar bedded calcisiltite with minor 2 cm thick interbeds of very fine-grained grainstone; beds have planar laminations and centimeter scale wave ripple laminations throughout; lenticular bedding is sparse; Basal carbonate member
2.3-8.7	Very coarse-grained to granular, fossiliferous grainstone; tabular cross-bedding showing bidirectional currents; Foresets dip 12° towards 120°/ 16° towards 309°; bedset thicknesses range from 10-20 cm for both current directions; bottom sets are planar to wave rippled and are almost entirely composed of fossils; Charophyte casts are discontinuous along bedding planes and are absent in the upper 4 meters; Basal carbonate member
8.7-12.6	Quaternary Gravel

Section KG-17

Height in section (m)	Description
0.0-1.2	Interbedded lime mud and very fine-grained grainstone with prominent wavy bedding; lime mud interbeds range from 1mm to 1cm; fines upward to become dominated by calcisiltite; lenticular and flaser bedding common in uppermost 20 cm; Basal carbonate member
1.2-1.5	Planar bedded, granular, fossiliferous grainstone with no internal bedding; Basal carbonate member
1.5-2.7	Fissile, poorly cemented carbonate paper shale with millimeter thick laminations; Upper marl
2.7-2.9	Moderately sorted, medium- to coarse-grained sandy grainstone with minor bivalve shell fragments;
2.9-3.1	Highly fissile pale green clay stone
3.1-4.3	Fissile red mudstone with minor thin (2-3 cm) siltstone interbeds
4.3-6.9	Quaternary Gravel

Section KG-18

Height in section (m)	Description
0.0-0.6	Fissile carbonate paper shale with 1 mm thick laminations; background dip is 6° towards 71° (possible local control)
0.6-0.7	Structureless, medium- to coarse-grained sandy grainstone;
0.7-1.2	Fissile pale green claystone with rare orange discoloration; possible DCL?
1.2-4.5	Thinly bedded red mudstone with minor 5 cm thick interbeds of massive red mudstone; unit has abundant white, concretions that appear to be carbonate
4.5-5.3	Quaternary Gravel

Section KG-19

Height in section (m)	Description
0.0-5.9	Highly weathered fissile red mudstone with silt interbeds (5 cm thick); Root traces visible in upper 10-20cm
5.9-6.0	Poorly sorted, clast supported, cobble conglomerate; subangular clasts;
6.0-6.2	Poorly sorted, clast supported, pebble conglomerate; subangular clasts;
6.2-6.4	Moderately sorted, pebbly granule conglomerate with a fine-grained sandy matrix; tabular cross-bedding with foresets (20 cm thick) dipping 16° towards 203°; subrounded to subangular clasts
6.4-8.2	Poorly sorted, granule to pebble conglomerate with medium-grained sandy matrix; unit is clast supported at base and matrix supported at the top; subrounded to subangular clasts; carbonate in matrix decreases upwards from 20% to <5%; Upper bioclastic member
8.2-12.7	Poorly sorted, angular to subangular; clast supported pebble to cobble conglomerate; weakly cemented; internal structures are weakly developed horizontal stratification; carbonate content decreases upwards from 5% to 0%; transition from upper bioclastic member to Tfg2

Section KG-20

Height in section (m)	Description
0.0-1.6	Silty, very fine-grained Colorado River sand; well sorted, well rounded, poorly consolidated; possible soft sediment deformation, some convolute bedding
1.6-4.1	Fissile red mudstone and siltstone; three thin (1-3 cm thick) interbeds of very fine-grained Colorado River sand in upper 60 m;

4.1-7.9	Trough cross bedded and ripple cross laminated, very fine-grained Colorado River sandstone; poorly consolidated; ripples indicate flow towards 287°; ripple height is 2 cm;
7.9-9.3	Fine- to medium-grained colorado river sandstone with abundant climbing ripples; trough crossbedding present but poorly preserved due to poor consolidation; ripples indicate flow towards 240°
9.3-9.5	Structureless siltstone interbed; thickens slightly towards the east;
9.5-9.7	Fine-grained Colorado River sandstone with abundant climbing ripples; background dip is 3° towards 115°
9.7-10.3	Siltstone with weakly developed horizontal laminations
10.3-13.4	Poorly sorted, subrounded, matrix supported, horizontal to low angle bedded , pebble to cobble conglomerate with a medium-grained sand matrix; carbonate content is ~30% and is made of shell fragments and coralline red algae; carbonate content decreases to <10% near the top of the unit; a concentration of cobbles is observed in the upper 40 cm of the unit; Upper bioclastic member
13.4-19.4	Poorly sorted, angular to subangular, clast supported, pebble to cobble conglomerate with a medium sand matrix; no carbonate; erosional basal contact with underlying unit; poorly consolidated; Tfg2.

Section KG-21

Height in section (m)	**Description**
0.0-9.7	Fissile red mudstone with interbedded siltstone; siltstone interbeds range from 5-8 cm thick;
9.7-11.2	Very fine-grained Colorado River sandstone with weak planar bedding; minor ripple laminations throughout; ripples are 2 cm thick

11.2-16.2	Poorly sorted, subrounded, planar bedded, matrix supported pebbly conglomerate; matrix composition is <50% carbonate in first meter, decreases to <30% in the next 3 m, and is <10% in the upper 40 cm; coralline red algae fragments common in the lower two meters
16.2-17.6	Quaternary Gravel

Section KG-22

Height in section (m)	**Description**
0.0-8.2	Fissile red mudstone; interbedded with siltstone and very fine-grained Colorado River Sandstone in the uppermost meter; bedding becomes increasingly convolute and deformed to the NE; individual silt and sand beds are no greater than 5 cm thick.
8.2-11.0	Moderately sorted, subrounded, clast supported granule conglomerate with minor pebbles and cobbles; planar bedding and tabular cross-bedding is observed; cross-beds are 30 cm thick and dip 22° towards 120°; granular reactivation surfaces can be found on many foresets; coralline red algae fragments are abundant in the lower 2 meters; carbonate in matrix is 40%; Upper bioclastic member
11.0-14.6	Poorly sorted, subangular to subrounded, clast supported granule to pebble conglomerate with minor cobbles; mostly horizontally stratified, with rare tabular cross-beds; cross-bedding has the same orientation as underlying unit; carbonate in matrix is <10%; coralline red algae fragments are not present

Section KG-23

Height in section (m)	Description
0.0-7.2	Poorly sorted, subangular to rounded, boulder rich, pebble to cobble conglomerate; matrix supported; 30-40 cm thick trough crossbreeds throughout; axis of trough oriented 95° on vertical face oriented 50°; no carbonates; well cemented; Miocene Conglomerate
7.2-7.4	Quaternary Gravel

Section KG-24

Height in section (m)	Description
0.0-1.8	Horizontally stratified, subangular to subrounded, poorly sorted, pebble to cobble conglomerate; matrix supported; no carbonate in matrix; upper 20 cm is a clast supported cobble lag; with almost no matrix; Miocene Conglomerate
1.8-2.1	Highly silicified travel tine with single 30cm tall bioherm; travertine thickness on either side of bioherm is 10 cm; battilaria fossils common; sample GB7
2.1-2.5	Poorly sorted, subrounded, pebble to cobble conglomerate with no distinct bedding; ungraded;
2.5-2.8	Massive calcisiltite with abundant mollusk and battilaria fossils
2.8-3.3	Interbedded calcisiltite, lime mud, and very fine-grained sandy grainstone; lime mud beds are 1cm thick; calcisiltite and sandy grainstone beds are 1-3cm thick and display wavy bedding;
3.3-7.9	Very fine-grained Colorado River derived sand with minor granitic granule sized gravel in patches. **Chemehuevi Fm.**
7.9-9.1	Quaternary Gravel

Section KG-25

Height in section (m)	Description
0.0-2.3	Interbedded, structureless very fine-grained Colorado River sand and red mudstones; tilted and deformed by large scale soft sediment deformation; bedding is increasingly convolute to the west; Siliciclastic member;
2.3-4.6	Tabular cross-bedded, moderately sorted, rounded to subangular, matrix supported, pebbly granule conglomerate; cross-beds are 20 cm thick and indicate transport towards 223; <20% carbonate in matrix; Upper bioclastic member
4.6-5.8	Poorly sorted, angular to subangular, horizontally stratified, matrix supported pebble conglomerate with minor cobbles; no carbonates present; Tfg2

Section KG-26

Height in section (m)	Description
0.0-0.2	Massive lime mud
0.2-1.6	Horizontally stratified and wavy-flaser-lenticular bedded calcisiltite, very fine-grained grainstone, and lime mud; lime mud beds are <1 cm thick; silt and grainstone beds are 3-5 cm thick; background dip is 5° towards 108°
1.6-5.2	Silty, very fine-grained Colorado River sands; massive to weakly crossbedded; trough crossbedding not visible due to cover, but is likely;
5.2-6.6	Quaternary Gravel

Section PVM-1

Height in section (m)	Description
0.0-2.4	Weakly stratified, poorly sorted, granular to pebbly grainstone with lenses of moderately sorted pebble to cobble conglomerate in channels; channels range from 0.1-0.4 m tall and 1.5m wide; Basal carbonate member
2.4-2.8	Unstratified, ungraded cobble conglomerate;
2.8-4.8	Moderately to poorly sorted, pebble to boulder conglomerate with no internal structures; cobbles and boulders are concentrated in pockets
4.8-7.0	Horizontally stratified pebbly grainstone with lenses of moderately to poorly sorted pebble to boulder conglomerate that form elongate bodies up to 30 cm thick; conglomerate clasts are angular to subrounded; matrix in conglomerate is >50% carbonate
7.0-8.2	Quaternary Gravel

Section PVM-2

Height in section (m)	Description
0.0-0.4	Poorly sorted, medium to very coarse-grained pebbly sandstone with minor cobbles; weakly stratified; Miocene Conglomerate
0.4-1.1	Very fine-grained grainstone and calcisiltite with planar to wave ripple laminations throughout; Basal carbonate member; end of section PVM 2a
1.1-1.8	Moderately sorted granule to pebble conglomerate with a medium- to coarse-grained sandy matrix; small cobble lenses throughout; ungraded; start of section PVM 2b; Basal carbonate member
1.8-2.3	Poorly sorted, pebble to boulder conglomerate, thins to 10 cm over a distance of 5 meters to the east; Basal carbonate member

2.3-2.8	Horizontlly stratified pebble conglomerate with a medium sand matrix; carbonate content is <10%; basal carbonate member;
2.6-6.2	Horizontally bedded pebble to cobble conglomerate with beds ranging from 0.8-1.1 meters thick; no internal stratification or imbrication; clasts are rounded-to subangular; clast composition is 90% locally derived volcanics and 10% from underlying carbonates; erosional basal contact; Quaternary inset gravel
6.2-7.4	Younger Quaternary Gravel

Section PVM-3

Height in section (m)	**Description**
0.0-0.9	Interbedded carbonate paper shale and 5 to 10 cm thick intedbeds of massive lime muds; upper marl; Sample 19PVM3-1 taken at 0.4m; Sample 19PMV3-2 taken at 0.6m;
0.9-1.0	Well sorted; fine-grained grainstone with minor siliciclastic component; pebble lag along base; weak horizontal stratification;
1.0-1.35	Well sorted, medium-grained grainstone; tabular cross-bedding along base is 15 cm thick and indicates currents directed towards 276°; upper 20 cm is horizontally stratified with abundant wave rippled tops; Sample 19PVM3-3 taken at 1.25m;
1.35-1.9	Rhythmically bedded, well sorted, fine-grained sandy grainstone; individual beds are 1-2 cm thick; bedding plane surface is highly bioturbated and shows burrow mottling; Sample 19PVM3-4 taken at 1.6m; Sample 190126-16 taken at 1.8m; Unit this to the west due to erosion and channelization from overlying unit;
1.9-2.6	Poorly sorted, pebble to cobble conglomerate with a coarse-grained grainstone matrix; unit fines upwards to a poorly sorted granule to pebble conglomerate; upper 15 cm is a pebble to cobble lag; coralline red algae fragments are abundant; unit fills a channel inset into underlying unit; Sample 190126-17 taken at 2.1m;

2.6-4.2	Interbedded bracciate red mudstone with sizable grainstone-filled desiccation cracks and root casts; rhizoliths and pedogenic features common; four interbeds of coarse grained pebbly grainstone with abundant shell fragments are each 10 cm thick; Sample 19PVM3-5 taken at 3.35m; Sample 19PVM3-6 taken at 3.55m;
4.2-5.0	Rhythmically bedded/laminated, well sorted, fine-grained sandy grainstone; Sample 19PVM3-7 taken at 4.4m; Sample 19PVM3-8 taken at 4.6m
5.0-5.6	Poorly sorted, coarse-grained, sandy, pebbly, fossiliferous grainstone; with thin (1-2 cm thick) planar bedding; 60% carbonate; fossils are dominantly barnacles and bivalves;
5.6-7.6	Quaternary Gravel

Section PVM-4

Height in section (m)	**Description**
0.0-0.9	Planar to wavy-flaser bedded calcisiltite with thin (1 mm) lime mud interbeds; unusual facies of the upper marl; upper surface has cracks and fissures; Sample 19PVM4-1 taken at 0.4 m;
0.9-1.02	Siliciclastic green clay rich carbonate paper shale; upper marl; Sample 19PVM4-2 taken at 0.95 m
1.02-1.2	Karst breccia with clasts ranging from1.5 cm to 15x25 cm; clasts are composed of underlying unit, large reworked charophytes; dissolution cracks common; matrix is a poorly sorted, fine- to coarse-grained grainstone; no siliciclastics; upper marl; Sample 19PVM4-3 taken at 1.1 m

1.2-2.45	Moderately sorted, coarse-grained grainstone with cobble to boulder lags; planar to long wavelength convex up bedding; heavily bioturbated; thalassinoides burrows, rhodoliths, and coralline red algae are abundant; individual beds average 10-15 cm; can trace beds laterally westward into overlying cross-bedded conglomerates; possibly distal bottomsets; upper bioclastic member; Sample 19PVM4-4 taken at 1.5 m; Sample 19PVM4-5 taken 1.75 m; Sample 19PVM4-6 taken at 2.35 m; Sample S190127-18 taken at 2.2 m
2.45-2.70	Calcareous matrix granule conglomerate that fines upward to coarse-grained sandy grainstone; Sample 19PVM4-7 taken at 2.6 m;
2.7-2.8	Poorly sorted, subrounded granule conglomerate with <30% carbonate in matrix; no internal structures;
2.8-3.8	Poorly sorted pebble to cobble conglomerate; clast supported; matrix is a very coarse grained sandy fossiliferous grainstone; foresets (1 m thick) dip to SE; Sample S190127-19 taken at 2.9 m

Section PVM-5

Height in section (m)	**Description**
0.0-0.25	Interbedded lime mud and calcisiltite with wavy to planar stratification; Basal carbonate member
0.25-0.75	Well sorted, very fine- to fine- grained sandy grainstone with 1-5 mm thick lime mud interbeds; grainstone beds are heavily bioturbated; grainstone bed thicknesses increase from 1-3 cm at the base to 10 cm at the upper contact; mud interbeds show desiccation cracks; abundance of mud decreases towards the top of the unit;
0.75-0.95	Massive, structureless, very fine-grained grainstone with minor siliciclastic component; heavily bioturbated;
0.95-1.0	Planar to wave ripple laminated, well sorted, medium-grained sandy grainstone with minor siliciclastic pebbles;
1.0-1.1	Very coarse-grained, barnacle rich grainstone with no internal structures

1.1-1.45	Well sorted, medium-grained sandy grainstone with wavy to planar bedding with minor bioturbation;
1.45-1.55	Massive calcisiltite
1.55-1.8	Well sorted, fine- to medium-grained sandy grainstone with low angle (18°) crossbedding dipping towards 137°;
1.8-1.95	Laterally discontinuous layer of well sorted; fine-grained sandy grainstone with cross-bedding indicating transport to 290°;
1.95-2.2	Well sorted, fine- to medium-grained sandy grainstone with cross-bedding dipping towards 130°
2.2-2.25	Massive calcisiltite interbed
2.25-2.7	Poorly sorted, granule-sized fossilferous grainstone with abundant barnacle and bivalve fragments; cross-bedding indicates transport towards 134°; cross-bed thickness is 0.5 m
2.7-2.8	Massive calcisiltite with minor siliciclastic pebbles
2.8-3.4	Poorly sorted, granule sized fossiliferous sandy grainstone; crossbedding indicates transport to the 128°; cross-bed thickness is 0.6 m
3.4-3.7	Moderately sorted, coarse-grained sandy grainstone; planar beds are 10-15 cm thick;
3.7-4.3	Moderately sorted, very coarse-grained fossiliferous grainstone beds (5-10 cm thick) interbedded with poorly sorted, subrounded to subangular pebble-cobble conglomerate; conglomerate matrix is <65% carbonate;
4.3-5.5	Quaternary Gravel

Section PVM-6

Height in section (m)	Description
0.0-3.5	Moderately sorted, granule to pebble conglomerate with low angle to horizontal stratification; clast supported with a fine- to medium-grained sand matrix; elongate 2-3 m lenses of cobble conglomerate are common; subangular clasts; large cobbles have in-situ barnacles; Basal carbonate member
3.5-3.7	Poorly sorted, pebble to cobble conglomerate with travertine encrusted clasts; subrounded clasts; matrix is a very fine-grained grainstone; clast supported
3.7-3.9	Moderately to poorly sorted, granule to pebble conglomerate with low angle cross-stratification; Carbonate in matrix is <10%
3.9-4.1	Poorly sorted, cobble conglomerate with medium sand matrix; clast supported; carbonate in matrix is <10%; subangular clasts; ungraded
4.1-4.5	Poorly sorted, granule to pebble conglomerate with sporadic, discontinuous cobble lags throughout; clasts are subangular; horizontally to low angle stratified
4.5-4.7	Massive calcisiltite bed
4.7-7.4	Interbedded calcisiltite and very fine-grained grainstone; individual beds range from 2-8cm thick; bedding surfaces are planar or wavy; Pebble-cobble conglomerate is inset into a channel from 6.7-7.0m; upper 40 cm contains wave ripple beds;
7.4-7.8	Poorly sorted, cobble conglomerate; angular clasts; ungraded; carbonate in matrix is >60%
7.8-8.2	Well sorted, coarse-grained grainstone with SE directed tabular cross-bedding (not a full bed-set);
8.2-9.2	Quaternary Gravel

Section PVM-7

Height in section (m)	Description
0.0-1.3	Moderately sorted, granule to pebble conglomerate with low angle to horizontal crossbedding; discontinuous cobble lags throughout; coarsens up to a cobble conglomerate in upper 25 cm; basal carbonate member
1.3-1.8	Channelized, well sorted, granule conglomerate with bi-directional crossbedding (point bars); subrounded clasts; matrix is <70% carbonate;
1.8-2.4	Moderately sorted, weakly stratified, granule conglomerate with minor pebble component; no lags visible; carbonate is <30%
2.4-2.5	Structureless, well sorted, fine-grained sandy grainstone
2.5-2.9	Poorly sorted, ungraded, cobble conglomerate; angular to subangular clasts; carbonate in matrix is <50%
2.9-3.1	Horizontally stratified, interbedded massive calcisiltate and very fine-grained sandy grainstone; individual beds range from 1-3 cm thick
3.1-4.9	Interbedded calcisiltite and very fine- to fine-grained grainstone; wavy to planar bedding throughout; charophyte beds occur discontinuously along bedding planes
4.9-5.5	Moderately sorted, lenticular to flaser bedded calcisiltite, very fine- to fine grained sandy grainstone, and lime mud; mud content decreases towards top of unit;
5.5-5.7	Moderately sorted, granule-sized fossiliferous grainstone with 20 cm thick cross-beds.
5.7-6.1	Poorly sorted, inversely graded pebble-cobble conglomerate; carbonate in matrix is ~50%

Section PVM-8

Height in section (m)	Description

0.0-0.35	Moderately sorted, angular to subangular, pebble to cobble conglomerate with weak horizontal stratification; <5% carbonate in matrix; Basal carbonate member
0.35-0.4	Poorly sorted, pebbly, fine-grained sandy grainstone with wavy bedding;
0.4-0.5	Moderately sorted, pebbly, coarse-grained sandy grainstone with no internal structures;
0.5-1.55	Poorly sorted, coarse-grained pebbly sandstone with low angle cross-stratification to horizontal bedding; Lenticular pebble-cobble conglomerate patches with angular clasts are abundant;
1.55-1.85	Massive, very fine- to fine-grained sandy grainstone with heavy bioturbation; thalassinoides burrows, barnacles, mollusks and ostracizes common;
1.85-2.8	Planar and wavy bedded calcisiltite and very fine- to fine-grained grainstone; individual beds range from 1-5 cm thick;
2.8-3.0	Horizontally stratified lime mud bed; individual beds are 1-2 mm thick;
3.0-4.3	Wavy-flaser-lenticular bedded very fine- to fine-grained calcarenite, lime mud, and calcisiltite; individual beds are very well sorted; minor planar bedding;
4.3-4.6	Poorly sorted, granule to pebble conglomerate with weakly developed horizontal to low angle stratification; subangular to surrounded clasts; carbonate in matrix is <20%;
4.6-4.7	Poorly sorted, granule-sized fossiliferous sandy grainstone with abundant barnacle and mollusk fragments; no internal structures;
4.7-5.0	Poorly sorted, inversely graded, pebble to cobble conglomerate with fine- to coarse-grained matrix; matrix is <60% carbonate;
5.0-9.5	Quaternary Gravel

Section PVM-9

Height in section (m)	Description
0.0-0.3	Poorly sorted, pebble conglomerate with sandy matrix; angular to subangular clasts; no internal structures; Basal carbonate member
0.3-0.55	Well sorted, very fine-grained grainstone with no internal structures; bivalve shells (<4 mm across) throughout;
0.55-0.65	Thinly bedded, wave ripple laminated, calcisiltite and very fine-grained sandy grainstone;
0.65-1.05	Very fine-grained grainstone with planar to wavy bedding; thin mud interbeds (5 mm thick) show dessication cracks on exposed bedding surfaces;
1.05-1.1	Massive lime mud
1.1-1.8	Very fine- to fine-grained sandy grainstone with planar and wavy bedding; lime mud interbeds are 2 mm thick; mud bedding plane surfaces show grainstone filled desiccation cracks;
1.8-2.4	Interbedded calcisiltite and very fine-grained grainstone with abundant wavy bedding; wavelengths of wavy bedding is 0.4 m; lime mud observed in discontinuous mud drapes on wavy bedforms; lime mud beds are <1 cm thick; grainstone and calcisiltite beds range from 2-5 cm thick;
2.4-2.65	Heavily bioturbated, structureless, very fine- to fine-grained sandy grainstone; rare ripple laminations preserved;
2.65-2.75	Poorly sorted, pebbly, granule conglomerate with abundant shell fragments; matrix is a coarse-grained grainstone; no internal structures or imbrication;
2.75-2.85	Structureless, poorly sorted, pebbly, medium-grained sandy grainstone
2.85-2.95	Poorly sorted, granule-sized, fossiliferous sandy grainstone; no internal structures
2.95-3.05	Structureless, poorly sorted, pebbly, medium-grained sandy grainstone

3.05-3.45	Structureless, poorly sorted, pebble conglomerate with a fossilferous grainstone matrix; 15 cm thick lenses of coarse-grained grainstone throighout; conglomerate is weakly stratified;
3.45-3.6	Poorly sorted, medium- to coarse-grained pebbly sandy grainstone with planar laminations throughout
3.6-4.3	Poorly sorted, unstratified, cobble to boulder conglomerate; matrix is a poorly sorted, coarse-grained to granule sized fossiliferous grainstone; no internal structures; clasts are angular to subangular;
4.3-4.5	Poorly sorted, medium-grained pebbly grainstone with weak internal stratification
4.5-5.1	Moderately sorted, granule-sized fossiliferous grainstone with abundant 10 cm thick granule to pebble conglomerate lenses; weakly stratified
5.1-5.9	Moderately sorted, coarse- to very-coarse grained fossiliferous sandy grainstone; low angle cross-bedding throughout; individual foresets are 1-5 cm thick; abundant barnacles, mollusks and rhodoliths;
5.9-7.7	Quaternary Gravel

Section PVM-10

Height in section (m)	**Description**
0.0-0.7	Interbedded calcisiltite and very fine-grained grainstone; beds are 1-3 cm thick and show both planar laminations and wave rippled surfaces;
0.7-1.9	Wavy-Flaser bedded very fine- to fine-grained grainstone with thin (1-2 mm thick) lime mud beds; interbedded with poorly sorted, very coarse-grained to granule-sized fossiliferous grainstone with tabular cross-beds; cross-beds are 10 cm thick; finer beds range from 5-10 cm thick;
1.9-2.1	Well sorted, interbedded calcisiltite and very fine-grained sandy grainstone with wavy-flaser bedding;
2.1-2.2	Very fine-grained grainstone and calcisiltite with abundant reed casts in life position;

2.2-2.3	Massive lime mud with minor reed casts;
2.3-2.6	Moderately sorted; coarse- to very coarse-grained grainstone and fossiliferous grainstone with low angle (10°) crossbedding; unit pinches out two meters to the east;
2.6-2.95	Horizontally bedded, medium- to coarse-grained grains tine with abundant reed casts at the base; individual beds range from 3-5 cm;
2.95-3.1	Poorly sorted, pebble conglomerate with subangular to surrounded clasts; no internal structures; matrix is a fine-grained sand with 30-40% carbonate
3.1-3.2	Wavy-flaser bedded very fine-grained grainstone and lime mud;
3.2-3.5	Heavily bioturbated, structureless, calcisiltite and very fine-grained grainstone;
3.5-3.8	Heavily bioturbated, structureless, fine-grained sandy grainstone
3.8-4.0	Wavy-flaser bedded, calcisiltite and very fine-grained sandy grainstone;
4.0-4.15	Weakly stratified, bioturbated, very fine- to fine-grained sandy grainstone;
4.15-4.45	Rhodolith bearing, barnacle rich, fine- to medium-grained grainstone with weak planar laminations;
4.45-4.6	Weakly stratified, ripple laminated fine-grained sandy grainstone;
4.6-4.9	Rhodolith bearing, fine-grained grainstone; heavily bioturbated;
4.9-5.3	Granule-sized, fossiliferous grainstone with abundant barnacles and bivalves; tabular cross-beds indicating SE transport (138°) are 40 cm thick
5.3-5.8	Tabular cross-bedded, moderately sorted, coarse to very coarse-grained fossiliferous sandy grainstone with abundant shell fragments; cross-bed sets are 0.5 m thick and indicate transport to the SE (143°)
5.8-7.8	Tabular cross-bedded, coarse- to very coarse-grained fossiliferous grainstone; cross-bed thickness unreliable due to heavy cover and lack of full sets;

7.8-8.8	1 meter thick tabular cross-bedded, medium- to coarse-grained sandy grainstone; upper bioclastic member; small coralline red algae fragments sparsely distributed throughout;
9.8	Quaternary Gravel

Section PVM-11

Height in section (m)	**Description**
0.0-2.2	Thinly bedded red mudstone; weakly developed soil horizons in upper 10 cm; horizontal and vertical zones of bright orange discoloration along bedding planes; white, vertical rhizocretions throughout;
2.2-2.25	Well sorted, fine-grained sandy grainstone; structureless
2.25-4.0	Thinly bedded to massive red mudstone; massive beds are 8 cm thick; fewer orange discolorations than lower unit;
4.0-4.35	Hortizontally laminated, well sorted, very fine- to fine-grained Colorado River derived sandstone;
4.35-4.45	Thinly bedded siltstone
4.45-6.45	Interbedded very fine-grained sandstone and siltstone with abundant planar laminations; orange discoloration common throughout; individual beds range from 1-4 cm thick;
6.45-8.8	Thinly bedded red mudstone with minor, discontinuous interbeds of siltstone; common orange discoloration along bedding plane surfaces;

8.8-9.4	Interbedded, poorly cemented siltstone and very fine-grained sandstone; minor granules throughout; individual beds are 3 cm thick;
9.4-12.2	Quaternary Gravel

Section PVM-12

Height in section (m)	**Description**
0.0-3.5	Well sorted, well rounded, medium-grained Colorado River sandstone with amalgamated, multi-storey trough crossbedding; trough axes oriented 176°
3.5-9.2	Well sorted, well rounded, fine- to medium grained Colorado River sandstone with amalgamated, multi story trough-cross-bedding; trough axes oriented 170°
9.2-9.6	Well sorted, well rounded, fine-grained Colorado River sandstone with planar laminations throughout;
9.6-11.5	Poorly sorted, medium- to coarse-grained pebbly sandy grainstone with long wavelength (40-50 cm) convex-up bedforms; pinch and swell geometry in pebble lenses throughout; pebbles concentrated in convex up lenses; pebbles are subangular to subrounded; upper bioclastic member;
11.5-13.0	Poorly sorted, pebble to cobble conglomerate with very weak stratification; subangular clasts; matrix is a fine-to medium grained sand with <50% carbonate;
13.0-16.3	Interbedded calcareous matrix, pebble to cobble conglomerate and poorly sorted, medium- to coarse-grained pebbly sandstone with minor carbonate; highly stratified; conglomerate and pebbly sandstone beds range from 40-50 cm thick; upper 50 cm has wave rippled surfaces in the pebbly sandstone and long wavelength (1 m) convex up bedrooms throughout;
16.3-17.8	Quaternary Gravel

Section PVM-13

Height in section (m)	Description
0.0-2.6	Tertiary volcanics; crystal tuff;
2.6-3.0	Angular cobble to boulder volcanic clasts; surrounded by tuffaceous matrix; lahar?
3.0-3.2	Poorly sorted, granule to cobble calcareous matrix conglomerate; inversely graded; basal carbonate member;
3.2-3.4	Moderately sorted, granule to pebble conglomerate; horizontally stratified; rounded to subrounded clasts;
3.4-3.7	Massive, well cemented, lime mud
3.7-5.2	Horizontally stratified, interbedded calcisiltite and very fine- to fine-grained grainstone; thin lime mud interbeds throughout; wavy bedding throughout; thalassinoides burrows observed on basal surfaces; ripples preserved on bedding plane surfaces;
5.2-6.15	Massive to highly laminated lime mud; well stratified; upper marl
6.15-6.8	Moderately sorted, granule-sized fossiliferous sandy grainstone; 0.5 m thick trough crossbedding with axes oriented 85°; bivalve and barnacle fragments throughout; upper bioclastic member
6.8-9.1	Horizontally stratified, very fine- to fine grained sandy grainstone with planar, medium-grained sandy grainstone interbeds (20 cm thick) throughout; Individual beds are 50 cm thick and are structureless
9.1-9.7	Moderately sorted, fine-grained pebbly sandy grainstone with abundant coralline red algae fragments; structureless
9.7-10.2	Planar bedded, granule-sized fossiliferous sandy grindstone with abundant bivalves and barnacles;
10.2-10.4	Wavy-flaser bedded, fine-grained sandy grainstone; thin (2 cm thick) interbed of granule-sized fossiliferous grainstone
10.4-10.7	Very coarse-grained fossiliferous sandy grainstone with minor cobbles; coralline red algae throughout; no pebbles or cobbles in upper 10 cm;

10.7-10.8	Wavy bedded, fine-grained sandy grainstone
10.8-11.7	Inversely graded; poorly sorted, pebbly granule-sized fossiliferous sandy grainstone that coarsens upwards into a calcareous matrix cobble conglomerate; abundant coralline red algae fragments
11.7-12.1	Wavy bedded, fine- to medium-grained sandy grainstone with abundant barnacles; wave ripple lamentations preserved throughout; minor pebble component
12.1-12.3	Coarse- to very-coarse grained pebbly sandy fossiliferous grainstone; long wavelength (3 m) convex up bedding
12.3-13.1	Horizontally to low angle stratified, well sorted, coarse-grained pebbly sandy grainstone; Long wavelength (3m) pinch and swell bedding sporadic throughout;
13.1-13.2	Wavy bedded and wave ripple laminated; fine-grained sandy grainstone;
13.2-13.55	Weakly stratified, coarse- to very-coarse grained sandy grainstone with abundant barnacle, bivalve, and coralline red algae fossils
13.55-13.7	Poorly sorted cobble conglomerate with subrounded clasts; matrix is a fine- to medium-grained grainstone;
13.7-13.95	Wavy bedded and wave ripple laminated; fine-grained sandy grainstone;
13.95-14.35	Coarse- to very coarse-grained pebbly fossiliferous sandy grainstone; lower 20 cm is structureless with abundant shell fragments; upper 20 cm are weakly stratified
14.35-14.4	Structureless, fine-grained sandy grainstone
14.4-15.35	Poorly sorted, coarse- to very coarse-grained pebbly sandy fossiliferous grainstone; lower 60 cm are structureless; upper 35 cm are horizontally stratified
15.35-15.45	Structureless, fine-grained sandy grainstone; discontinuous cobble lag along base; wave rippled top;
15.45-16.1	Planar bedded, moderately sorted, very coarse-grained, pebbly sandy grainstone; individual beds range from 1-5 cm thick;

16.1-21.1	Cover/Quaternary Gravel

Section PP-1

Height in section (m)	Description
0.0-0.2	Interbedded calcisiltite and very-fine-grained grainstone with abundant thalassinoides burrows; thinly bedded (0.5-1 cm thick beds)
0.2-1.6	Well sorted, medium- to coarse-grained sandy grainstone; planar tabular cross-bedding indication southward transport; cross-bed thickness is 1.4m thick; granule-sized fossiliferous grainstone concentrated on sigmoidal reactivation surfaces along foresets; climbing ripples common near upper portions of foresets
1.6-1.95	Well sorted, fine-grained grainstone with low angle stratification; heavily bioturbated; bottom sets
1.95-3.65	Well sorted, medium- to coarse- grained sandy grainstone; granule-sized fossiliferous grainstone concentrated along sigmoidal reactivation surfaces; cross-bedding is 1.7 meters thick and indicates transport towards 178°;
3.65-4.3	Well sorted, medium- to coarse- grained sandy grainstone; granule-sized fossiliferous grainstone concentrated along sigmoidal reactivation surfaces; cross-bedding is 0.65 meters thick and indicates transport towards 181°;
4.3-4.7	Well sorted, medium- to coarse- grained sandy grainstone; granule-sized fossiliferous grainstone concentrated along sigmoidal reactivation surfaces; cross-bedding is 0.4 meters thick and indicates transport towards 174°;
4.7-4.85	Well sorted, medium- to coarse- grained sandy grainstone; granule-sized fossiliferous grainstone concentrated along sigmoidal reactivation surfaces; cross-bedding is 0.15 meters thick and indicates transport towards 184°;

Section PP-2

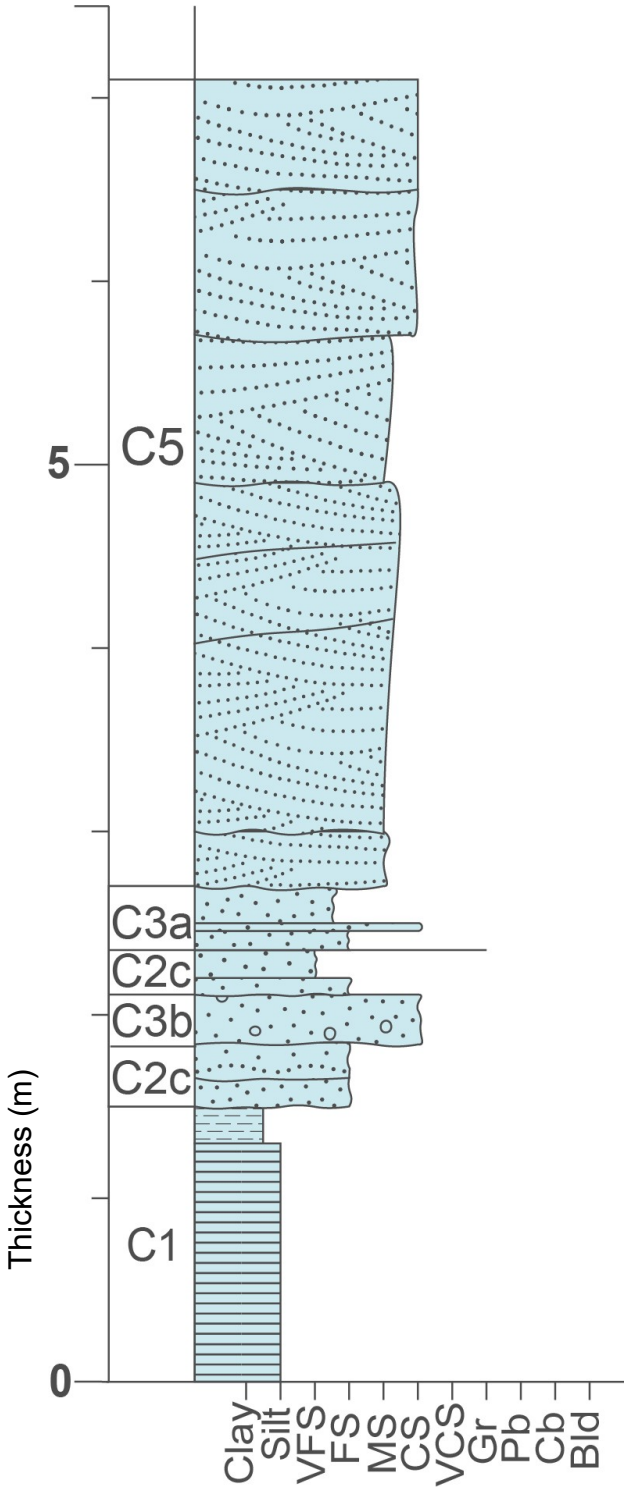
Thickness (m)
5
0
C5
C3a
C2c
C3b
C2c
C1
Clay
Silt
VFS
FS
MS
CS
VCS
Gr
Pb
Cb
Bld

Section SR-1

Height in section (m)	Description
0.0-0.65	Poorly sorted, medium- to very coarse-grained fossiliferous sandy grainstone; ~30% siliciclastics; south east directed 65 cm thick cross-bedding;
0.65-0.8	Very coarse-grained fossiliferous sandy grainstone with southeast directed 15 cm thick cross-bedding
0.8-1.0	Well sorted, fine- to medium-grained sandy grainstone with planar and wave rippled bedding;
1.0-1.7	Moderately to poorly sorted, medium- to coarse-grained pebbly grainstone with 35 cm thick, SE directed crossbedding (127°)
1.7-1.95	Festoon cross-bedded pebbly fossiliferous sandy grainstone; 50% siliciclastics; axes of cross-beds trend 178°;
1.95-2.2	Granule-sized fossiliferous sandy grainstone with abundant bivalve and barnacle fragments; 25 cm thick cross-beds indicate transport towards 136°
2.2-2.95	Well sorted, fine-grained grainstone with planar bedding; individual beds are heavily burrow mottled and contain thalassinoides burrows;
2.95-3.15	Fine- to medium-grained grainstone with abundant shell fragments; low angle to horizontal stratification.

Section SR-2

Height in section (m)	Description
0.0-0.3	Interbedded calcisiltite and very fine-grained sandy grainstone; planar to wavy bedding throughout; individual beds are 1-3 cm thick
0.3-1.3	Moderately to well sorted, coarse- to very-coarse grained pebbly grainstone with tabular cross-bedding; cross-beds range from 30-35 cm thick and foresets dip towards 88°;

1.3-2.0	Moderately sorted granule-sized sandy fossiliferous grainstone with minor pebble component; 0.7 m thick tabular cross-beds have foresets that dip 25° towards 90°;
2.0-2.55	Well sorted, medium-grained fossiliferous sandy grainstone; tabular cross-bed sets range from 10-25 cm thick and indicate transport towards 93°;
2.55-2.85	Interbedded granule-sized fossiliferous sandy grainstone and fine-grained wave rippled grainstone; individual beds are 10 cm thick;
2.85-3.65	Medium- to very coarse-grained sandy grainstone and granule sized fossiliferous pebbly grainstone; East directed tabular cross-beds range from 15-30 cm thick;
3.65-4.4	Well sorted, very fine- to fine grained grainstone with a single 10 cm thick siliclastic and carbonate mud interbed; grainstone is burrow mottled and mildly bioturbated;
4.4-4.6	Well sorted, fine- to medium-grained sandy fossiliferous grainstone with low angle, east directed cross-beds (20 cm thick)
4.6-4.9	Well sorted, very coarse-grained to granule-sized fossiliferous grainstone with <10% siliciclastics; tabular cross-beds (10 cm thick) are oriented 92°
4.9-5.15	Well sorted, granule-sized fossiliferous sandy grainstone with abundant bivalve and barnacle shell fragments; low angle cross-bedding (25 cm thick) indicates eastward transport

Section SR-3

Height in section (m)	**Description**
0.0-0.35	Medium- to coarse-grained, moderately sorted, sandy grainstone; 35 cm thick cross-bed indicates transport towards 96°
0.35-0.45	Well sorted, fine- to medium grained sandy grainstone; planar stratification minor shell fragments

0.45-0.75	Poorly sorted, very coarse-grained to granule-sized pebbly fossiliferous grainstone; cross-bed sets (20 cm thick) indicate transport towards 85°
0.75-1.6	Well sorted, interbedded calcisiltite and very fine- to fine-grained grainstone; wavy and planar bedding; wave ripple laminations preserved throughout
1.6-1.8	Poorly sorted, granule-sized fossiliferous grainstone; unit grades laterally eastward into underlying unit; low angle stratification
1.8-2.15	Well sorted, medium-grained sandy grainstone; 35 cm thick cross-bed sets indicate transport towards 87°
2.15-2.85	Poorly sorted, coarse-grained to granule-sized fossiliferous sandy grainstone; sigmoidal cross-bedding is 40 cm thick and indicates transport towards 95°; single 10 cm thick, laterally discontinuous cross-bed indicates transport towards 277°
2.85-3.0	Poorly sorted, granule-sized fossiliferous grainstone; 15 cm thick cross-bed set indicates transport towards 268°;

Section SR-4

Height in section (m)	**Description**
0.0-0.4	Moderately to well sorted, coarse- to very coarse-grained fossiliferous grainstone with weakly preserved east directed sigmoidal crossbedding
0.4-0.55	Very well cemented fine-grained, well sorted sandy grainstone; structureless
0.55-0.8	Well sorted, fine-grained grainstone with poorly preserved wave ripple laminations; burrow mottling throughout
0.8-0.9	Very coarse-grained fossiliferous grainstone with 30 cm wavelength rippled surfaces; barnacle and bivalve fragments abundant;
0.9-0.95	Structureless, fine-grained sandy grainstone

0.95-1.95	Poorly sorted, coarse-grained to granule-sized fossiliferous grainstone; nearly pure carbonate; abundant barnacle and mollusk fragments; sigmoidal cross-beds 50 cm thick indicate transport towards 94°; pebbles appear in upper 20 cm
1.95-2.15	Structureless, fine-grained sandy grainstone
2.15-2.4	Interbedded coarse-grained grainstone and fine-grained grainstone; individual beds are 5 cm thick; base of uppermost coarse-grained grainstone bed has cobble lag
2.4-2.7	Well sorted, very fine-grained sandy grainstone; heavily bioturbated in basal 20 cm; upper 10 cm shows wavy bedding and lime mud drapes
2.7-3.05	Medium-grained sandy grainstone with minor granules; coarsens upward into pebbly granule-sized fossiliferous sandy grainstone; sigmoidal cross-bed 35 cm thick indicates transport towards 93°
3.05-3.75	Coarse- to very coarse grained grainstone and granule-sized fossiliferous sandy grainstone; minor pebbles throughout; sigmoidal cross-beds ranging from 20-30 cm thick are eastward directed; highly weathered
3.75-4.05	Structureless calcisiltite; heavily bioturbated
4.05-4.4	Heavily bioturbated, structureless, very fine-grained sandy grainstone; single 10 cm thick clam bed interbedded from 4.1-4.2 m;
4.4-4.75	Poorly sorted, very coarse-grained to granule-sized fossiliferous sandy grainstone with low angle stratification dipping 10° to the east;
4.75-5.65	Moderately sorted, granule-sized fossiliferous sandy grainstone with abundant barnacle and mollusk fragments; east directed cross-bedding is amalgamated

Continued on following page

Section SR-5

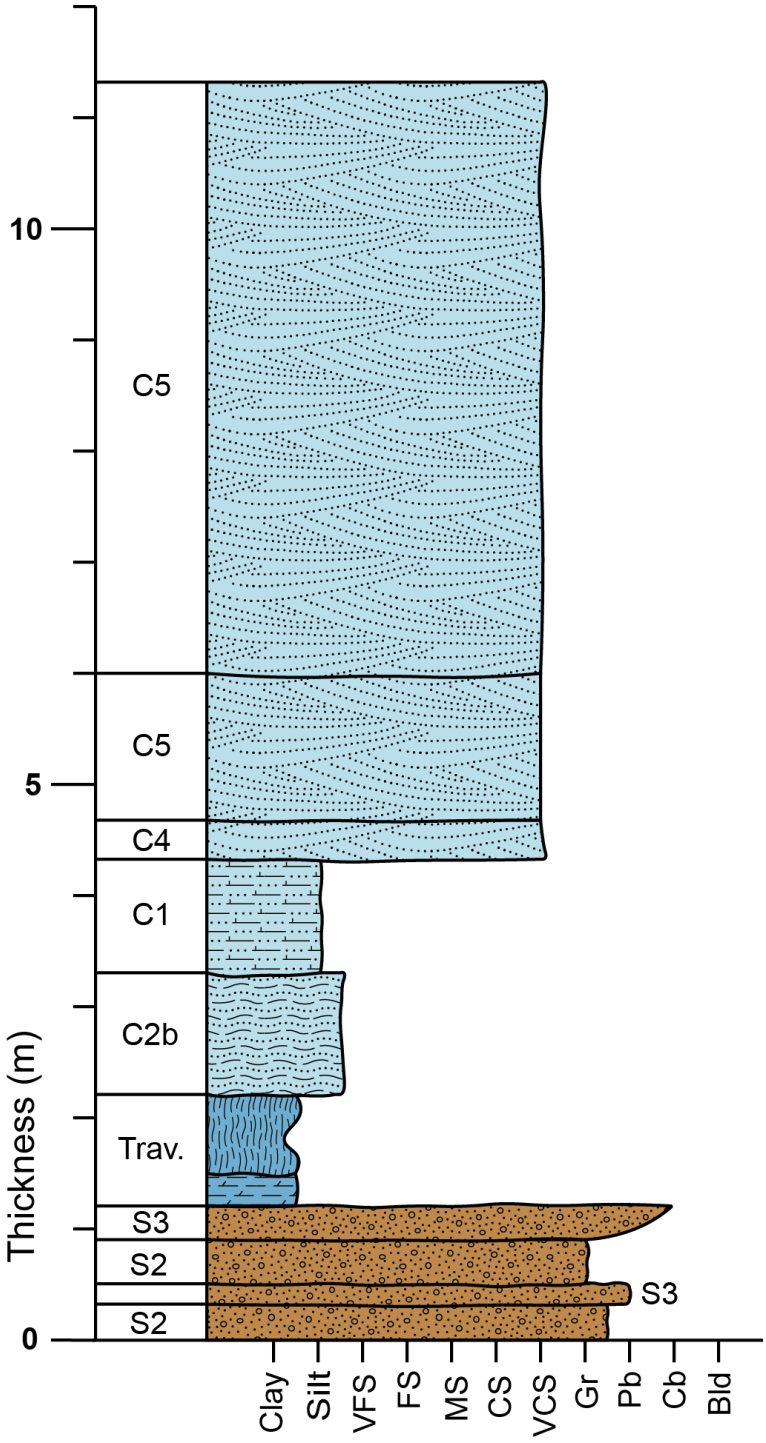
Thickness (m)
10
5
0
C5
C5
C4
C1
C2b
Trav.
S3
S2
S2
S3
Clay
Silt
VFS
FS
MS
CS
VCS
Gr
Pb
Cb
Bld

APPENDIX C

PETROGLYPH PARK PALEOCURRENT DATA

Latitude	Longitude	Dip	Dip Direction	Simple Dune Thickness (cm)	Surface Order
33.41242	-114.69668	29	196	15	1
33.41242	-114.69668	19	6	12	1
33.41242	-114.69668	22	355	15	1
33.41242	-114.69668	20	2	10	1
33.41242	-114.69668	27	202	x	1
33.41242	-114.69668	26	198	80	1
33.41242	-114.69668	27	186	123	1
33.41242	-114.69668	29	183	180	1
33.41242	-114.69668	23	188	55	1
33.41242	-114.69668	27	179	40	1
33.41242	-114.69668	29	181	1.2	1
33.41242	-114.69668	23	174	40	1
33.41242	-114.69668	27	184	50	1
33.41242	-114.69668	32	178	150	1
33.41242	-114.69668	22	177	60	1
33.41242	-114.69668	34	175	100	1
33.33576	-114.72308	35	141	x	1
33.33572	-114.72304	34	161	x	1
33.33572	-114.72305	36	146	x	1
33.33663	-114.72230	29	175	x	1
33.33706	-114.72189	15	357	x	1
33.33702	-114.72183	11	148	x	1
33.33699	-114.72188	10	9	x	1
33.33703	-114.72188	14	211	x	1

Latitude	Longitude	Dip	Dip Direction	Simple Dune Thickness (cm)	Surface Order
33.33654	-114.72185	9	322	x	1
33.33656	-114.72189	22	162	x	1
33.33658	-114.72146	23	209	x	1
33.33658	-114.72146	25	183	x	1
33.33659	-114.72136	15	356	x	1
33.33657	-114.72151	29	183	x	1
33.33653	-114.72144	29	179	x	1
33.33658	-114.72146	15	352	x	1
33.33657	-114.72143	22	334	x	1
33.33646	-114.72145	33	171	x	1
33.33648	-114.72149	37	171	x	1
33.33640	-114.72140	43	175	x	1
33.33637	-114.72154	23	179	x	1
33.33651	-114.72144	23	180	x	1
33.33650	-114.72144	35	172	x	1
33.33644	-114.72144	30	170	x	1
33.33653	-114.72150	26	172	x	1
33.33651	-114.72153	25	152	x	1
33.35907	-114.72657	38	335	x	1
33.35908	-114.72657	31	137	15	1
33.35906	-114.72655	23	134	12	1
33.35908	-114.72655	18	263	10	1
33.35899	-114.72662	29	264	x	1
33.33647	-114.72146	28	182	180	1
33.33673	-114.72134	21	181	100	1
33.33686	-114.72097	33	191	110	1
33.33677	-114.72124	20	175	x	1
33.33676	-114.72119	31	161	x	1
33.33685	-114.72116	26	161	x	1

Latitude	Longitude	Dip	Dip Direction	Simple Dune Thickness (cm)	Surface Order
33.33685	-114.72116	11	330	x	1
33.33693	-114.72134	16	164	x	1
33.33486	-114.72310	34	150	x	1
33.33531	-114.72350	28	144	x	1
33.33524	-114.72346	23	142	x	1
33.33516	-114.72324	31	149	x	1
33.35906	-114.72647	24	86	15	1
33.35905	-114.72645	13	90	5	1
33.35909	-114.72645	18	190	8	1
33.35918	-114.72620	20	185	4	1
33.35925	-114.72623	17	196	4	1
33.35928	-114.72629	19	266	3	1
33.35908	-114.72614	15	267	5	1
33.35914	-114.72629	18	265	5	1
33.35919	-114.72622	17	175	40	1
33.35922	-114.72624	15	100	35	1
33.35928	-114.72621	18	96	38	1
33.35915	-114.72646	15	96	15	1
33.35915	-114.72646	15	98	32	1
33.35914	-114.72657	21	86	40	1
33.35909	-114.72649	25	75	35	1
33.35909	-114.72649	31	72	25	1
33.33632	-114.72144	25	179	x	1
33.33594	-114.72264	29	149	x	1
33.33594	-114.72266	30	157	x	1
33.33591	-114.72271	31	134	x	1
33.33594	-114.72280	31	143	x	1
33.33594	-114.72280	32	152	x	1
33.33591	-114.72276	24	155	x	1

Latitude	Longitude	Dip	Dip Direction	Simple Dune Thickness (cm)	Surface Order
33.33638	-114.72075	24	284	x	1
33.33637	-114.72071	27	286	x	1
33.33641	-114.72142	39	160	x	1
33.33700	-114.72121	15	232	x	1
33.33704	-114.72122	19	226	x	1
33.33704	-114.72127	19	230	x	1
33.33548	-114.72314	16	168	x	1
33.33717	-114.72366	21	81	x	1
33.33706	-114.72366	28	83	x	1
33.33699	-114.72362	28	261	x	1
33.33722	-114.72368	29	281	x	1
33.33590	-114.72245	24	184	x	1
33.41242	-114.69668	14	190	N/A	2
33.41242	-114.69668	21	183	N/A	2
33.41242	-114.69668	22	185	N/A	2
33.41242	-114.69668	12	185	N/A	2
33.41242	-114.69668	13	190	N/A	2
33.41242	-114.69668	17	177	N/A	2
33.41242	-114.69668	11	192	N/A	2
33.41242	-114.69668	18	189	N/A	2
33.41242	-114.69668	18	181	N/A	2
33.41242	-114.69668	17	179	N/A	2
33.41242	-114.69668	14	186	N/A	2
33.41242	-114.69668	23	181	N/A	2
33.41242	-114.69668	13	175	N/A	2
33.41242	-114.69668	24	179	N/A	2
33.33580	-114.72307	26	133	N/A	2
33.33579	-114.72304	28	154	N/A	2
33.33658	-114.72146	9	210	N/A	2

Latitude	Longitude	Dip	Dip Direction	Simple Dune Thickness (cm)	Surface Order
33.33658	-114.72146	10	191	N/A	2
33.33659	-114.72153	29	186	N/A	2
33.33655	-114.72149	16	191	N/A	2
33.33650	-114.72139	27	170	N/A	2
33.33643	-114.72138	23	180	N/A	2
33.33640	-114.72139	20	180	N/A	2
33.33641	-114.72142	11	170	N/A	2
33.33648	-114.72156	21	167	N/A	2
33.33651	-114.72143	27	170	N/A	2
33.33639	-114.72152	37	164	N/A	2
33.33650	-114.72145	29	177	N/A	2
33.33651	-114.72151	23	153	N/A	2
33.33651	-114.72147	19	175	N/A	2
33.33681	-114.72117	13	181	N/A	2
33.33675	-114.72131	14	179	N/A	2
33.33679	-114.72120	12	193	N/A	2
33.33678	-114.72123	9	185	N/A	2
33.33684	-114.72121	22	160	N/A	2
33.33705	-114.72130	9	157	N/A	2
33.33483	-114.72313	20	123	N/A	2
33.33517	-114.72322	23	140	N/A	2
33.35909	-114.72654	19	77	N/A	2
33.35910	-114.72651	6	86	N/A	2
33.35913	-114.72652	18	99	N/A	2
33.35912	-114.72649	19	81	N/A	2
33.35913	-114.72655	19	77	N/A	2
33.35914	-114.72655	18	77	N/A	2
33.35915	-114.72652	12	107	N/A	2
33.33593	-114.72264	29	168	N/A	2

Latitude	Longitude	Dip	Dip Direction	Simple Dune Thickness (cm)	Surface Order
33.33596	-114.72266	30	152	N/A	2
33.33591	-114.72279	25	157	N/A	2
33.33596	-114.72279	24	143	N/A	2
33.33594	-114.72278	24	146	N/A	2
33.33589	-114.72281	16	140	N/A	2
33.33637	-114.72073	13	263	N/A	2

APPENDIX D

STALLARD AREA PALEOCURRENT DATA

Latitude	Longitude	Dip	Dip Direction	Simple Dune Thickness (cm)	Surface Order
33.35479	-114.72755	17	230	4	1
33.35481	-114.72741	12	262	10	1
33.35910	-114.72616	5	253	5	1
33.35479	-114.72755	20	85	25	1
33.35917	-114.72617	7	262	6	1
33.35485	-114.72742	18	96	20	1
33.35479	-114.72755	10	244	11	1
33.35487	-114.72745	10	273	15	1
33.35919	-114.72612	2	264	16	1
33.35479	-114.72755	21	96	50	1
33.35479	-114.72755	23	93	35	1
33.35299	-114.72734	20	100	120	1
33.35918	-114.72616	16	238	15	1
33.35482	-114.72744	25	97	25	1
33.35478	-114.72705	23	110	23	1
33.35479	-114.72755	35	349	80	1
33.35479	-114.72755	23	93	50	1
33.35479	-114.72755	6	265	10	1
33.35299	-114.72734	20	82	45	1
33.35918	-114.72618	24	80	22	1
33.35479	-114.72745	22	263	25	1
33.35911	-114.72649	23	209	15	1
33.35469	-114.72709	24	104	20	1
33.35479	-114.72755	35	100	40	1
33.35479	-114.72755	15	98	30	1

Latitude	Longitude	Dip	Dip Direction	Simple Dune Thickness (cm)	Surface Order
33.35479	-114.72755	15	259	15	1
33.35479	-114.72755	16	263	5	1
33.35299	-114.72734	24	103	40	1
33.35910	-114.72651	26	81	25	1
33.35908	-114.72642	21	181	5	1
33.35340	-114.72743	20	99	30	1
33.35915	-114.72621	7	179	8	1
33.35485	-114.72759	27	101	30	1
33.35466	-114.72705	16	106	30	1
33.35479	-114.72755	21	86	30	1
33.35479	-114.72755	14	265	12	1
33.35479	-114.72755	19	100	30	1
33.35299	-114.72734	21	102	110	1
33.35299	-114.72734	30	109	20	1
33.35339	-114.72747	13	277	30	1
33.35900	-114.72648	6	261	5	1
33.35913	-114.72646	24	80	20	1
33.35913	-114.72616	17	217	10	1
33.35484	-114.72753	33	96	130	1
33.35461	-114.72717	20	105	40	1
33.35479	-114.72755	26	96	25	1
33.35479	-114.72755	21	93	50	1
33.35479	-114.72755	17	258	10	1
33.35299	-114.72734	19	100	31	1
33.35299	-114.72734	20	101	25	1
33.35920	-114.72650	23	71	30	1
33.35905	-114.72640	23	91	45	1
33.35911	-114.72633	25	88	60	1
33.35491	-114.72754	30	96	130	1

Latitude	Longitude	Dip	Dip Direction	Simple Dune Thickness (cm)	Surface Order
33.35475	-114.72705	22	100	30	1
33.35923	-114.72623	25	80	50	1
33.35921	-114.72625	24	79	70	1
33.35908	-114.72629	26	79	65	1
33.35916	-114.72615	23	77	40	1
33.35482	-114.72738	26	104	15	1
33.35479	-114.72755	36	87	70	1
33.35479	-114.72755	21	89	15	1
33.35299	-114.72734	18	94	30	1
33.35299	-114.72734	24	91	20	1
33.35335	-114.72750	21	87	35	1
33.35872	-114.72669	26	101	40	1
33.35912	-114.72633	32	95	70	1
33.35479	-114.72755	25	82	60	1
33.35898	-114.72646	32	82	20	1
33.35892	-114.72644	25	93	35	1
33.35486	-114.72762	38	99	150	1
33.35474	-114.72721	23	93	120	1
33.35329	-114.72745	7	264	3	1
33.35479	-114.72755	6	97	N/A	2
33.35914	-114.72612	9	95	N/A	2
33.35482	-114.72746	9	101	N/A	2
33.35479	-114.72755	12	87	N/A	2
33.35915	-114.72622	12	92	N/A	2
33.35487	-114.72747	3	90	N/A	2
33.35479	-114.72755	8	87	N/A	2
33.35918	-114.72615	10	83	N/A	2
33.35475	-114.72739	11	87	N/A	2
33.35479	-114.72755	9	85	N/A	2

Latitude	Longitude	Dip	Dip Direction	Simple Dune Thickness (cm)	Surface Order
33.35479	-114.72755	10	91	N/A	2
33.35299	-114.72734	7	89	N/A	2
33.35921	-114.72623	16	81	N/A	2
33.35481	-114.72744	16	99	N/A	2
33.35473	-114.72707	8	100	N/A	2
33.35479	-114.72755	8	98	N/A	2
33.35479	-114.72755	9	82	N/A	2
33.35479	-114.72755	7	97	N/A	2
33.35299	-114.72734	8	92	N/A	2
33.35908	-114.72642	13	94	N/A	2
33.35918	-114.72623	15	85	N/A	2
33.35487	-114.72752	11	95	N/A	2
33.35469	-114.72709	8	94	N/A	2
33.35479	-114.72755	8	94	N/A	2
33.35479	-114.72755	8	91	N/A	2
33.35479	-114.72755	7	85	N/A	2
33.35479	-114.72755	9	86	N/A	2
33.35299	-114.72734	9	97	N/A	2
33.35341	-114.72749	7	100	N/A	2
33.35906	-114.72646	9	88	N/A	2
33.35905	-114.72640	13	81	N/A	2
33.35917	-114.72615	14	88	N/A	2
33.35471	-114.72712	8	106	N/A	2
33.35479	-114.72755	8	89	N/A	2
33.35479	-114.72755	8	89	N/A	2
33.35479	-114.72755	10	98	N/A	2
33.35299	-114.72734	5	102	N/A	2
33.35299	-114.72734	8	101	N/A	2
33.35908	-114.72644	11	87	N/A	2

Latitude	Longitude	Dip	Dip Direction	Simple Dune Thickness (cm)	Surface Order
33.35920	-114.72631	16	86	N/A	2
33.35486	-114.72751	20	97	N/A	2
33.35473	-114.72705	10	94	N/A	2
33.35479	-114.72755	7	83	N/A	2
33.35479	-114.72755	10	87	N/A	2
33.35479	-114.72755	10	92	N/A	2
33.35299	-114.72734	7	93	N/A	2
33.35299	-114.72734	7	100	N/A	2
33.35919	-114.72653	18	77	N/A	2
33.35904	-114.72633	9	102	N/A	2
33.35914	-114.72629	15	94	N/A	2
33.35489	-114.72756	13	93	N/A	2
33.35467	-114.72708	11	101	N/A	2
33.35921	-114.72623	15	78	N/A	2
33.35917	-114.72621	10	83	N/A	2
33.35922	-114.72614	15	84	N/A	2
33.35480	-114.72740	12	97	N/A	2
33.35479	-114.72755	13	84	N/A	2
33.35479	-114.72755	10	93	N/A	2
33.35299	-114.72734	8	97	N/A	2
33.35299	-114.72734	10	98	N/A	2
33.35328	-114.72743	12	92	N/A	2
33.35907	-114.72651	20	79	N/A	2
33.35906	-114.72648	16	95	N/A	2
33.35915	-114.72636	13	89	N/A	2
33.35482	-114.72772	20	90	N/A	2
33.35475	-114.72710	13	88	N/A	2
33.35481	-114.72756	10	97	N/A	2
33.35337	-114.72745	7	87	N/A	2

Latitude	Longitude	Dip	Dip Direction	Simple Dune Thickness (cm)	Surface Order
33.35911	-114.72651	13	85	N/A	2
33.35318	-114.72736	16	90	N/A	2
33.35913	-114.72631	12	93	N/A	2
33.35867	-114.72668	14	98	N/A	2
33.35479	-114.72755	10	102	N/A	2

APPENDIX E

BEDDING MEASUREMENTS

(DATUM: WGS84); STRIKE/DIP FOLLOW RIGHT HAND RULE

Latitude	Longitude	Strike	Dip	Facies
33.29334134	-114.7685605	25	8	Bioclastic Grainstone
33.29537735	-114.76512115	2	4	Bioclastic Grainstone
33.29537437	-114.76449863	329	5	Bioclastic Grainstone
33.29530837	-114.7645138	36	6	Bioclastic Grainstone
33.31260505	-114.74223286	358	5	Bioclastic Grainstone
33.29916806	-114.75978926	12	11	Bioclastic Grainstone
33.29407493	-114.77170522	15	7	Bioclastic Grainstone
33.29537735	-114.76512115	2	4	Bioclastic Grainstone
33.33637131	-114.72073437	167	6	Bioclastic Grainstone
33.31260505	-114.74223286	358	5	Bioclastic Grainstone
33.29530837	-114.7645138	36	6	Bioclastic Grainstone
33.29407493	-114.77170522	15	7	Bioclastic Grainstone
33.29537735	-114.76512115	2	4	Bioclastic Grainstone
33.33611914	-114.72151648	175	5	Bioclastic Grainstone
33.33633581	-114.72147734	211	5	Bioclastic Grainstone
33.41241757	-114.69667553	27	2	Bioclastic Grainstone
33.41241757	-114.69667553	37	3	Bioclastic Grainstone
33.35901276	-114.72673791	8	9	Bioclastic Grainstone
33.29537735	-114.76512115	2	4	Bioclastic Grainstone
33.29334134	-114.7685605	25	8	Bioclastic Grainstone
33.29921094	-114.76009268	11	21	Bioclastic Grainstone
33.29919841	-114.76006703	31	32	Bioclastic Grainstone
33.29925046	-114.76006385	30	29	Bioclastic Grainstone
33.29923893	-114.76005899	21	26	Bioclastic Grainstone
33.29916806	-114.75978926	12	11	Bioclastic Grainstone
33.29537437	-114.76449863	329	5	Bioclastic Grainstone

Latitude	Longitude	Strike	Dip	Facies
33.29530837	-114.7645138	36	6	Bioclastic Grainstone
33.29532861	-114.76472762	1	6	Bioclastic Grainstone
33.35865397	-114.72603492	350	3	Bioclastic Grainstone
33.35864161	-114.72607926	349	2	Bioclastic Grainstone
33.35903212	-114.72648134	356	3	Bioclastic Grainstone
33.35918081	-114.72644337	351	8	Bioclastic Grainstone
33.33633581	-114.72147734	211	5	Bioclastic Grainstone
33.33633581	-114.72147734	210	5	Bioclastic Grainstone
33.33637131	-114.72073437	167	6	Bioclastic Grainstone
33.33637123	-114.7207047	191	11	Bioclastic Grainstone
33.33699878	-114.72121314	142	15	Bioclastic Grainstone
33.3370396	-114.72121792	136	19	Bioclastic Grainstone
33.33703826	-114.72127374	140	19	Bioclastic Grainstone
33.33528732	-114.72281174	78	3	Bioclastic Grainstone
33.29407493	-114.77170522	15	7	Bioclastic Grainstone
33.29230034	-114.7736755	219	16	Bioclastic Grainstone
33.29230435	-114.7736797	224	23	Bioclastic Grainstone
33.29223234	-114.7735846	112	7	Bioclastic Grainstone
33.29233776	-114.7736421	121	8	Bioclastic Grainstone
33.29234606	-114.7736491	144	7	Bioclastic Grainstone
33.2923466	-114.7736413	122	12	Bioclastic Grainstone
33.29234814	-114.7736785	124	10	Bioclastic Grainstone
33.29235212	-114.7736735	140	12	Bioclastic Grainstone
33.29236214	-114.7736692	156	8	Bioclastic Grainstone
33.29236839	-114.7736538	154	8	Bioclastic Grainstone
33.29236078	-114.7736637	143	8	Bioclastic Grainstone
33.2918629	-114.7764816	99	6	Bioclastic Grainstone
33.2919358	-114.7764584	102	9	Bioclastic Grainstone
33.29192782	-114.7764561	100	8	Bioclastic Grainstone
33.29188818	-114.7764673	85	6	Bioclastic Grainstone

Latitude	Longitude	Strike	Dip	Facies
33.29184421	-114.7765077	30	6	Bioclastic Grainstone
33.29185063	-114.7764738	82	7	Bioclastic Grainstone
33.29186042	-114.7764869	63	8	Bioclastic Grainstone
33.29289291	-114.7716174	4	13	Bioclastic Grainstone
33.29289291	-114.7716174	350	21	Bioclastic Grainstone
33.29289291	-114.7716174	347	18	Bioclastic Grainstone
33.29289291	-114.7716174	359	20	Bioclastic Grainstone
33.29289291	-114.7716174	330	19	Bioclastic Grainstone
33.29289291	-114.7716174	338	12	Bioclastic Grainstone
33.29289291	-114.7716174	332	13	Bioclastic Grainstone
33.30166244	-114.7612532	232	18	Bioclastic Grainstone
33.30169501	-114.7612611	218	12	Bioclastic Grainstone
33.30164705	-114.7612657	210	16	Bioclastic Grainstone
33.30162896	-114.7612289	215	18	Bioclastic Grainstone
33.30161145	-114.7612241	24	7	Bioclastic Grainstone
33.30162549	-114.7612263	31	15	Bioclastic Grainstone
33.30160584	-114.761225	26	15	Bioclastic Grainstone
33.30163822	-114.761201	26	11	Bioclastic Grainstone
33.30168689	-114.7611678	42	14	Bioclastic Grainstone
33.301757	-114.7618128	13	2	Bioclastic Grainstone
33.30180807	-114.7618352	29	4	Bioclastic Grainstone
33.30174179	-114.7618145	27	2	Bioclastic Grainstone
33.30174889	-114.7618305	52	5	Bioclastic Grainstone
33.3017477	-114.7618281	356	2	Bioclastic Grainstone
33.30171856	-114.7618144	340	9	Bioclastic Grainstone
33.30170917	-114.761831	333	10	Bioclastic Grainstone
33.30170603	-114.7618655	359	8	Bioclastic Grainstone
33.30171077	-114.7618759	349	6	Bioclastic Grainstone
33.30170634	-114.7618645	12	9	Bioclastic Grainstone
33.30172628	-114.7618784	192	5	Bioclastic Grainstone

Latitude	Longitude	Strike	Dip	Facies
33.30174117	-114.7618631	162	9	Bioclastic Grainstone
33.30172206	-114.7618773	157	8	Bioclastic Grainstone
33.3017164	-114.7618946	183	10	Bioclastic Grainstone
33.30172942	-114.7618718	176	14	Bioclastic Grainstone
33.30175241	-114.7618324	170	17	Bioclastic Grainstone
33.30175221	-114.7618292	172	18	Bioclastic Grainstone
33.30173546	-114.7618265	160	20	Bioclastic Grainstone
33.30174795	-114.7618365	170	18	Bioclastic Grainstone
33.29537164	-114.765151	348	4	Bioclastic Grainstone
33.29535053	-114.7651487	57	3	Bioclastic Grainstone
33.29535341	-114.7651491	28	2	Bioclastic Grainstone
33.29532182	-114.7650552	53	16	Bioclastic Grainstone
33.29532032	-114.7650577	57	19	Bioclastic Grainstone
33.29533121	-114.7650332	56	23	Bioclastic Grainstone
33.2953133	-114.7650416	57	16	Bioclastic Grainstone
33.29531461	-114.7650457	47	16	Bioclastic Grainstone
33.29530986	-114.7650366	54	16	Bioclastic Grainstone
33.32087652	-114.736756	355	8	Bioclastic Grainstone
33.32039261	-114.7365388	14	6	Bioclastic Grainstone
33.32050692	-114.7365883	348	13	Bioclastic Grainstone
33.29546691	-114.7621652	59	36	Bioclastic Grainstone
33.29547971	-114.7621655	68	33	Bioclastic Grainstone
33.29547256	-114.762138	84	26	Bioclastic Grainstone
33.29546189	-114.7621183	100	18	Bioclastic Grainstone
33.29546235	-114.7621078	81	22	Bioclastic Grainstone
33.29553771	-114.7619751	355	25	Bioclastic Grainstone
33.29555946	-114.76203	14	30	Bioclastic Grainstone
33.29552322	-114.7619819	19	24	Bioclastic Grainstone
33.29550942	-114.7620092	53	33	Bioclastic Grainstone
33.29549239	-114.7620435	69	26	Bioclastic Grainstone

Latitude	Longitude	Strike	Dip	Facies
33.29549722	-114.7621049	62	25	Bioclastic Grainstone
33.29549056	-114.7621535	66	37	Bioclastic Grainstone
33.29550921	-114.7621539	66	33	Bioclastic Grainstone
33.29553159	-114.7621363	90	31	Bioclastic Grainstone
33.29552905	-114.7621109	87	29	Bioclastic Grainstone
33.30034232	-114.7600729	297	21	Bioclastic Grainstone
33.30034492	-114.7600738	323	22	Bioclastic Grainstone
33.30032845	-114.7600752	316	20	Bioclastic Grainstone
33.30033306	-114.7600933	320	24	Bioclastic Grainstone
33.30030116	-114.7600375	288	27	Bioclastic Grainstone
33.30030827	-114.7600525	288	27	Bioclastic Grainstone
33.30029384	-114.7600651	299	24	Bioclastic Grainstone
33.30177537	-114.7618764	178	11	Bioclastic Grainstone
33.30175741	-114.7618854	186	17	Bioclastic Grainstone
33.30176084	-114.7618482	159	18	Bioclastic Grainstone
33.30185843	-114.7621914	11	4	Bioclastic Grainstone
33.3017866	-114.7622135	22	11	Bioclastic Grainstone
33.30150876	-114.76322	285	2	Bioclastic Grainstone
33.41241757	-114.69667553	39	6	Green Claystone
33.41241757	-114.69667553	39	6	Green Claystone
33.41241757	-114.69667553	33	7	Green Claystone
33.41241757	-114.69667553	45	5	Heterolithic Facies
33.41241757	-114.69667553	95	6	Heterolithic Facies
33.35483534	-114.72762831	9	4	Heterolithic Facies
33.35915186	-114.72623616	5	3	Heterolithic Facies
33.33592426	-114.72377909	32	7	Heterolithic Facies
33.35324924	-114.72752715	1	7	Heterolithic Facies
33.41241757	-114.69667553	29	3	Heterolithic Facies
33.41241757	-114.69667553	37	2	Heterolithic Facies
33.41241757	-114.69667553	26	6	Heterolithic Facies

Latitude	Longitude	Strike	Dip	Facies
33.41241757	-114.69667553	323	4	Heterolithic Facies
33.41241757	-114.69667553	38	6	Heterolithic Facies
33.41241757	-114.69667553	22	2	Heterolithic Facies
33.41241757	-114.69667553	308	4	Heterolithic Facies
33.41241757	-114.69667553	30	6	Heterolithic Facies
33.41241757	-114.69667553	7	6	Heterolithic Facies
33.41241757	-114.69667553	42	6	Heterolithic Facies
33.41241757	-114.69667553	45	5	Heterolithic Facies
33.35479222	-114.72755393	64	7	Heterolithic Facies
33.35479222	-114.72755393	94	3	Heterolithic Facies
33.35479222	-114.72755393	94	3	Heterolithic Facies
33.35479222	-114.72755393	38	2	Heterolithic Facies
33.35479222	-114.72755393	74	5	Heterolithic Facies
33.35324924	-114.72752715	1	7	Heterolithic Facies
33.35915186	-114.72623616	5	3	Heterolithic Facies
33.35478975	-114.72776217	360	7	Heterolithic Facies
33.35483534	-114.72762831	9	6	Heterolithic Facies
33.35459751	-114.72726387	6	6	Heterolithic Facies
33.30208092	-114.7624066	23	5	Heterolithic Facies
33.3020978	-114.7624418	11	3	Heterolithic Facies
33.30209455	-114.7624317	46	3	Heterolithic Facies
33.30210887	-114.7624119	19	4	Heterolithic Facies
33.30209308	-114.7624028	27	4	Heterolithic Facies
33.30210105	-114.7623707	60	5	Heterolithic Facies
33.30205384	-114.7623778	53	4	Heterolithic Facies
33.35459751	-114.72726387	6	6	Heterolithic Facies
33.33592426	-114.72377909	32	7	Heterolithic Facies
33.2957667	-114.7653923	64	4	Heterolithic Facies
33.29569606	-114.7653429	50	6	Heterolithic Facies
33.29573717	-114.7654733	17	5	Heterolithic Facies

Latitude	Longitude	Strike	Dip	Facies
33.2957585	-114.7655232	41	3	Heterolithic Facies
33.29573708	-114.7654912	6	3	Heterolithic Facies
33.29581661	-114.765369	33	23	Heterolithic Facies
33.29583842	-114.7653751	47	6	Heterolithic Facies
33.29618687	-114.7667968	83	5	Heterolithic Facies
33.29619205	-114.7667993	39	3	Heterolithic Facies
33.29620557	-114.7667918	114	3	Heterolithic Facies
33.29620082	-114.7667856	48	3	Heterolithic Facies
33.29619892	-114.7667862	79	3	Heterolithic Facies
33.29618142	-114.7667759	84	4	Heterolithic Facies
33.29619749	-114.7668306	51	5	Heterolithic Facies
33.29619631	-114.7668237	66	5	Heterolithic Facies
33.29619767	-114.7668724	91	4	Heterolithic Facies
33.29619669	-114.7668835	74	5	Heterolithic Facies
33.2967167	-114.7670405	32	9	Heterolithic Facies
33.2967111	-114.7670802	38	8	Heterolithic Facies
33.29671915	-114.7670555	13	8	Heterolithic Facies
33.29673201	-114.7670554	11	7	Heterolithic Facies
33.2967384	-114.767002	70	4	Heterolithic Facies
33.29674882	-114.7669558	74	4	Heterolithic Facies
33.29674415	-114.7669495	95	6	Heterolithic Facies
33.29675075	-114.7669512	85	5	Heterolithic Facies
33.29675208	-114.7669494	80	5	Heterolithic Facies
33.29676332	-114.7669546	71	6	Heterolithic Facies
33.30549374	-114.7538809	19	9	Heterolithic Facies
33.30547201	-114.7538981	33	5	Heterolithic Facies
33.30544416	-114.7538834	112	1	Heterolithic Facies
33.3055135	-114.7540241	47	4	Heterolithic Facies
33.30516029	-114.7550061	61	4	Heterolithic Facies
33.30517381	-114.7550005	98	4	Heterolithic Facies

Latitude	Longitude	Strike	Dip	Facies
33.30514613	-114.7549816	70	4	Heterolithic Facies
33.3051434	-114.7549723	89	4	Heterolithic Facies
33.30513922	-114.7549829	81	4	Heterolithic Facies
33.30513609	-114.754991	65	6	Heterolithic Facies
33.3051291	-114.7549916	51	4	Heterolithic Facies
33.30512898	-114.7549841	34	5	Heterolithic Facies
33.30512629	-114.7549888	51	4	Heterolithic Facies
33.30713895	-114.7481669	359	3	Heterolithic Facies
33.30711906	-114.7481969	3	6	Heterolithic Facies
33.30695345	-114.7479986	40	5	Heterolithic Facies
33.30699386	-114.7480735	33	4	Heterolithic Facies
33.30709338	-114.7480849	24	5	Heterolithic Facies
33.30709727	-114.7481065	10	6	Heterolithic Facies
33.30708795	-114.7481292	7	4	Heterolithic Facies
33.30708999	-114.7481175	3	6	Heterolithic Facies
33.30710237	-114.7481802	23	6	Heterolithic Facies
33.30710047	-114.7481712	21	5	Heterolithic Facies
33.30707464	-114.7481633	9	5	Heterolithic Facies
33.30705664	-114.7481363	72	4	Heterolithic Facies
33.30704654	-114.7481401	31	6	Heterolithic Facies
33.30706441	-114.7481522	24	5	Heterolithic Facies
33.30707419	-114.7481519	27	4	Heterolithic Facies
33.31157759	-114.7421445	43	5	Heterolithic Facies
33.30949522	-114.7450357	27	5	Heterolithic Facies
33.31237961	-114.7412016	19	2	Heterolithic Facies
33.31205648	-114.7415502	89	7	Heterolithic Facies
33.31206869	-114.7415451	94	8	Heterolithic Facies
33.31232628	-114.7440408	356	3	Heterolithic Facies
33.31233363	-114.7440306	352	3	Heterolithic Facies
33.31233302	-114.744043	26	5	Heterolithic Facies

Latitude	Longitude	Strike	Dip	Facies
33.31236227	-114.7440753	18	5	Heterolithic Facies
33.31230849	-114.7439903	23	5	Heterolithic Facies
33.31230671	-114.7439875	49	6	Heterolithic Facies
33.31226055	-114.7439528	67	7	Heterolithic Facies
33.31223806	-114.7439658	3	4	Heterolithic Facies
33.31227244	-114.7439911	346	4	Heterolithic Facies
33.32042668	-114.7370554	21	5	Heterolithic Facies
33.3203748	-114.7370791	9	7	Heterolithic Facies
33.32062881	-114.7369897	357	11	Heterolithic Facies
33.32062013	-114.7369681	357	8	Heterolithic Facies
33.32062502	-114.7369896	22	10	Heterolithic Facies
33.32061735	-114.7369814	25	7	Heterolithic Facies
33.32058023	-114.7369245	5	6	Heterolithic Facies
33.32053736	-114.736902	353	3	Heterolithic Facies
33.32054909	-114.7369708	33	7	Heterolithic Facies
33.30152188	-114.7632462	4	6	Heterolithic Facies
33.30154452	-114.7632065	141	6	Heterolithic Facies
33.30142097	-114.7632252	81	4	Heterolithic Facies
33.30155026	-114.7632644	2	4	Heterolithic Facies
33.30151964	-114.7632306	324	6	Heterolithic Facies
33.41241757	-114.69667553	23	3	Red MS/Siltstone
33.29403465	-114.75639132	27	10	Red MS/Siltstone
33.29403465	-114.75639132	27	10	Red MS/Siltstone
33.30047735	-114.7421773	26	7	Red MS/Siltstone
33.30047842	-114.7421734	48	10	Red MS/Siltstone
33.30045095	-114.7421839	32	7	Red MS/Siltstone
33.30042956	-114.7421751	48	8	Red MS/Siltstone
33.30046644	-114.7421838	47	6	Red MS/Siltstone
33.29339126	-114.76855455	28	6	Reworked Conglomerate
33.34892442	-114.72953964	339	58	Tv

Latitude	Longitude	Strike	Dip	Facies
33.34892442	-114.72953964	339	58	Tv
33.30117572	-114.7724227	346	39	Tv
33.30122484	-114.7724182	355	47	Tv
33.30122551	-114.7724743	357	55	Tv
33.30120394	-114.7724773	355	57	Tv
33.31539547	-114.74147455	52	13	UBM
33.29289858	-114.7716139	7	125	UBM
33.29289868	-114.771636	8	134	UBM
33.29486856	-114.7669698	44	8	UBM
33.29485064	-114.7669498	46	6	UBM
33.29481946	-114.7668464	46	6	UBM
33.29474443	-114.7668726	38	7	UBM
33.29481398	-114.7668645	15	5	UBM
33.29482367	-114.7668584	42	6	UBM
33.30144013	-114.7599591	344	5	Upper Marl
33.30147128	-114.7599686	1	4	Upper Marl
33.30145459	-114.7599862	343	5	Upper Marl
33.30142297	-114.759962	343	5	Upper Marl
33.30142809	-114.7599467	348	6	Upper Marl
33.30139209	-114.7599128	338	7	Upper Marl
33.30139691	-114.7599398	325	7	Upper Marl
33.29478249	-114.7670179	42	6	Upper Marl
33.29481811	-114.7669522	44	6	Upper Marl
33.29477241	-114.7668693	37	4	Upper Marl
33.29471349	-114.7668937	31	5	Upper Marl
33.29481185	-114.7672068	63	5	Upper Marl

REFERENCES CITED

Ainsworth, R.B., Hasiotis, S.T., Amos, K.J., Krapf, C.B.E., Payenberg, T.H.D., Sandstrom, M.L., Vakarelov, B.K., Lang, S.C., 2012. Tidal signatures in an intracratonic playa lake. Geology 40, 607–610. https://doi.org/10.1130/G32993.1

Allen, J.R.L., 1980. Sand waves: A model of origin and internal structure. Sedimentary Geology 26, 281–328. https://doi.org/10.1016/0037-0738(80)90022-6

Allen, J.R.L., 1982. Sedimentary structures, their character and physical basis (Vol. 2). Developments in Sedimentology 30B 2, 645.

Ashley, G.M., 1990. Classification of Large-Scale Subaqueous Bedforms: A New Look at an Old Problem. Journal of Sedimentary Petrology 60, 160–172. https://doi.org/10.2110/jsr.60.160

Beard, L.S., Haxel, G.B., Dorsey, R.J., McDougall, K., Jacobson, C.E., 2016. Late Neogene deformation of the Chocolate Mountains Anticlinorium: implications for deposition of the Bouse Formation and early evolution of the Lower Colorado River. Going LOCO, investigations along the Lower Colorado River 176–184.

Beletsky, D., Saylor, J.H., Schwab, D.J., 1999. Mean circulation in the Great Lakes. Journal of Great Lakes Research 25, 78–93. https://doi.org/10.1016/S0380-1330(99)70718-5

Berné, S., 2000. Architecture, dynamics and preservation of marine sand waves (large dunes). Marine Sandwave Dynamics, International Workshop 25–28.

Blair, T.C., 1999. Sedimentology of gravelly Lake Lahontan highstand shoreline deposits, Churchill Butte, Nevada, USA. Sedimentary Geology 123, 199–218. https://doi.org/10.1016/S0037-0738(98)00138-9

Bright, J., Cohen, A.S., Dettman, D.L., Pearthree, P.A., 2018a. Freshwater plumes and brackish lakes: Integrated microfossil and O-C-Sr isotopic evidence from the late Miocene and early Pliocene Bouse Formation (California-Arizona) supports a lake overflow model for the integration of the lower Colorado River corridor. Geosphere 14, 1875–1911. https://doi.org/10.1130/GES01610.1

Bright, J., Cohen, A.S., Dettman, D.L., Pearthree, P.A., Dorsey, R.J., Homan, M.B., 2016. Did a Catastrophic Lake Spillover Integrate the Late Miocene Early Pliocene Colorado River and the Gulf of California?: Microfaunal and Stable Isotope Evidence From Blythe Basin, California-Arizona, Usa. Palaios 31, 81–91. https://doi.org/10.2110/palo.2015.035

Bright, J., Cohen, A.S., Starratt, S.W., 2018b. Distinguishing brackish lacustrine from brackish marine deposits in the stratigraphic record: A case study from the late Miocene and early Pliocene Bouse Formation, Arizona and California, USA. Earth-Science Reviews.

Brown, J.M., Davies, A.G., 2010. Flood/ebb tidal asymmetry in a shallow sandy estuary and the impact on net sand transport. Geomorphology 114, 431–439. https://doi.org/10.1016/j.geomorph.2009.08.006

Buising, A. V, 1990. The Bouse Formation and bracketing units, southeastern California and western Arizona: Implications for the evolution of the Proto-Gulf of California and the lower Colorado River. Journal of Geophysical Research 95, 20111–20132. https://doi.org/10.1029/jb095ib12p20111

Bye, J.A.T., Will, G.D., 1989. The hydrogeology of the filling, in: Bonython, C.W., Fraser, A.S. (Eds.), The Great Filling of Lake Eyre in 1974. Royal Geographical Society of Australasia, South Australia Branch, pp. 32–43.

Crossey, L.C., Karlstrom, K.E., Dorsey, R., Pearce, J., Wan, E., Beard, L.S., Asmerom, Y., Polyak, V., Crow, R.S., Cohen, A., Bright, J., Pecha, M.E., 2015. Importance of groundwater in propagating downward integration of the 6–5 Ma Colorado River system: Geochemistry of springs, travertines, and lacustrine carbonates of the Grand Canyon region over the past 12 Ma. Geosphere 11, 660–682. https://doi.org/10.1130/GES01073.1

Daidu, F., Yuan, W., Min, L., 2013. Classifications, sedimentary features and facies associations of tidal flats. Journal of Palaeogeography 2, 66–80. https://doi.org/10.3724/SP.J.1261.2013.00018

Dalrymple, R.W., 1984. Morphology and internal structure of sandwaves in the Bay of Fundy. Sedimentology 31, 365–382. https://doi.org/10.1111/j.1365-3091.1984.tb00865.x

Dalrymple, R.W., Choi, K., 2007. Morphologic and facies trends through the fluvial-marine transition in tide-dominated depositional systems: A schematic framework for environmental and sequence-stratigraphic interpretation. Earth-Science Reviews 81, 135–174. https://doi.org/10.1016/j.earscirev.2006.10.002

Dalrymple, R.W., Knight, R.J., Zaitlin, B.A., Middleton, G. V., 1990. Dynamics and facies model of a macrotidal sand-bar complex, Cobequid Bay-Salmon River Estuary (Bay of Fundy). Sedimentology 37, 577–612. https://doi.org/10.1111/j.1365-3091.1990.tb00624.x

Dalrymple, R.W., Zaitlin, B.A., Boyd, R., 1992. Estuarine facies models; conceptual basis and stratigraphic implications. Journal of Sedimentary Research 62, 1130–1146.

Davis Jr, R.A., Fox, W.T., Hayes, M.O., Boothroyd, J.C., 1972. Comparison of ridge and runnel systems in tidal and non-tidal environments. Journal of Sedimentary Research 42.

Davis, Richard A, 2012. Tidal signatures and their preservation potential in stratigraphic sequences, in: Principles of Tidal Sedimentology. Springer, pp. 35–55.

Davis, Richard A., 2012. Principles of Tidal Sedimentology, Principles of Tidal Sedimentology. Springer Netherlands, Dordrecht. https://doi.org/10.1007/978-94-007-0123-6

Dillon, J.T., 1976. Geology of the Chocolate and Cargo Muchacho Mountins, southeasternmost California. University of California (Doctoral Dissertation).

Dorsey, R.J., Connell, B.O., Homan, M.B., Howard, K.A., 2016. Upper limestone of the southern Bouse Formation: evidence for unsteady origins of the Colorado River. Going LOCO, investigations along the Lower Colorado River 145–153.

Dorsey, R.J., O'Connell, B., Homan, M., Bennett, S.E.K., 2017. Influence of the Eastern California Shear Zone on deposition of the Mio–Pliocene Bouse Formation: Insights from the Cibola area, Arizona, in: Desert Symposium Field Guide and Proceedings. California State University Desert Studies Center, Zzyzx, CA. pp. 150–157.

Dorsey, R.J., O'Connell, B., McDougall, K., Homan, M.B., 2018. Punctuated Sediment Discharge during Early Pliocene Birth of the Colorado River: Evidence from Regional Stratigraphy, Sedimentology, and Paleontology. Sedimentary Geology 363, 1–33. https://doi.org/10.1016/j.sedgeo.2017.09.018

Dronkers, J., 1986. Tidal asymmetry and estuarine morphology. Netherlands Journal of Sea Research 20, 117–131. https://doi.org/10.1016/0077-7579(86)90036-0

Fenies, H., Tastet, J.P., 1998. Facies and architecture of an estuarine tidal bar (the Trompeloup bar, Gironde Estuary, SW France). Marine Geology 150, 149–169. https://doi.org/10.1016/S0025-3227(98)00059-0

Flemming, B.W., 2000. The role of grain size, water depth and flow velocity as scaling factors controlling the size of subaqueous dunes, in: Proceedings of Marine Sandwave Dynamics. pp. 55–61.

Fortunato, A.B., Oliveira, A., 2005. Influence of intertidal flats on tidal asymmetry. Journal of Coastal Research 1062–1067.

Fraser, G.S., Hester, N.C., 1977. Sediments and Sedimentary Structures of a Beach-Ridge Complex, Southwestern Shore of Lake Michigan. SEPM Journal of Sedimentary Research Vol. 47, 1187–1200. https://doi.org/10.1306/212F7306-2B24-11D7-8648000102C1865D

Gierlowski-Kordesch, E.H., 2010. Lacustrine carbonates, in: Developments in Sedimentology. Elsevier, pp. 1–101.

Homan, M.B., 2014. Sedimentology and stratigraphy of the Miocene-Pliocene Bouse Formation near Cibola, Arizona and Milpitas Wash, California: Implications for the early evolution of the Colorado River. Unpub. M.S. Thesis, University of Oregon Eugene, OR.

House, P.K., Pearthree, P.A., Perkins, M.E., 2008. Stratigraphic evidence for the role of lake spillover in the inception of the lower Colorado River in southern Nevada and western Arizona. Late Cenozoic Drainage History of the Southwestern Great Basin and Lower Colorado River Region: Geologic and Biotic Perspectives: Geological Society of America Special Paper 439 80301, 335–353. https://doi.org/10.1130/2008.2439(15).

Ingram, B.L., Conrad, M.E., Ingle, J.C., 1996. Stable isotope and salinity systematics in estuarine waters and carbonates: San Francisco Bay. Geochimica et Cosmochimica Acta 60, 455–467. https://doi.org/10.1016/0016-7037(95)00398-3

Kang, J.W., Jun, K.S., 2003. Flood and ebb dominance in estuaries in Korea. Estuarine, Coastal and Shelf Science 56, 187–196.

Kvale, E.P., Cutright, J., BIlodeau, D., Archer, A., Johnson, H.R., Pickett, B., 1995. Analysis of modern tides and implications for ancient tidalites. Continental Shelf Research 15. https://doi.org/10.1016/0278-4343(95)00001-H

Lichter, J., 1995. Lake Michigan Beach-Ridge and Dune Development, Lake Level, and Variability in Regional Water Balance. Quaternary Research 44, 181–189. https://doi.org/10.1006/qres.1995.1062

Longhitano, S.G., 2013. A facies-based depositional model for ancient and modern, tectonically-confined tidal straits. Terra Nova 25, 446–452. https://doi.org/10.1111/ter.12055

Longhitano, S.G., Mellere, D., Steel, R.J., Ainsworth, R.B., 2012. Tidal depositional systems in the rock record: A review and new insights. Sedimentary Geology 279, 2–22. https://doi.org/10.1016/j.sedgeo.2012.03.024

Longhitano, S.G., Steel, R.J., 2017. Deflection of the progradational axis and asymmetry in tidal seaway and strait deltas: insights from two outcrop case studies. Geological Society, London, Special Publications 444, 141–172. https://doi.org/10.1144/SP444.8

McDougall, K., 2008. Late Neogene marine incursions and the ancestral Gulf of California Late Neogene marine incursions and the ancestral Gulf of California. Late Cenozoic Drainage History of the Southwestern Great Basin and Lower Colorado River Region: Geologic and Biotic Perspectives 439, 355–373. https://doi.org/10.1130/2008.2439(16).

McDougall, K., Miranda-Martínez, A.Y.M., 2014. Evidence for a marine incursion along the lower Colorado River corridor. Geosphere 10, 842–869. https://doi.org/10.1130/GES00975.1

Metzger, D.G., 1968. The Bouse Formation (Pliocene) of the Parker-Blythe-Cibola area, Arizona and California, U.S. Geological Survey Professional Paper 600-D.

Metzger, D.G., Loeltz, O.J., Irelan, B., 1973. Geohydrology of the Parker-Blythe-Cibola area, Arizona and California.

Miller, D.M., Reynolds, R.E., Bright, J.E., Starratt, S.W., 2014. Bouse formation in the Bristol basin near Amboy, California, USA. Geosphere 10, 462–475. https://doi.org/10.1130/GES00934.1

Moore, R.D., Wolf, J., Souza, A.J., Flint, S.S., 2009. Morphological evolution of the Dee Estuary, Eastern Irish Sea, UK: a tidal asymmetry approach. Geomorphology 103, 588–596.

O'Connell, B., 2016. Sedimentology and Depositional History of the Miocene-Pliocene Bouse Formation, Arizona and California. M.S. Thesis, University of Oregon, Eugene OR.

O'Connell, B., Dorsey, R.J., Humphreys, E.D., 2017. Tidal rhythmites in the southern Bouse Formation as evidence for post-Miocene uplift of the lower Colorado River corridor. Geology 45, 99–102. https://doi.org/10.1130/G38608.1

Olariu, C., Steel, R.J., Dalrymple, R.W., Gingras, M.K., 2012. Tidal dunes versus tidal bars: The sedimentological and architectural characteristics of compound dunes in a tidal seaway, the lower Baronia Sandstone (Lower Eocene), Ager Basin, Spain. Sedimentary Geology 279, 134–155. https://doi.org/10.1016/j.sedgeo.2012.07.018

Olariu, M.I., Olariu, C., Steel, R.J., Dalrymple, R.W., Martinius, A.W., 2012. Anatomy of a laterally migrating tidal bar in front of a delta system: Esdolomada Member, Roda Formation, Tremp-Graus Basin, Spain. Sedimentology 59, 356–378. https://doi.org/10.1111/j.1365-3091.2011.01253.x

Olmstead, F.H., Loeltz, O.J., Irelan, B., 1973. Geohydrology of the parker-blythe-cibola area, Arizona and California. Geological Survey professional Paper.

Otvos, E.G., 2000. Beach ridges — definitions and significance. Geomorphology 32, 83–108. https://doi.org/10.1016/S0169-555X(99)00075-6

Pearthree, P.A., House, P.K., 2014. Paleogeomorphology and evolution of the early Colorado River inferred from relationships in Mohave and Cottonwood valleys, Arizona, California, and Nevada. Geosphere 10, 1139–1160. https://doi.org/10.1130/GES00988.1

Pethick, J., 1994. Estuaries and wetlands: function and form, in: Wetland Management: Proceedings of the International Conference Organized by Institution of Civil Engineers and Held in London on 2–3 June 1994. Thomas Telford Publishing, pp. 75–87.

Poulson, S.R., John, B.E., 2003. Stable isotope and trace element geochemistry of the basal Bouse Formation carbonate, southwestern United States: Implications for the Pliocene uplift history of the Colorado Plateau. Bulletin of the Geological Society of America 115, 434–444. https://doi.org/10.1130/0016-7606(2003)115<0434:SIATEG>2.0.CO;2

Pugh, D.T., 1988. D. T. Pugh Tides, Surges and Mean Sea-Level, xiv, 472 pp. John Wiley, 1987. Price £50.00. Journal of the Marine Biological Association of the United Kingdom 68, 361–361. https://doi.org/10.1017/S0025315400052309

Pye, K., 1990. Physical and human influences on coastal dune development between the Ribble and Mersey estuaries, northwest England, in: Coastal Dunes: Form and Process. Wiley Chichester, pp. 339–359.

Reineck, H.-E., Wunderlich, F., 1968. Classification and origin of flaser and lenticular bedding. Sedimentology 11, 99–104.

Reynaud, J.-Y., Dalrymple, R.W., 2012. Shallow-Marine Tidal Deposits, in: Davis Jr., R.A., Dalrymple, R.W. (Eds.), Principles of Tidal Sedimentology. Springer Netherlands, Dordrecht, pp. 335–369. https://doi.org/10.1007/978-94-007-0123-6_13

Richard, S.M., 1993. Palinspastic reconstruction of southeastern California and southwestern Arizona for the Middle Miocene. Tectonics 12, 830–854. https://doi.org/10.1029/92TC02951

Ricketts, J.W., Girty, G.H., Sainsbury, J.S., Muela, K.K., Sutton, L. a., Biggs, M. a., Voyles, E.M., 2011. Episodic Growth of the Chocolate Mountains Anticlinorium Recorded By the Neogene Bear Canyon Conglomerate, Southeastern California, U.S.A. Journal of Sedimentary Research 81, 859–873. https://doi.org/10.2110/jsr.2011.66

Roskowski, J.A., Patchett, P.J., Spencer, J.E., Pearthree, P.A., Dettman, D.L., Faulds, J.E., Reynolds, A.C., 2010. A late Miocene-early Pliocene chain of lakes fed by the Colorado River: Evidence from Sr, C, and O isotopes of the Bouse Formation and related units between Grand Canyon and the Gulf of California. Bulletin of the Geological Society of America 122, 1625–1636. https://doi.org/10.1130/B30186.1

Santoro, V.C., Amore, E., Cavallaro, L., Cozzo, G., Foti, E., 2002. Sand Waves in the Messina Strait, Italy. Journal of Coastal Research 36, 640–653. https://doi.org/10.2112/1551-5036-36.sp1.640

Schuster, M., Nutz, A., 2017. Lacustrine wave-dominated clastic shorelines: modern to ancient littoral landforms and deposits from the Lake Turkana Basin (East African Rift System, Kenya). Journal of Paleolimnology 59, 221–243. https://doi.org/10.1007/s10933-017-9960-4

Shaw, J., You, Y., Mohrig, D., Kocurek, G., 2015. Tracking hurricane-generated storm surge with washover fan stratigraphy. Geology 43, 127–130. https://doi.org/10.1130/G36460.1

Sherrod, D.R., Tosdal, R.M., 1991. Geologic setting and tertiary structural evolution of southwestern Arizona and southeastern California. Journal of Geophysical Research 96, 12407. https://doi.org/10.1029/90JB02688

Smith, P.B., 1970. New evidence for a pliocene marine embayment along the lower colorado river area, california and arizona. Bulletin of the Geological Society of America 81, 1411–1420. https://doi.org/10.1130/0016-7606(1970)81[1411:NEFAPM]2.0.CO;2

Spencer, J.E., Jonathan Patchett, P., Pearthree, P.A., Kyle House, P., Sarna-Wojcicki, A.M., Wan, E., Roskowski, J.A., Faulds, J.E., 2013. Review and analysis of the age and origin of the pliocene bouse formation, lower Colorado River Valley, southwestern USA. Geosphere 9, 444–459. https://doi.org/10.1130/GES00896.1

Spencer, J.E., Patchett, P.J., 1997. Sr isotope evidence for a lacustrine origin for the upper Miocene to Pliocene Bouse Formation, lower Colorado River trough, and implications for timing of Colorado Plateau uplift. Bulletin of the Geological Society of America 109, 767–778. https://doi.org/10.1130/0016-7606(1997)109<0767:SIEFAL>2.3.CO;2

Spencer, J.E., Pearthree, P.A., 2001. Headward Erosion Versus Closed-basin Spillover as Alternative Causes of Neogene Capture of the Ancestral Colorado River by the Gulf of California. Colorado River origin and evolution 215–220.

Spencer, J.E., Peters, L., McIntosh, W.C., Patchett, P.J., 2001. 40Ar/39Ar Geochronology of the Hualapai Limestone and Bouse Formation and Implications for the Age of the Lower Colorado River. Colorado River origin and evolution 89–91.

Stride, A.H., 1982. Offshore tidal deposits: sand sheet and sand bank facies, in: Offshore Tidal Sands. Springer Netherlands, Dordrecht, pp. 95–125. https://doi.org/10.1007/978-94-009-5726-8_5

Taylor, D.W., 1983. Later Tertiary Mollusks from the Lower Colorado River Valley. Museum of Paleontology, The University of Michigan.

Townend, I.H., 2003. Coastal and estuary behaviour systems. ABP Marine Environment Research, Southampton, UK.

Turak, J., 2000. Re-evaluation of the Miocene/Pliocene depo- sitional history of the Bouse Formation, Colorado River trough, southern Basin and Range (CA, NV, and AZ). M.S. Thesis University of Wyoming, Laramie.

Winterer, J.I., 1975. Biostratigraphy of the Bouse Formation: A Pliocene Gulf of California deposit in California, Arizona, and Nevada. M.S. Thesis California State University, Long Beach CA.

Zanor, G.A., Piovano, E.L., Ariztegui, D., Vallet-Coulomb, C., 2012. A modern subtropical playa complex: Salina de Ambargasta, central Argentina. Journal of South American Earth Sciences 35, 10–26. https://doi.org/10.1016/j.jsames.2011.10.007